Middle Holocene SST record (7,518±46 to 5,944±28 ybp) based on corals from the Enriquillo Valley, Dominican Republic

by

Yesenia Herrera

Thesis submitted in partial fulfillment of the requirements for the degree of

MASTER OF SCIENCE

in

GEOLOGY

UNIVERSITY OF PUERTO RICO

MAYAGÜEZ CAMPUS

2018

Approved by:

_____	_____
Wilson R. Ramírez Martínez Ph.D President of Graduate Committee	Date
_____	_____
Amos Winter, Ph.D Member of Graduate Committee	Date
_____	_____
Hernán Santos Mercado, PhD Member of Graduate Committee	Date
_____	_____
Rafael Mendez-Tejeda, PhD Member of Graduate Committee	Date
_____	_____
Roy A. Armstrong, Ph.D. Representative of Graduate Studies	Date
_____	_____
Lizzette Rodríguez Iglesias, Ph.D, Chairperson of the Department of Geology	Date

ABSTRACT

Corals are important paleo-climatological tools because as they accrete their aragonite skeletons they also store a record of fluctuations in the chemical and physical conditions that existed in the sea water surrounding them. The Cañada Honda outcrop located in Enriquillo Valley in southwestern Dominican Republic is a rare and excellently preserved fossil coral reef which allows for the collection of paleo-climate information from the early Holocene. *Orbicella species* complex coral samples were collected from this outcrop ranging in age from 7,518 ±46 to 5,944 ±28 years before present. Slabs from these corals were x-rayed to show annual growth bands which were analyzed for annual growth rates. Powdered samples were taken at millimeter intervals across the maximum growth axis of each coral slab. The powders were analyzed for $\delta^{18}O$ and Sr/Ca ratios which were used to calculate sea surface temperatures (SST) and estimate residual $\delta^{18}O$ which is correlated to sea surface salinity. Results from these mid-Holocene corals show that annual growth rates range from 2.5 to 5.3±0.2 mm/yr, which is expected for corals growing at 17 to 20±1 meters depth. Sr/Ca derived SST range on average from 21.95 to 20.28°C. $\delta^{18}O$ derived SST range from 11.09 to 16.79°C which are temperatures outside the tolerance of corals (18-30 C). Residual $\delta^{18}O$ suggest that the corals grew in an environment with high variability in sea surface salinity. $\delta^{18}O$ derived salinity values suggest that that the coral reefs accreted in the mid-Holocene Enriquillo paleo-embayment were subject to the upper limit of coral salinity tolerance. Sr/Ca-SST from Cañada Honda corals are 5.5 to 8°C cooler than other Caribbean SST proxies suggesting that the Sr/Ca-SSTs from this study do not show absolute temperature. Regardless, Sr/Ca-SSTs do capture a warming trend in the mid-Holocene also seen other Caribbean SST proxies.

RESUMEN

Los corales son importantes herramientas paleo-climatológicas porque a medida que crecen almacenan en sus esqueletos de aragonita un registro de las fluctuaciones en las condiciones químicas y físicas que existe en el agua de mar en su alrededor. El afloramiento de Cañada Honda, ubicado en el Valle de Enriquillo, en el suroeste de la República Dominicana, es un arrecife de coral fósil único y altamente preservado lo cual permite la recolección de información paleo-climática del Holoceno medio. Se recolecto de este afloramiento muestras de coral del complejo *Orbicella sp*. Las edades de estos corales están entre 7,518 ± 46 y 5,944 ± 28 años antes del presente. Transectos de estos corales se sometieron a radiografías para mostrar las bandas de crecimiento anual, las cuales se analizaron para determinar las tasas de crecimiento anual. Se tomaron muestras en polvo a intervalos de milímetro a través del eje de crecimiento máximo de cada transecto de coral. Los polvos se analizaron para determinar las razones de $\delta^{18}O$ y Sr/Ca que se usaron para calcular las temperaturas de la superficie del mar (TSM) y estimar el $\delta^{18}O$ residual que se correlaciona con la salinidad de la superficie del mar. Los resultados de estos corales del Holoceno medio muestran que las tasas de crecimiento anual varían de 2.5 a 5.3±0.2 mm/año, lo que se espera para los corales que crecen a una profundidad de 17 a 20±1 metros. El rango de TSM derivado de Sr/Ca en promedio es de 21.95 a 20.28°C. TSM derivado de $\delta^{18}O$ da rango de TSM de 11.09 a 16.79°C en promedio, cuales son temperaturas fuera de la tolerancia de los corales (18 a 30°C). $\delta^{18}O$ residual sugiere que los corales crecieron en un ambiente con alta variabilidad en la salinidad de la superficie del mar. Los valores de salinidad derivados de $\delta^{18}O$ sugieren que los arrecifes coralinos acrecidos en el paleo-bahía de Enriquillo a mediados del Holoceno estuvieron sujetos al límite superior de la tolerancia a la salinidad del coral. TSM-Sr/Ca de los corales Cañada Honda son de 5.5 a 8°C más fríos que otros paleo-registros de TSM en el Caribe, lo que sugiere que las TSM-Sr/Ca de este estudio no muestran la temperatura absoluta. Independientemente, las TSM-Sr/Ca captan una tendencia de calentamiento en el Holoceno medio cual también se ha observado en otros paleo-registros de TSM en el Caribe.

ACKNOWLEDGEMENTS

I would first like to express my gratitude and appreciation to my thesis advisor Dr. Wilson Ramirez of the Geology department at the University of Puerto Rico-Mayaguez Campus. Dr. Ramirez's office was always open whenever I needed guidance or had a question about my research. He consistently allowed this paper to be my own work but steered me in the right the direction whenever he thought I needed it. I would also like to thank the members of my committee who provided guidance and their expertise for this research project: Dr. Hernan Santos, Dr. Amos Winter, and Dr. Rafael Mendez-Tejeda. Without their disposition, participation, and input, this research could not have been successfully conducted. I would also like to thank the experts whose contribution was essential and vital for this research. Thank you to Ivette Roche and her staff in the radiology laboratory at the San Antonio Hospital in Mayagüez, Yelitsa I. Gonzalez of the Gas Analysis Stable Isotope Laboratory, Miguel Santiago of the geology department UPR-NSF Earth X-ray Analysis Center, Dr. Ali Pourmand from the Rosenstiel School of Marine and Atmospheric Sciences, and José Almodovar of the UPRM-Biology microscopy center as their work and disposition was crucial for the fulfillment of this project. Thanks to Sociedad Geológica de República Dominicana and MESCyT who funded the field work and laboratory analysis required for this project. I would also like to express my gratitude from the staff of the UPRM-Geology Department and my fellow graduate students and undergraduate students for their aid and support. Last but not least, I must express my very profound gratitude to my parents and to my husband for providing me with unwavering support and continuous encouragement throughout my years of study and through the process of researching and writing this thesis. This accomplishment would not have been possible without them. Thank you.

TABLE OF CONTENTS

List of tables

List of figures

List of appendices

CHAPTER 1 – INTRODUCTION

1.1 Climate Science

Climate science is young and increasingly relevant. Regional climatic events during the last thousand years, such as the Little Ice Age (LIA, 500–100 years B.P.), indicate that natural centennial-scale climate variability is superimposed by anthropogenically forced climate change (Saenger et al., 2008). Recently rising sea level, record-breaking climatic events, and the escalated bleaching of the Great Barrier Reef has further fueled the desire to understand anthropogenic and natural climate change (Ainsworth et al., 2016).

The specific effect of anthropogenic versus natural radiative forcing on climate is still not well understood. The climate system is composed of five major components, the ocean, atmosphere, cryosphere, biosphere, and land (Karl and Trenberth, 2003). Natural processes that force changes, at different time scales, in the climate system include tectonic processes and large volcanic eruptions, earth orbital changes, and changes in the total solar irradiance (Myhre et al., 2013). Anthropogenic forcing is a result of human industry and agriculture that add greenhouse gasses to the atmosphere. The rate of human-induced climate change is projected to be much faster than most natural processes (Karl and Trenberth, 2003). However, there are thresholds that could abruptly switch the climate to a different regime. For example, approximately 11,500 to 12,700 years ago rapid warming resulted in freshwater discharge from melting ice sheets into the North Atlantic Ocean and changed ocean thermohaline circulation causing cooling (Karl and Trenberth, 2003). This is known as the Younger Dryas cold event. Characterization of the anthropogenic influence on climate in the future requires understanding climate change at a fine temporal scale for long intervals of time in earth's recent history but without modern anthropogenic activity (Karl and Trenberth, 2003). This study used fossil corals to create sea

surface temperature and sea surface salinity records from the mid-Holocene as an effort to contribute to our understanding of climate variation before modern climate records and before modern anthropogenic forcing.

1.1.1 Corals as Climate Proxies

Climate proxies are indirect measurements of climatic conditions obtained through physical and/or chemical measurement of climate archives. Climate archives include tree rings, ice cores, sediment cores, speleothems, and corals. In the tropics, corals are important climate archives (Grottoli, 2001). As corals accrete their aragonite skeletons they record changes in chemical and physical conditions in the environment surrounding them (Druffel, 1997). Coral skeletons provide records of annual density banding, isotopic ratios, elemental ratios, skeletal stress bands, and skeletal fluorescence. Annual density bands are skeletal structures in corals that consist of one high and one low-density band deposited by the coral each year and they are discernible by radiographs. High and low-density band couplets are used to determine chronology and thus enhancing the time resolution of the climate records obtained from corals (Brachert et al., 2006). Therefore, corals provide high-resolution climate information obtained by combining isotope geochemistry and trace element analysis with annual density band analysis.

Grottoli (2001), states that massive stony corals are good climate proxies due to their wide distribution in the tropics, their annual skeletal banding pattern, their growth rates of 5-25 mm/year permit sub-annual sampling resolution, and their ability to record changes in paleo-sea surface temperature (SST), sea surface salinity (SSS), ocean circulation, ocean mixing patterns, and other climatic and oceanic features. Changes in Caribbean SST can influence hurricane intensity and paths further highlighting the importance of understanding the cause of changes in SST. Studying paleo-SST can also help us better understand the frequency of climate events that

influence Caribbean SST such as North Atlantic Oscillation (NAO) and El Niño Southern Oscillation (ENSO) (Birgmark, 2014). NAO is a large-scale movement of atmospheric mass between the Icelandic low-pressure system and the North Atlantic subtropical high-pressure system (Charlery et al., 2006). The NAO is negatively correlated with Caribbean rainfall due to anomalous SST's (Giannini et al., 2001). ENSO is a major contributor to annual climate variability. ENSO is characterized by the pressure difference between Tahiti (central Pacific) and Darwin (northern Australia), reduction of coastal upwelling, and an increase in SST along the western coast of South America (Donders, 2005). In the Caribbean, rainfall is associated with annual changes in sea level pressure (SLP) and SST. ENSO events correlate to anomalously high SLP in the North Atlantic high which translates into stronger trade winds resulting in cooler SSTs and therefore less Caribbean rainfall (Giannini et al. 2000). Cobb et al. (2013), used oxygen isotope ($\delta^{18}O$) analysis of fossil corals from the Pacific Northern Line Islands to create a reconstruction of ENSO in the Holocene. ENSO brings warmer and rainier conditions to the Northern Line Islands and decrease the coral $\delta^{18}O$. The ENSO reconstruction from Northern Line Island corals was combined with previously published ENSO reconstructions to cover 1.3 to 6.9 ky. This study found no evidence of orbitally induced insolation forcing or systematic trends in ENSO variance which suggests that ENSO variance in the past 7ky are the result of internal variability (Cobb et al., 2013). Cobb et al. (2013), also found that twentieth-century ENSO variance is significantly higher (although not unheard of) than average fossil coral ENSO variance. Determining whether the twentieth-century ENSO variance is a result of anthropogenic greenhouse forcing may be undetectable due to large internal variability and requires much longer data sets.

Sea surface temperature studies from fossil corals are used to validate climate models and provide insight into the cause of climate fluctuations in the past. Beck et al. (1992), coupled strontium/calcium (Sr/Ca) ratio analysis by thermal ionization mass spectrometry and $\delta^{18}O$ thermometry of modern and fossil *Porites sp.* corals of the southwestern Pacific. In this study the modern corals were taken from sites near SST recording stations to calibrate and assess the Sr/Ca ratio method. The fossil coral indicated that approximately 10,200 years ago SST's in the southwestern Pacific were 5°C colder and variations in SST were greater than modern variations (Beck et al., 1992). Beck et al. (1992), were able to therefore determine that during times of deglaciation, tropical climate zones were restricted closer to the equator. Winter et al. (2000), used oxygen isotopes in cores of *Orbicella faveolata* colonies from La Parguera, Puerto Rico, to obtain an SST record from the Little Ice Age (LIA). They were able to determine that during the LIA Caribbean SST was between 2-3°C cooler than modern sea surface temperatures. Giry et al. (2012), used Sr/Ca ratio records from both modern and fossil *Diploria strigosa* corals from Bonaire in the south Caribbean. Using Sr/Ca ratio records to reconstruct sea surface temperatures Giry et al. (2012), found that the southern Caribbean Sea during the mid- to late Holocene SST was characterized by clear seasonal cycles, persistent quasi-biennial and prominent interannual as well as inter- to multidecadal-scale variability. Flannery and Poore (2013), obtained Sr/Ca ratio records from one modern and one Holocene *Orbicella faveolata* coral in the Dry Tortugas National Park in Florida. The Sr/Ca record from the modern coral was regressed against a local SST record to create a calibration between SST and Sr/Ca. This calibration generated an SST record from 1961 to 2008 and a 7-year Holocene record about six thousand years old. As a result, Flannery and Poore (2013) reported that the Sr/Ca from *Orbicella faveolata* have a high potential for developing Holocene SST records because Sr/Ca values and calculated SST records of the

Holocene, compared to the modern, are very similar. Like these discussed studies, this investigation seeks to use corals as proxies to better understand Holocene climate.

Sea surface salinity (SSS) is an important physical parameter in climate studies. Temperature and salinity are the driving forces of thermohaline circulation and precipitation/ evaporation trends. Therefore, salinity has the potential to give information on atmospheric components of climate (Corrège, 2006). Oxygen isotope ($\delta^{18}O$) ratios of coral skeletons reflect a blend of SST and the $\delta^{18}O$ of the seawater surrounding the coral. SSS is related to the $\delta^{18}O$ of the seawater ($\delta^{18}O_w$). If either the SSS or SST are known to be constant in a region, the $\delta^{18}O$ of coral skeletons can be used to determine variability of SST or SSS, respectively. Both SSS and SST vary seasonally in the Caribbean therefore trace element ratios such as Sr/Ca, Mg/Ca, and U/Ca are used to provide SST independent of SSS (Watanabe et al., 2001). Gagan et al. (2000) coupled Sr/Ca and $\delta^{18}O$ to reconstruct the $\delta^{18}O_w$ of seawater for corals in the Pacific and Indian Ocean. Residual $\delta^{18}O$ or $\delta^{18}O_w$ of seawater is defined by the difference between coral Sr/Ca and $\delta^{18}O$ curves. Gagan et al. (2000) found that residual $\delta^{18}O$ records can explain the regional balance between precipitation and evaporation in high resolution datasets. This study will use Sr/Ca and $\delta^{18}O$ to reconstruct the $\delta^{18}O_w$ of seawater for fossil mid-Holocene corals in the Caribbean.

While fossil corals are powerful tools in climate science, their study is complicated by the major susceptibility of coral aragonitic skeletons to be diagenetically altered by recrystallization, micritization, neomorphism, and dissolution, all of which are processes that alter the original character, texture, and geochemical character of the corals (Sayani et al., 2011). Aragonite is a polymorph of the mineral calcite; it has the same chemical formula, $CaCO_3$, but differs in its crystallographic structure. Aragonite coral skeletons can suffer diagenetic alteration in both the marine and vadose environments. As a result, well-preserved corals with their original

mineralogy are few and difficult to find. Evidence of diagenesis takes form in the precipitation of secondary aragonite, calcite cement in skeletal voids, or calcite replacement of the coral skeleton. These digenetic processes alter the geochemical signature of the coral skeleton, therefore, altering the SST record calculated from Sr/Ca and $\delta^{18}O$ ratios (McGregor and Gagan, 2003).

McGregor and Gagan (2003), used *Porites* corals from Papua New Guinea to study the implications of vadose zone diagenesis on coral skeletons used in paleoclimate research. McGregor and Gagan (2003), analyzed coral samples that had diagenetic features varying from leaching of primary aragonite, fine calcite overgrowths, calcite void filling and neomorphic, fabric selective replacement of the coral skeleton. Through comparison of altered and unaltered coral they found that Sr/Ca ratios were more impacted than $\delta^{18}O$ due to the partition coefficient of strontium into calcite being much lower relative to aragonite. As a result, McGregor and Gagan (2003), found that calculated SST sensitivity to vadose-zone calcite diagenesis from Sr/Ca was 1.1 to 1.5°C warmer per percent calcite and calculated SST from $\delta^{18}O$ was -0.2 to 0.2°C cooler or warmer per percent calcite (See Figure 1). Quinn and Taylor (2006), also studied *Porites* corals from Papua New Guinea to examine the influence early marine diagenesis of coral skeleton diagenesis (in the form of secondary aragonite) on Sr/Ca and $\delta^{18}O$ derived SST. They found that alteration by secondary aragonite resulted in cooler SSTs by 2.5°C for $\delta^{18}O$ calculated SST's and 6°C for Sr/Ca calculated SST's. Secondary aragonite can be identified by X-radiography, scanning electron microscope (SEM) analysis, and analysis of petrographic thin-sections, therefore these types of analyses should be a part of all coral based paleoclimate reconstructions (Quinn and Taylor, 2006). The negative implications of diagenesis to paleoclimate reconstructions based on corals highlight the importance of the pristine conditions

in coral skeletons of the Cañada Honda outcrop present in the Enriquillo Valley, Dominican Republic.

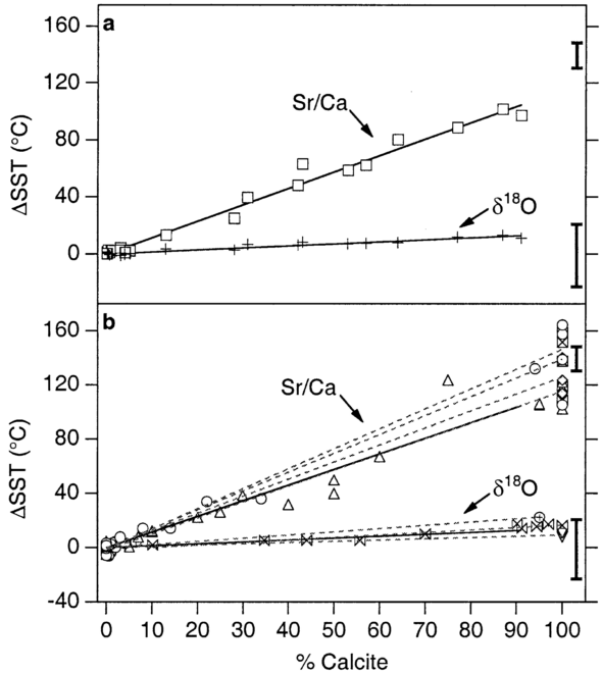

Figure 1. Diagenetic influence, obtained by McGregor and Gagan (2003), on Sr/Ca and $\delta^{18}O$ expressed as a change in SST. All data were converted to SST using the average of published Sr/Ca and $\delta^{18}O$ SST slopes (See McGregor and Gagan, 2003). (a) Weighted mean linear 18O(+) and Sr/Ca (□) data and regression lines (solid lines) from corals from uplifted reefs at Muschu Island. (b) Comparison of SST regressions from (a)(solid lines) with those for various coral species with varying percentages of vadose-zone calcite (dashed lines). $\delta^{18}O$-ΔSST regression for Martin et al. (1986, ▽), Stein et al. (1993, ⊕), and Wei et al. (1998, ⋈). Sr/Ca-ΔSST regression for Seigel (1960, Δ), Zhu (1990, ○), Zhu et al. (1988, ⊠), and Zhu et al. (1994, ◊). The bars at 100% calcite represent the range of calculated end-member Sr/Ca- ΔSST (upper vertical line) and calculated end-member $\delta^{18}O$-ΔSST (lower vertical line). Figure from McGregor and Gagan (2003).

1.1.2 Cañada Honda Corals

The Cañada Honda outcrop located in the hillside of the Enriquillo Lake, southwestern Dominican Republic, is a rare and excellently preserved example of a Holocene shallow-water coral reef (Hubbard et al., 2004). Its mid-Holocene age (9,000 to 5,000 yr BP; Hubbard et al., 2008) where no modern anthropogenic influences were present, and its high sedimentation environment adds to the importance of this outcrop. The lack of modern anthropogenic influence is important because it allows the study of climate in the recent past before anthropogenic forcing was a large contributor to climate change. The high sedimentation environment was key in its pristine preservation because sediments protected the coral from bioerosion by burying it very fast. The subaerial exposure exhibits excellent preservation of aragonite coral skeletons and provides a unique opportunity to study fine temporal scale aspects of climate change (Greer, 2001). Cañada Honda presents a unique opportunity to study a fossil marine ecosystem, very similar if not identical to that of modern Caribbean. The location provides pristine corals that can be used as proxies to obtain sea surface temperature (SST) and sea surface salinity (SSS). Furthermore, it provides a continuous 4,000 years record which can be used to determine the SST rate of change during the mid-Holocene without modern anthropogenic influence.

1.1.3 Holocene Climate

The Holocene epoch spans from 11,700 years before present (ybp) to the present and has undergone considerable change in climate (Walker et al., 2012). The beginning of the Holocene is marked by the start of deglaciation predicted by the Milankovitch theory as the result of a summer insolation maximum in the northern hemisphere near 10,000 years before present. Holocene climate is dominated by millennial-scale variations although the cause of these variations is still not well understood (Maslin et al., 2001). Mayewiski et al. (2004), examined 50 globally distributed paleoclimate records to discover six periods of rapid climate change (RCC). Two of these RCC

periods overlap with the ages from Cañada Honda, 9,000-8,000 and 6,000-5,000 ybp. These RCC periods are marked by polar cooling, tropical aridity, and major atmospheric circulation changes. From 9,000 to 8,000 ybp is the only RCC to occur when large Northern Hemisphere ice sheets were still present (Mayewiski et al., 2004). Within this period is the 8.2ka event that lasted approximately 150 years and was characterized by dry windy conditions and regional cooling. This event is documented by methane and nitrogen isotopes collected from air bubbles trapped in Greenland ice cores which suggest that during the 8.2ka event temperatures over Greenland dropped by 3.3-7.4°C (Kobashi et al., 2007). This event is believed to have been caused by disruption of oceanic circulation by massive freshwater flows from proglacial lakes into the ocean (Kobashi et al., 2007). This event was associated with increased precipitation in the Eastern Caribbean resulting in accelerated stalagmite growth rates (Winter et al., 2013). The RCC period that occurred from 6,000-5,000 ybp is characterized by cool poles and dry-tropics. Although, during this time the Caribbean, unlike other tropical regions, underwent increasing rainfall and became wetter. The 6,000-5,000 ybp RCC has no evidence of massive freshwater pluses as in the 9,000 to 8,000 ybp RCC. There is also no evidence cooling trends could have been caused by changes in the concentrations of volcanic aerosols or atmospheric CO_2. The decline in solar output is suggested by $\delta^{14}C$ and ^{10}Be records are the most plausible cause (Mayewiski et al., 2004). Holocene climate is proven to be highly variable by a multitude of proxy records highlighting the importance of studying the Mid-Holocene Cañada Honda reef outcrop.

1.2 Study Area

Enriquillo Valley is an east-west trending feature bounded by active faults located in the southwestern part of the Dominican Republic (See Figure 2). The valley extends into Haiti where it is known as the Cul-de-Sac Plain. The Enriquillo-Cul-de-Sac Valley is a compression ramp valley, depressed by the overthrust loads of neighboring mountain blocks (Mann et al., 1984).

Located in this valley is Cañada Honda a uniquely well-preserved shallow-water coral reef outcrop with preservation of original aragonite coral skeletons. The excellent preservation is attributed to the warm temperatures and relatively dry climate of the area (Greer, 2001). Radiocarbon dating of the subaerially exposed coral reef revealed that the reef existed from approximately 9,000 to 5,000 years before present (Hubbard et al., 2008).

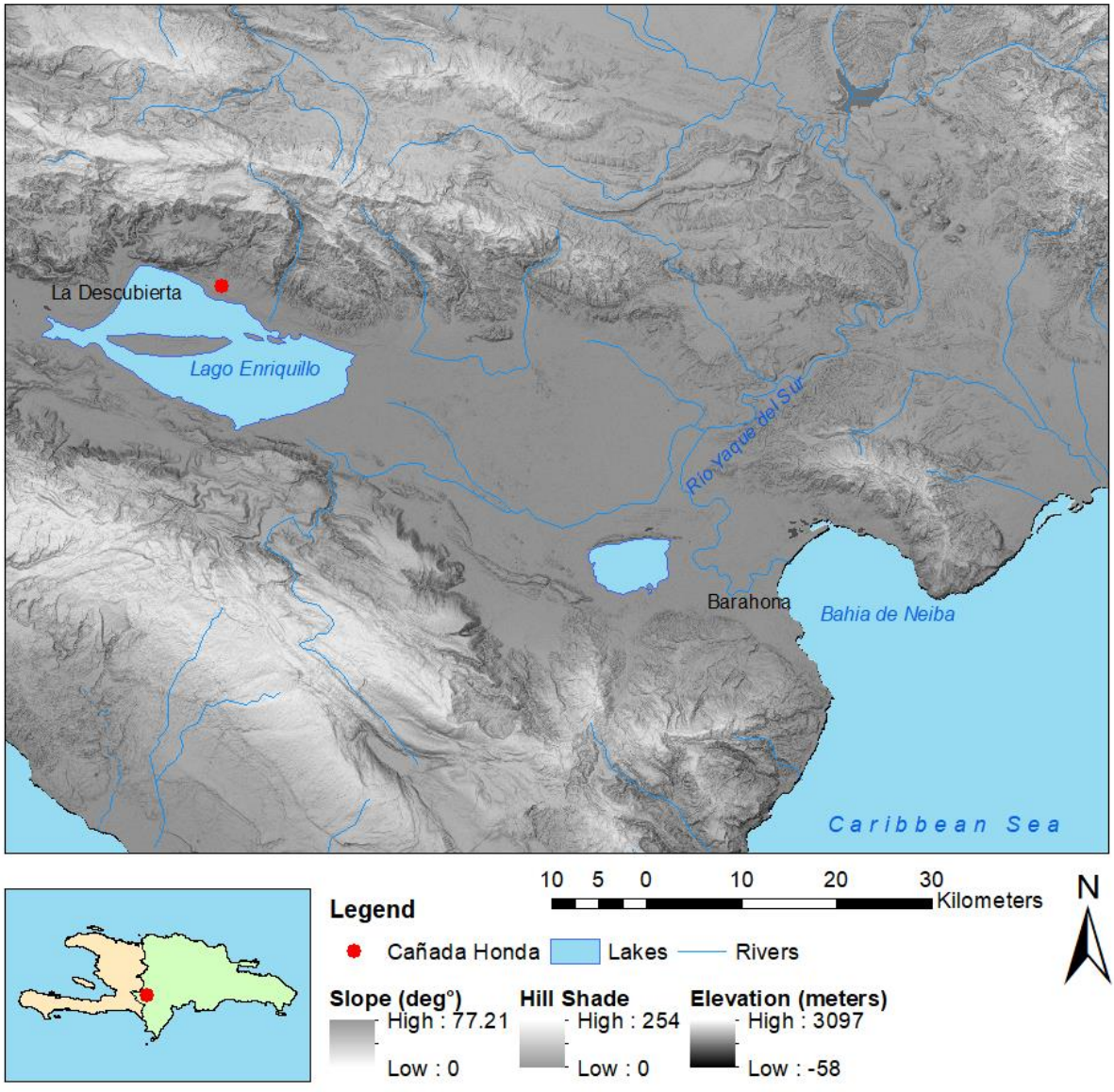

Figure 2. This map shows Enriquillo vallley topography. The red circle indicated the location of Cañada Honda. The elevation raster is overlain by slope and hillshade rasters with transparency.

(Figure 2 caption continued) The elevation raster was created with data from the Shuttle Radar Topography Mission (SRTM) 1 Arc-Second Global and obtained from the USGS Earth Explorer.

The Enriquillo Valley flooded about 10,000 years ago (Taylor et al., 1985) due to rising sea level that gave the name to geological epoch (Lighty et al., 1982). This created a bay connected to the Caribbean Sea resulting in transgressive deposits that eventually formed shallowing-upward sequences (Cuevas et al., 2005). Submerged alluvial fan deposits in the Enriquillo-Cul-de-Sac Valley were colonized by corals approximately 8,000 years ago and creating a thriving reef community by 7,000 years ago (Mann et al., 1984). The community flourished until approximately 4 to 5,000 years ago when fluvial deposits from Río Yaque del Sur coupled with left lateral movement along the Enriquillo fault zone isolated the open bay separating it from the Caribbean Sea and forming the present day hypersaline Lake Enriquillo (Mann et al., 1984). The reef became very well preserved by the influx of abundant fluvial sediment (Cuevas et al., 2005).

Because of the unique preservation of all kinds of fossils in the paleo-reefs present in the Enriquillo Valley, the region has been the focus of many studies. According to Stemann and Johnson (1992), much of the ecology, species richness, and diversity of the fossilized reef in Enriquillo are similar to modern reefs of the Caribbean with limited wave exposure with the exception that *Diploria sp.* corals are not present. The absence of *Diploria sp.* commonly known as brain corals in Cañada Honda is a mystery because the presence of *Diploria sp.* has been documented in the modern coral reef environments of Barahona Bay, just a few tens of kilometers away (Guzmán, 2017). Mann et al. (1984) also determined that the zonation displayed by the fossil reef is similar to a typical modern Caribbean reef found in offshore low energy environment. Mann et al. (1984) suggested that the fossil reefs of Enriquillo formed in a tectonic

depression approximately 85 kilometers long and 12 kilometers wide. The deep embayment resulted in limited wave action which accounts for the large volume of *Acropora cervicornis* (Geister, 1977), as well as the absence of *Acropora palmata* who relies on wave action to remove sediment from its colony surfaces (Cuevas et al., 2005). Greer and Swart (2006) proposed the paleogeography of the area is most likely preserved because there are no major unconformities observed and no evidence of folding or faulting of Holocene reef sediments. Paleo sea level during reef accretion is difficult to determine due to the absence of *A. palmata*. Mann et al. (1984) proposed the minimum paleo sea level to be 5 meters below sea level (BSL) by using the elevation of the youngest (highest elevation) *Orbicella annularis* colony with sub-columnar form. The *Orbicella annularis* colonies are understood to have lived near low-tide level at the reef crest, substantiated by the presence of beachrock deposits that occur just above and landward from the highest elevation *Orbicella annularis* sub-columnar colony. The dates of these proposed *Orbicella annularis* reef crest corals is 4,760±90 ybp, which correlate well with *A. palmata* sea-level indicators of the same elevation in the western Atlantic (Mann et al., 1984).

The ancient embayment in which the Cañada Honda fossil reef accreted was bounded by the Sierra de Neiba mountain range to the north and Sierra de Bahoruco to the south. The average elevation of both mountain ranges is 1,500 m (Cuevas et al., 2005). This high relief produced large amounts of sedimentation discharge into the valley. The stress of sediments produced a low-diversity assemblage of corals dominated by coral from the *Orbicella species* complex (*Orbicella sp.* complex) and *Siderastrea siderea* (Greer and Swart, 2006).

High sediment influx conditions result in smothering and block out necessary sunlight in modern reefs (Rogers, 1990). The main contributor of sediments to the Cañada Honda reef was Sierra de Neiba. This mountain range is primarily composed of Paleocene to middle Miocene

limestones of the Neiba and Sombrerito Formations (Mann and Lawrence, 1991). Accreting reefs produce and are adapted to manage large amounts of carbonate sediments (Rogers, 1990) therefore the high influx of carbonate sediments from the Sierra de Neiba did not halt the accretion, however it was not at optimal conditions. Hubbard et al. (2008), proposed that high sedimentation resulted in suppressed growth rates of *Sideastrea sp.* and *Orbicella sp.* from the published 5-10 mm/yr to 1-3 mm/yr in Cañada Honda. The Cañada Honda corals show skeletal morphologies that suggest limited lateral growth caused by excessive sedimentation. The coral colonies present hemispheric, conical, and columnar morphologies, with abundant foliations (See Figure 4). High sedimentation and nutrient influx are also deduced from the abundant presence of boring lithophagid mollusks and barnacles associated with this type of environment (Hubbard et al., 2008).

Since the first descriptions of Cañada Honda corals were made the taxonomic classification of the genus *Montastraea* has changed to the genus *Orbicella*. The genus *Montastraea* remains exclusively for *Montastraea cavernosa*. This new classification comes from the integration of morphological and molecular data (Budd et al., 2012). This study focuses on the use of skeletons of *Orbicella sp.* complex corals from Cañada Honda to create paleoclimate reconstructions. The 450 meters long exposure of Cañada Honda was separated into facies by Hubbard et al. (2004) and Cuevas et al. (2005). Hubbard et al. (2004), quantified coral species and morphologies through point counting of quadrants along 16 vertical transects. Six coral reef facies were described including three massive coral facies named; M1, M2, and M3 as well as, mixed, branching and platy coral facies (See Figure 3). The branching coral facies is dominated by thick accumulations of the stag-horn coral *Acropora cervicornis.* The thick accumulations of *Acropora cervicornis* possibly formed near paleo sea-level (Cuevas et al.,

2005). Above the thick *Acropora cervicornis* layer serpulid worm reefs are present. These worm reefs typically form in brackish waters (Greer, 2001).

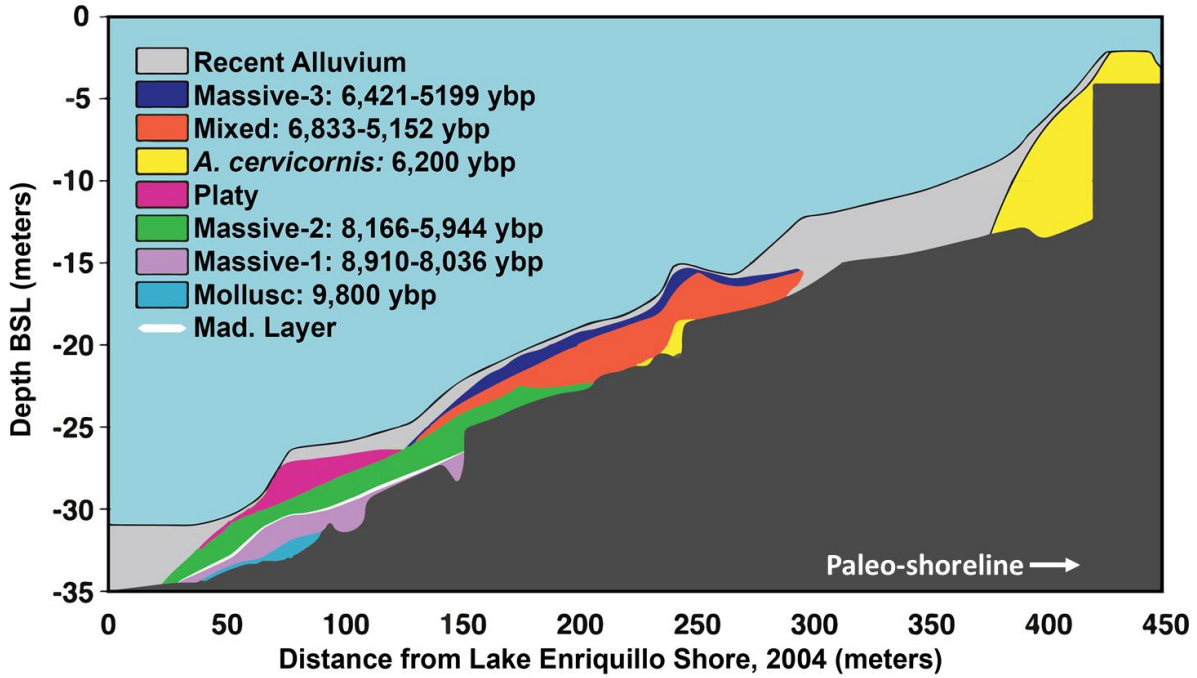

Figure 3. Facies model of Cañada Honda outcrop. The focus of this study is to analyze coral samples within Massive Zone 2, shown in green. Figure modified from Hubbard et al. (2004) and Cuevas et al. (2005).

1.2.1 Massive Coral Facies 2

The focus of this study is the massive-2 (M2) coral facies. The massive coral facies M1 and M2 are very similar in terms of coral assemblage but separated by a horizon with abundant displaced and broken *Madracis sp.* coral fragments and gastropods, bivalves, and other displaced and broken corals, plus sediment. The horizon was named the Mad layer and is interpreted as a storm deposit formed by one or several short-term disturbances (See Figure 4). Hubbard et al. (2004) used a *Madracis sp.* coral to radiocarbon date the deposit between 9,400-9,000 ybp. The most abundant coral in M1 and M2 facies is *Siderastrea siderea* followed by *Orbicella sp.* complex and then some *Stephanocoenia intersepta*. Based on quadrant point counts the M2 coral facies has 56.3% of *Siderastrea siderea* colonies, 10.1% of *Orbicella sp.* complex

colonies,18.5% sediment, and an overall total of 13 distinct coral species (See Table 1). Sediment character was also studied in the paleo-reef by Cuevas et al. (2005), which found that sediments were composed mostly of carbonate with insoluble residue that varied from 2-9%. The M2 facies produced the second lowest quantity of insoluble material at about 2.5%. Quartz and vermiculite were reported from XRD analyses of the insoluble residue (Cuevas, 2010). Growth rates of *O. faveolata* specimens were measured, using X-rays, in all the facies and the corals in the M2 facies produced growth rates that varied from 0.13 to 0.45 cm per year (Cuevas et al., 2005). A recent study by Morales (2015) produced unpublished U/Th dates for the M1 facies indicating this facies formed from 8,000 to 8,900 ybp. This highlights the importance of dating the M2 facies because the Mad layer was dated to be 9,400-9,000 ybp but it should be younger than the M1 facies since the Mad layer is stratigraphically above the M1 facies. This suggests the *Madracis sp.* coral dated from the Mad Layer storm deposit was sourced from older deposits. Dating corals present in the M2 facies will help restrain the age of the event that produced the Mad layer.

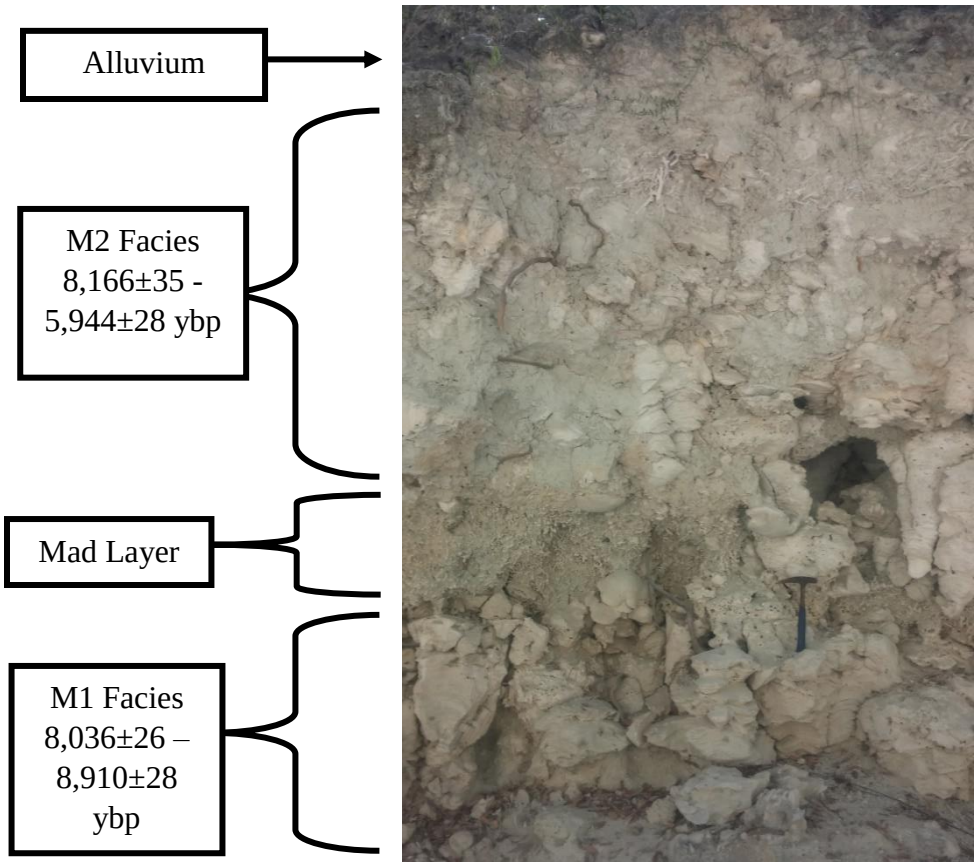

Figure 4. Cañada Honda outcrop approximately 53 meters inland from Lake Enriquillo shore as of 2004. M1 and M2 facies are labeled with U/Th dates. The Mad layer separating the M1 and M2 facies is composed primarily of sediment and broken *Madracis sp.* corals. Note coral morphologies are conical with abundant foliations. Hammer for scale.

Table 1. Distribution (% counts) of coral species and sediment for the M2 facies from quadrant point counts by Cuevas et al. (2005).

Coral Species	Distribution (% counts)
Siderastrea siderea	56.3
Orbicella sp. complex	10.1
Stephanocoenia intersepta	1
Madracis spp.	0.6
Dichocoenia stokesi	0.9
Colpophyllia natans	3.3
Undaria agaricites	0.6
Porites	0.2
Siderastrea radians	0.4
Helioceris cucullata	0.3
Manicinia aerolata	0.2
Eusmilia fastigiana	1.5
Porites astreoides	0.1
Unrecognizable	0.8
Sediment	18.5
Mad layer	5.2
Total %	100

2 CHAPTER – METHODOLOGY

2.1 Field Work

2.1.1 Fossil Corals Sampling

The fossil coral specimens used in this project were collected by students from the geology department of the University of Puerto Rico at Mayaguez (Jose Morales, Elson Core, and Kevin Velez) the summer of 2014 in an expedition lead by Dr. Wilson Ramirez. *Orbicella sp.* complex corals were used for this project because the genus is still present in the Caribbean and because they are present throughout the mid-Holocene reef deposits of the Enriquillo Valley. Both modern and fossil *Orbicella sp.* complex (formerly *Montastraea sp.*) corals have been featured in published paleoclimate studies (Saegner et al., 2008; Dodge et al., 1993; Swart et al., 2002; Greer and Swart, 2006; and others). Only fossil corals in growth position were collected from the M2 facies. It is crucial fossil corals be in growth position to ensure that the location of the paleoclimate record obtained from the coral is accurate. Before a coral sample was removed from the outcrop it was labeled with an alphanumeric code. The first two digits represent the facies the sample was taken from according to Hubbard et al. (2004); all samples in this study are from the M2 facies. The second number is based on the distance in meters from the shore of Lake Enriquillo. The final number of the alphanumeric code represents the stratigraphic height from the base of the gully. The edges of the samples were cut preserving only the central part of the coral skeleton. Samples were cut in the field using a portable Nakita Doc 7301 cutting machine with the purpose of easier transportation and to assess the degree of preservation of the coral and the presence of bioerosion in the skeleton. Corals were wrapped in newspaper and packed into medium sized plastic trash cans for transportation to Puerto Rico on the American Cruise Ferry. Fourteen of these samples were initially chosen for processing into five-millimeter

thick slabs based on preservation and size. Five-millimeter thick samples were cut from the selected coral samples to ensure good quality radiographies; this is because five-millimeters is the average diameter of an *Orbicella sp.* complex corallite. After analysis of the coral radiographies, ten corals were selected for physical and geochemical analysis (See Table 2).

During the summer of 2015 the Enriquillo Valley was visited by the author with the objective to learn about the exposure, sample locations, character of the outcrop, and local geology. Field observations were made of the M2 facies and surrounding facies (see Figure 4 and Section 1.2.1 for additional description of the M2 facies). The M1 facies was observed to have a higher coral density than the M2 facies. The M2 facies had similar coral types but corals were separated by more sediment than in the M1 facies (see Figure 4). It seems that it took some time for the reef to stabilize after the Mad layer event which separates M1 and M2 facies.

Table 2. Sample list of the ten corals that were collected from the M2 facies. The table provides a summary of the physical and geochemical analyses conducted on the coral sample. * Indicates the coral was samples but results were not received due to technical difficulties. Radiographies of each coral are in Appendix 9. XRD diffractograms for each coral are in Appendix 1. Stable isotope data is in Appendix 5. Sr/Ca data is in Appendix 6. U/Th dates are in table 7 in section 3.3. SEM images for each coral are in figures 13-14 in section 3.1.

Analysis Type	Geochemical			Physical and Preservation		
Sample List	Stabe Isotopes	Sr/Ca	U/Th	X-ray	XRD	SEM
M2 120.5-0.5	✓		✓	✓	✓	✓
M2 148.0-0.6	*			✓	✓	
M2 140.7-0.7	✓	✓	✓	✓	✓	✓
M2 140.0-0.8	✓			✓	✓	✓
M2 136.3-1.1	✓		✓	✓	✓	✓
M2 134.4-1.2	✓			✓	✓	
M2 150.7-1.3	*			✓	✓	✓
M2 120.4-1.5	✓			✓	✓	✓
M2 144.8-3.1	✓			✓	✓	✓
M2 145.7-3.1	✓	✓	✓	✓	✓	✓
M2 120.4-1.5-sed					✓	

2.2 Laboratory Work

2.2.1 Sclerochronology

Fossil coral samples were cut into slabs five-millimeter thick using a SMI Fulker DiMet C/149B masonry and concrete saw. The average corallite diameter of the coral samples is five-millimeters therefore cutting the coral to this thickness is important to better detect differences in skeletal density bands by radiographs. If the slabs are too thick the differences in skeletal density do not show as well. The fossil coral slabs were taken to the San Antonio Hospital in Mayagüez for radiographs with Ivette Roche. Scleractinian corals deposit a high density (HD) band and a low density (LD) band within the interval of one year (Brachert et al., 2006). The linear extension differences of these seasonal variations in density that produce bands were used to measure growth rates.

Radiographs taken of the coral slabs were scanned to produce images and analyzed in a program called Coral XDS (Helmle et al., 2002). This program detects relative changes in luminosity as a proxy to discern between the high and low-density bands in the image and then measure their extension (see Figure 5). Appendix 2 contains the coral growth rate data and transects from all corals in this study. High density bands are brighter than low density bands because HD bands allow less x-rays to pass through and underexpose the film. The length of HD and LD bands are known as couplets and are interpreted as one year of skeletal growth meaning the annual growth can be determined by Coral XDS measurements. Average growth rates for the whole coral was calculated using equation 1. These HD and LD bands can possess a relationship to the SST obtained from $\delta^{18}O$ and Sr/Ca analysis. Aragonite from HD bands is expected to show higher SST values then aragonite sampled from low density bands. Coral radiographies were also taken after the corals were sampled for geochemical analysis. These radiographies were used to

determine if the geochemical samples were taken from an HD or LD band. Density band analysis is also essential to assign ages to geochemical samples by coupling the density band information with uranium thorium geochronometry.

Many corals in the Cañada Honda paleo reef exhibit foliations which are interpreted to be caused by high but periodic sedimentation (Hubbard et al., 2008). The present climate in the Enriquillo Valley is characterized by very dry conditions seasonally interrupted by intense, flash rains typical of a desert region. Assuming, climate conditions in the mid-Holocene were similar, these foliations could have been caused by high sedimentation events (Hubbard et al., 2008). Corals M2 140.7-0.7b and M2 136.3-1.1 show well defined foliations. The extension of each foliation was determined by measuring the HD and LD bands related to that foliation then dividing by the number of couplets for the sedimentation rate (see Equation 2). Many studies present sedimentation rates as mg/cm^2*d. Assuming the sediment was 100% calcite (density 2.71mg/cm^3) the sedimentation rates are converted to mg/cm^2*d using equation 3.

Equation 1. $Growth\ rate = \frac{annual\ extension\ in\ mm/yr}{number\ of\ years}$

Equation 2. $Sedimentation\ rate = \frac{Foliation\ extention\ (mm)}{number\ of\ couplets\ (yr)}$

Equation 3. $Sedimentation\ rate\ \left(\frac{mg}{cm^2 \times d}\right) = Sed.rate\ \left(\frac{cm}{d}\right) \times sed.density\left(\frac{mg}{cm^3}\right)$

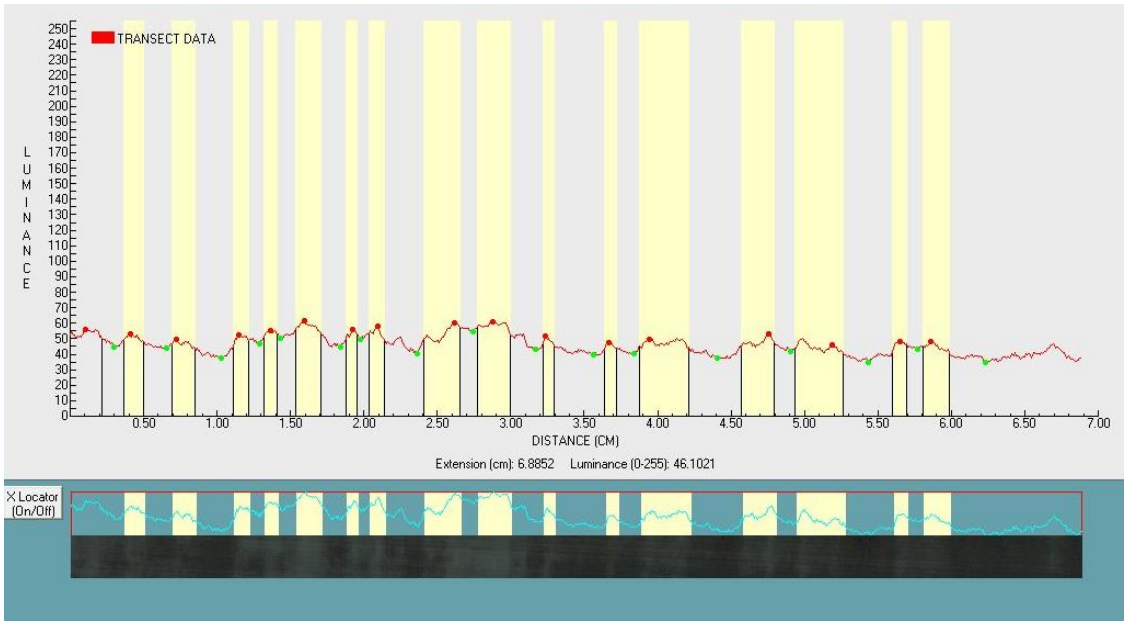

Figure 5. Luminance transect showing high density band delimiters (yellow) on a coral radiograph transect image (sample shown M2 140.7-0.7).

2.2.2 Preservation of Samples

A mineralogical analysis was done to verify the sample integrity and determine that the coral has not been altered. This is necessary due to the high susceptibility of aragonite in both early marine and vadose environment to suffer from diagenetic processes which will alter the geochemical signature of the coral (Sayani et al., 2011). The UPRM Geology Department's Siemens X-Ray Diffractometer (XRD) D500 was used to verify the mineralogy of the coral is still 100% aragonite (see Figure 6 for the XRD spectra expected from aragonite). Aragonite diffraction data published by the American Mineralogist Crystal Structure Database indicates that the highest intensity peaks should be located at the following 2 theta positions: 26.24, 45.9, 27.25, 33.16, 37.92, 48.36, 52.51, and 50.28. Calcite highest intensity peaks should be located at the following 2 theta positions: 29.42, 39.44, 48.54, 47.54, 43.19, and 36. Note that both aragonite and calcite have high intensity peaks close to 37, 42, and 48. Therefore, the high

intensity peak locations at 29.42 and 39.44 will be used to detect the presence of calcite. The detection limit for calcite concentrations is 1–2% (Reuter et al., 2005).

Since XRD analysis only can verify mineralogy the Scanning Electron Microscopy (SEM) was necessary to determine if secondary aragonite was present (See Figure 7 for an example of corals with and without secondary aragonite). Secondary aragonite produced by early marine diagenesis can produce values of SSTs that are incorrect (Quinn and Taylor, 2006). SEM analysis were conducted at the University of Puerto Rico at Mayaguez Biology Department with José Almodovar. 5mm cubes were cut from coral samples for SEM analysis. Samples were taken adjacent to the sampling transects used for geochemical analysis.

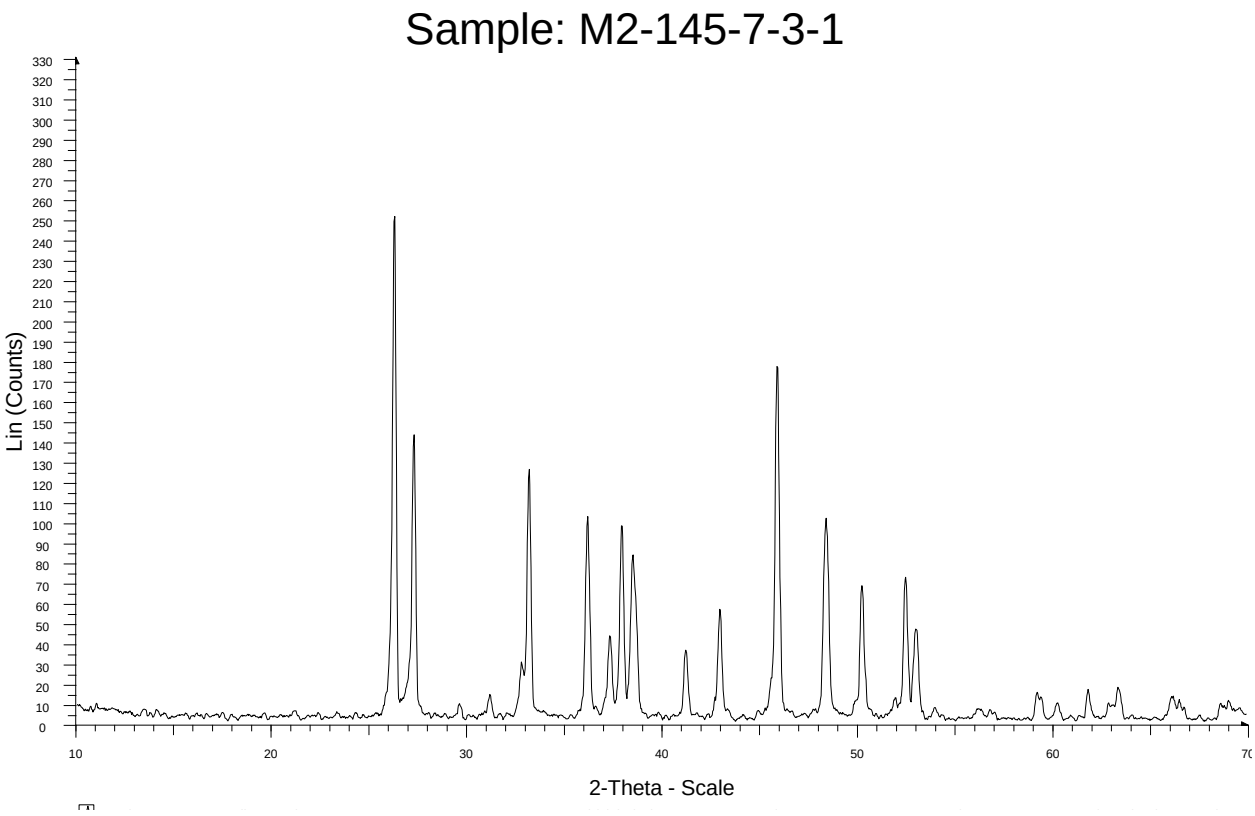

Figure 6. XRD spectra fossil coral aragonite (sample shown M2 145.7-3.1). Note the double peak at 26 and 27 2-theta a defining trait of aragonite XRD spectra.

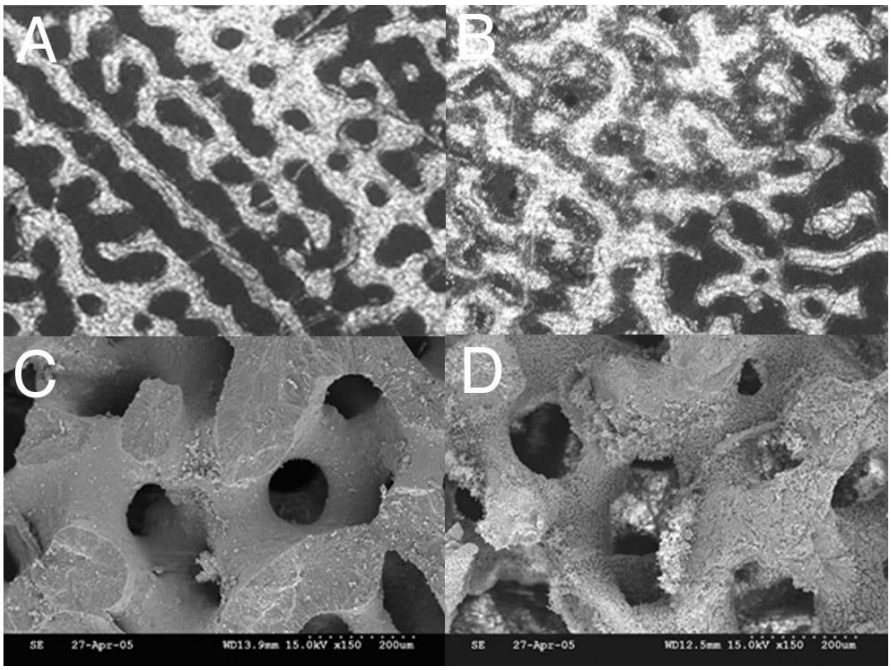

Figure 7. Comparison of an unaltered and altered *Porites sp.* coral from Papua New Guinea. Images (A) and (B) are thin section images and (C) and (D) are SEM images (Quinn and Taylor, 2006).

2.2.3 Paleoenvironmental Analysis

2.2.3.1 Fossil Coral Dating

Uranium Thorium (U/Th) geochronometry of four coral samples (M2-140.7-0.7, M2-120.5-0.5, M2-136.3-1.1, M2-145.7-3.1) was conducted at Rosenstiel School of Marine and Atmospheric Science (RSMAS), in Miami Florida. Four samples were collected from the base of each coral slab. The Neptune Isotope Laboratory (NIL) at RSMAS contains a Thermo-Fisher Neptune Plus, high performance Multi-Collector Inductively Coupled Plasma Mass Spectrometer (MC-ICP-MS) which was used for the U/Th analysis. Areas that show sedimentation in the interstices of the skeleton, bio-erosion, dissolution or any other alteration to the original physical or chemical integrity of the coral were avoided when collecting the sample.

Relative age of each coral was estimated using the corals with U/Th geochronometry ages and stratigraphic position (See Figure 19 from section 3.4). For example, coral M2 148-0.6

is in a lower stratigraphic position and located closer to the paleo shore than M2140.7-0.7a suggesting it is older than M2140.7-0.7a. Corals in order of oldest to youngest are as follows: M2 148-0.6, M2 140.7-0.7a, M2 140.7-0.7b, M2 150.7-1.3, M2 120.5-0.5, M2 140.0-0.8, M2 120.4-1.5, M2 134.4-1.2, M2 136.3-1.1, M2 144.8-3.1, and M2 145.7-3.1. Accretion rates were also estimated using methods cited by Hubbard et al. (2009) where accretion rates are equal to the vertical distance (ΔD) between two corals divided by the age difference (Δt) (See Equation 4.)

Equation 4. $Accretion\ rate = \frac{\Delta D}{\Delta t}$

The paleodepth of the four corals dated in this study was calculated using the vertical difference between the elevation of the sample and sea level at the time it grew the paleodepth of the coral. This same method was previously used in the M2 facies by Cuevas (2010). This study used the corrected Lighty et al. (1982) sea level curve by Hubbard et al., (2005) to determine paleodepth (See Figure 29 and 31).

2.2.3.2 Paleothermometer Sample Preparation

Using the coral radiographs as a baseline the coral growth bands were micro-sampled with a Micromeritics Micromill with a 1mm drill bit at the University of Puerto Rico. Samples traversed the corallite between two parallel thecal walls at a continuous 1 mm sampling interval parallel to the axis of primary growth, a method which does not influence original stable isotope composition of the coral skeleton (Gill et al.,1995) (See Figure 8). Powders obtained were split for Sr/Ca ratio and $\delta^{18}O$ isotopic analyses. Powders were carefully collected and weighted using a Mettler UMT2 Micro-balance consecutively for both stable isotope analysis with sample weights

between 350-500μg and Sr/Ca ratio analysis with sample weights between 1000-3000 μg. This sampling method constructed a geochemical record with sub-annual resolution.

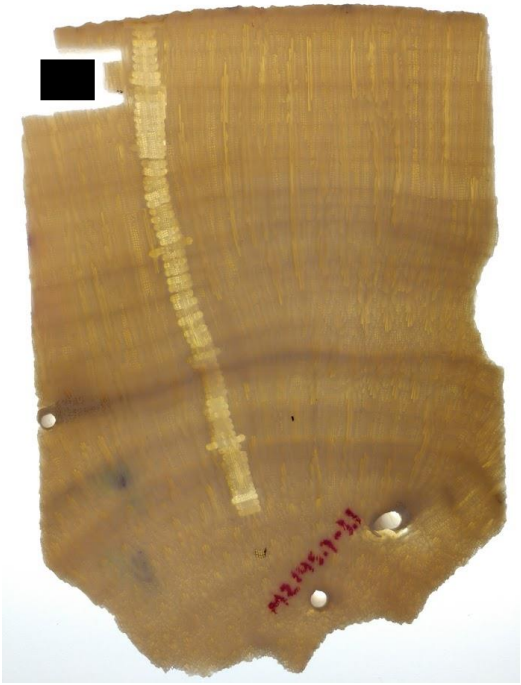

Figure 8. Image of coral M2 145.7-3.1 on a light table to show the sampling method used in this study to obtain powders for Sr/Ca ratio and $\delta^{18}O$ isotopic analyses. The black rectangle shows where the sample was taken for SEM analysis.

2.2.3.3 Stable Isotope Analysis

$\delta^{18}O$ and $\delta^{13}C$ isotopic values were analyzed using an IsoPrime JB079 Micromass Gas source isotope ratio Mass Spectrometer (MS) with a gas precision of 0.1‰ and linearity of 0.3 ‰ and NBS-19 as a standard in the UPRM Geology Department. NBS-19 standard is defined by the values -2.2 for $\delta^{18}O$ and 1.95 $\delta^{13}C$ therefore the standard error from these analyses were used to determine instrumentation error. Instrumentation error was used for error bars in the stable isotope graphs (See Table 3).

Table 3. Calculated error for stable isotope analyses. Count refers to the number of times the NBS-19 standard was run alongside the coral samples.

Coral Sample	Analysis	Count	Mean (‰)	Standard Deviation (‰)	Standard Error (‰)
M2 120.5-0.5	$\delta^{13}C$	17	1.93	0.080	0.019
	$\delta^{18}O$	17	-2.20	0.070	0.017
M2 140.7-0.7b	$\delta^{13}C$	18	1.95	0.058	0.014
	$\delta^{18}O$	18	-2.20	0.096	0.023
M2 140.7-0.7a	$\delta^{13}C$	20	1.96	0.053	0.012
	$\delta^{18}O$	20	-2.19	0.136	0.030
M2 140.0-0.8	$\delta^{13}C$	16	1.94	0.052	0.013
	$\delta^{18}O$	16	-2.20	0.055	0.014
M2 136.3-1.1	$\delta^{13}C$	27	1.95	0.043	0.008
	$\delta^{18}O$	27	-2.20	0.046	0.009
M2 134.4-1.2	$\delta^{13}C$	7	1.95	0.034	0.013
	$\delta^{18}O$	7	-2.24	0.065	0.024
M2 120.4-1.5	$\delta^{13}C$	12	1.95	0.043	0.012
	$\delta^{18}O$	12	-2.20	0.078	0.023
M2 144.8-3.1	$\delta^{13}C$	12	1.95	0.038	0.011
	$\delta^{18}O$	12	-2.20	0.054	0.016
M2 145.7-3.1	$\delta^{13}C$	17	1.96	0.055	0.013
	$\delta^{18}O$	17	-2.20	0.064	0.016

2.2.3.4 Sr/Ca Ratios Analysis

Powder samples for Sr/Ca analysis were selected by analyzing the peaks and valleys of the oxygen isotope records (See Figures 1 and 2 in Appendix 6). Sr/Ca ratios were measured at Rosenstiel School of Marine and Atmospheric Science (RSMAS), in Miami Florida in the NIL laboratory. Thirty powder samples were dissolved in 3 mL of 0.45M HNO3 and diluted by a factor of 80 and then directly analyzed by peak-jumping mode on the ThermoFisher Neptune Plus, high performance Multi-Collector Inductively Coupled Plasma Mass Spectrometer (MC-ICP-MS) using standard-sample bracketing technique for elemental concentrations and Sr/Ca ratios. Standard deviation of the standard dilution was used to determine instrumental error.

2.2.3.5 $\delta^{18}O$ derived Sea Surface Temperature

SSTs were calculated from $\delta^{18}O$ isotopic values using the same method as the study by Greer and Swart (2006) for Enriquillo corals. The calibration between $\delta^{18}O$ and the obtained temperature by Leder et al. (1996) is shown in equation 5. $\delta^{18}O_w$ was assigned a value of zero keeping the oxygen isotope values of the water constant using the assumption that variations in $\delta^{18}O$ will attributed only to changes in temperature due to fractionation (Greer and Swart, 2006).

Equation 5. $SST = 5.33 – 4.519\ (\pm 19) * (\delta^{18}Oc - \delta^{18}Ow)$

2.2.3.6 Sr/Ca derived Sea Surface Temperature

Sr/Ca ratios are also used to calculate SSTs. The use of both $\delta^{18}O$ and Sr/Ca produces more reliable SST results (Grottoli, 2001). Calibration equations of Sr/Ca ratios to SSTs have been conducted in many studies from different locations and using different species of corals. Table 4 contains a list of all the Sr/Ca ratio calibrations to SST used to calculate Sr/Ca-SSTs in this study.

Table 4. Calibration equations of Sr/Ca ratios to SST.

Author	Location	Coral Species	Environment	Calibration
Jimenez, 2018	Barahona Bay, Dominican Republic	*Orbicella sp.* complex	Semi enclosed	Sr/Ca = 10.7867– 0.0676 * SST
Swart et al., 2002	Ball Buoy Reef, Southern Florida	*Orbicella annularis*	Small patch reef	Sr/Ca = 10.165 – 0.0471 * SST
Flannery and Poore, 2013	Pulaski Shoal, Dry Tortugas, Florida	*Orbicella faveolata*	Shoal, ~3 meters depth	Sr/Ca = 10.205 – 0.0392 * SST
Saenger et al. 2008 (1)	South shore reef, Bermuda	*Orbicella franksi*	Open-ocean, 13-m depth	Sr/Ca = 11.74 – 0.095 * SST
Saenger et al. 2008 (2)	St. Croix, U.S. Virgin Islands	*Orbicella faveolata*.	~ 1 meter depth	Sr/Ca = 10.98 – 0.077 * SST
Smith, 2006	Looe Key, Florida	*Orbicella faveolata*	4 meters depth	Sr/Ca = 9.962 – 0.0282 * SST

2.2.3.7 Residual $\delta^{18}O$ ($\Delta\delta^{18}O$)

It is known that there is not one δ^{18}Osw–SSS relationship in the world's oceans. There are multiple relationships depending on the latitude and the ocean basin considered (Bigg and Rohling, 2000). δ^{18}Osw–SSS relationship in the tropics varies because the isotopic composition of rainfall and river water is not constant (Benway and Mix, 2004). The residual $\delta^{18}O$ ($\Delta\delta^{18}O$) was calculated using the equation 5 (Gagan et al., 1998; Yu et al., 2005). In equation 6 $d\delta^{18}O$ /dT is the slope of the empirical δ^{18}O–SST relationship for this study. $T_{\delta 18O}$ and $T_{Sr/Ca}$ represent calculated SSTs based on the empirical δ^{18}O– and Sr/Ca–SST relationships, respectively.

Equation 6. $\Delta\delta^{18}O = \frac{d\delta^{18}O}{dT(℃)} \times (T_{\delta^{18}O} - T_{\frac{Sr}{Ca}})$

3 CHAPTER – RESULTS

3.1 Coral Skeleton Preservation

3.1.1 XRD Analysis

X-ray Diffraction analysis of all coral samples in this study was conducted and compared to the powder diffraction data of aragonite and calcite from the American Mineralogist Crystal Structure database (ID 0006302 and 0000098). The XRD result output show intensity counts in the Y-axis versus 2theta in the X-axis. Table 5 lists the peak locations and relative intensity used to identify the presence of aragonite and calcite in addition to the mineralogy analysis provided by the UPR-NSF Earth X-ray Analysis Center XRD technician. All coral samples (M2 120.5-0.5, M2140.7-0.7ab, M2 148-0.6, M2 140.0-0.8, M2 136.3-1.1, M2 134.4-1.2, M2 150.7-1.3, M2 120.4-1.5, M2144.8-3.1, and M2 145.7-3.1) analyzed in this study show only aragonite diffraction data peaks (See Figure 10). Sayani et al. (2011), conducted XRD analysis of mixtures of aragonite and calcite powders with known calcite to aragonite ratios and determined the detection limit of calcite was 1%. Reuter et al. (2005), also cited the detection limit of calcite as 1-2%. For comparison, Cañada Honda corals that show dissolution, sediment infilling the interstices, and surfaces where growth stopped and were later recolonized were sampled for XRD analysis as well. Figure 9 shows examples of these features. Coral M2 120.5-0.4 (located near the base of the M2 facies near the *Madracis* Layer) had intervals with and without sediment. All samples with sediment infilling the interstices of the coral exhibited a 10-20 count peak at 29° of 2theta which is the highest intensity peak angle expected for calcite. Smaller intensity peaks among the 2theta spectrum for calcite were not detected since they may be indistinguishable from the background signal. Figures 11 and 12 show XRD results of a section with and without sediment infilling the interstices of the coral. Coral sample M2 148-0.6 shows

sediment and dissolution features and produced an XRD where calcite was present. The coral sample M2 150.7-1.3 has a surface where growth was discontinuous (See Figure 9) and XRD analysis of this sample indicated it was composed of aragonite. XRD results from all corals can be found in Appendix 1.

Table 5. Published diffraction data for calcite and aragonite with 2theta peak locations and relative intensity. Data published by the American Mineralogist Crystal Structure database (ID 0006302 and 0000098).

Calcite		Aragonite	
2-Theta	Intensity	2-Theta	Intensity
29.42	100	26.24	100
39.44	20.16	45.9	72.67
48.54	20.02	27.24	56.69
47.54	19.67	33.16	53.24
43.19	14.26	37.92	41.57
36	13.71	48.36	31.96
		52.51	31.92
		50.28	30.28
		38.44	28.5
		36.14	28.46
		42.94	21.5
		38.65	19.57
		48.49	19.19

Figure 9. From left to right: Sample M2 150.7-1.3, M2 148-0.6, and M2 120.5-0.4. M2 150.7-1.3. Sample M2 150.7-1.3 shows a surface where growth was discontinuous. M2 148-0.6 shows signs

of dissolution and sediment inside coral interstices and M2 120.5-0.4 shows alternate layers with and without sediment inside coral interstices.

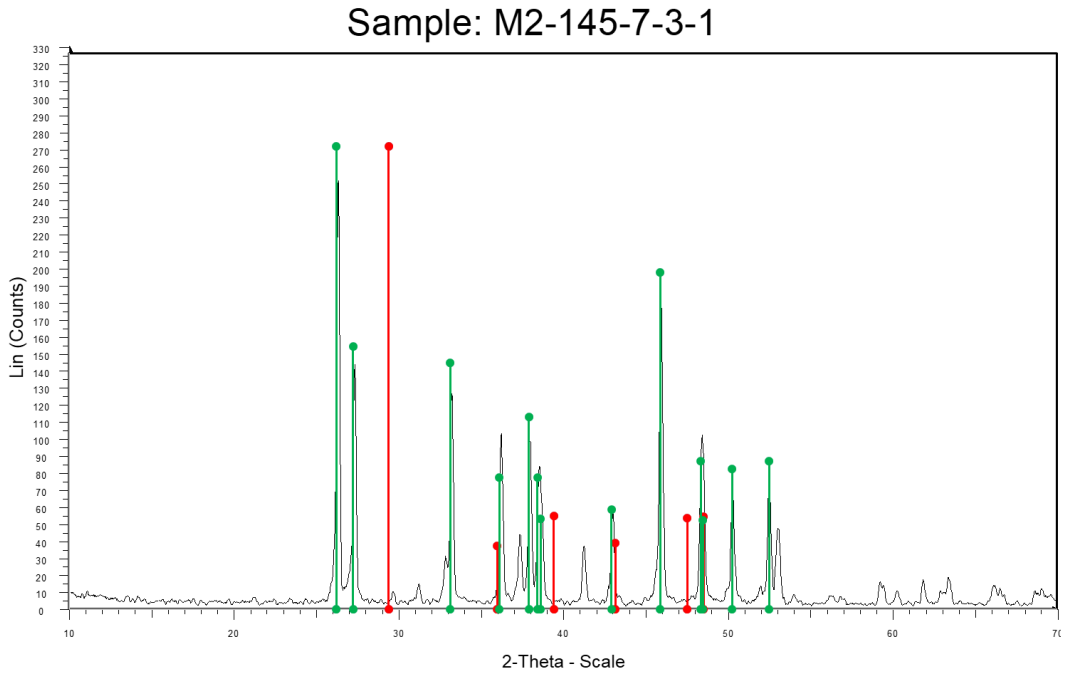

Figure 10. XRD diffractogram of a coral M2 145.7-3.1. Only aragonite was detected by XRD analysis. Green lines represent 2theta locations of aragonite peaks, and red lines correspond to calcite peaks. The detection limit for calcite is 1-2% (Sayani et al., 2011; Reuter et al., 2005).

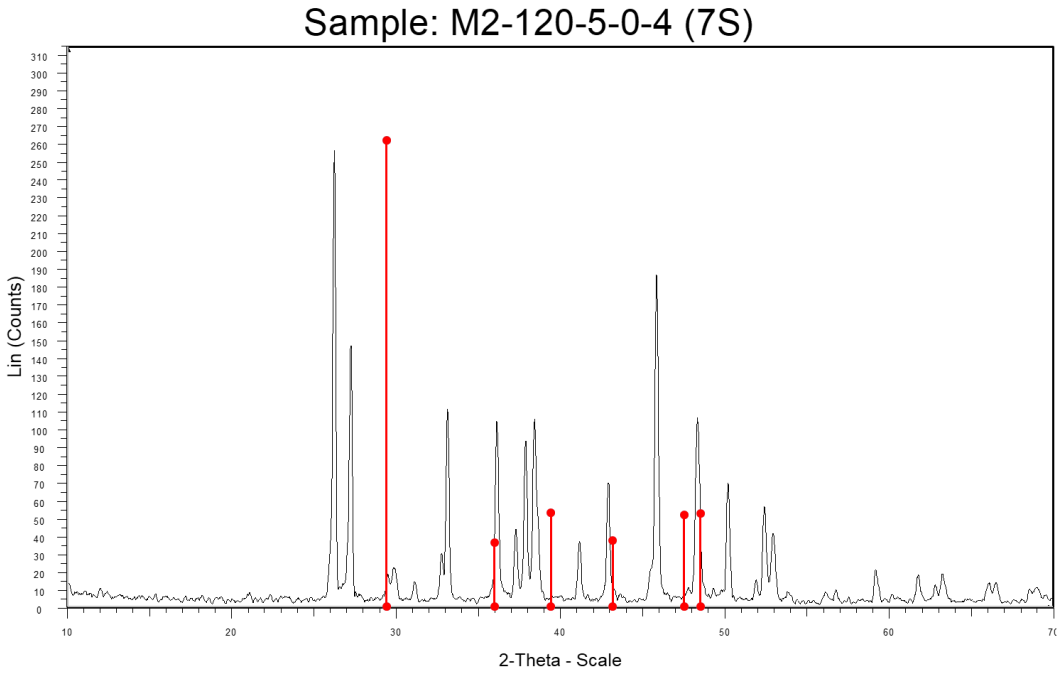

Figure 11. XRD diffractogram of coral M2 120.5-0.4. Sediment was identified within the structure of the coral. Note the ~20 count peak located at 29° 2theta. Red lines represent 2theta locations of major calcite peaks. The detection limit for calcite is 1-2% (Sayani et al., 2011; Reuter et al., 2005).

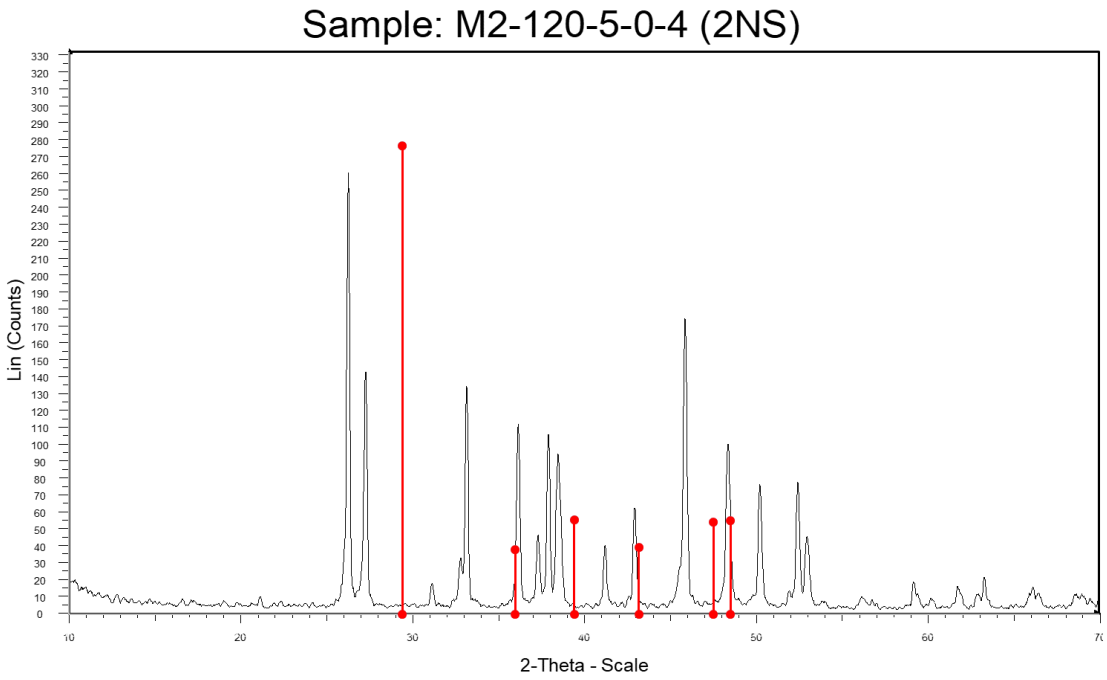

Figure 12. XRD diffractogram of a section of coral M2 120.5-0.4. This section of the coral did not show discontinuities, dissolution, or sediment in the coral structure. No calcite was detected in the analysis. Red lines represent 2theta locations of major calcite peaks. The detection limit for calcite is 1-2% (Sayani et al., 2011; Reuter et al., 2005).

3.1.2 SEM Analysis

Early marine diagenesis can cause problems in coral geochemical analysis as aragonite cement precipitated on the coral skeleton from marine water. Since corals are composed of aragonite, this secondary aragonite cannot be detected by XRD analysis. Eight coral samples (M2 140.7-0.7, M2 150.7-1.3, M2 140-0.8, M2 136.3-1.1, M2 145.7-3.1, M2 144.8-3.1, M2 120.4-1.5, and M2 120.5-0.5C) were inspected with a scanning electron microscope (SEM) to determine if secondary aragonite was present in the coral skeletons. Secondary aragonite takes the form of long and thin needles or fibers often in bundles (Hendy et al. 2007, Quinn and Taylor, 2006 and others). Figure 7 from Section 2.2.2 contains SEM figures from Quinn and Taylor (2006), showing an example of a pristine coral skeleton versus a coral that shows

secondary aragonite. Inspection of the images produced by the SEM from the corals M2 140.7-0.7, M2 150.7-1.3, M2 140-0.8, M2 136.3-1.1, M2 145.7-3.1, and M2 144.8-3.1 indicate there is no secondary aragonite present. Coral samples M2 120.4-1.5, and M2 120.5-0.5C, show a small amount of secondary aragonite (See Figures 13-14). Overall, secondary aragonite is not common or widespread.

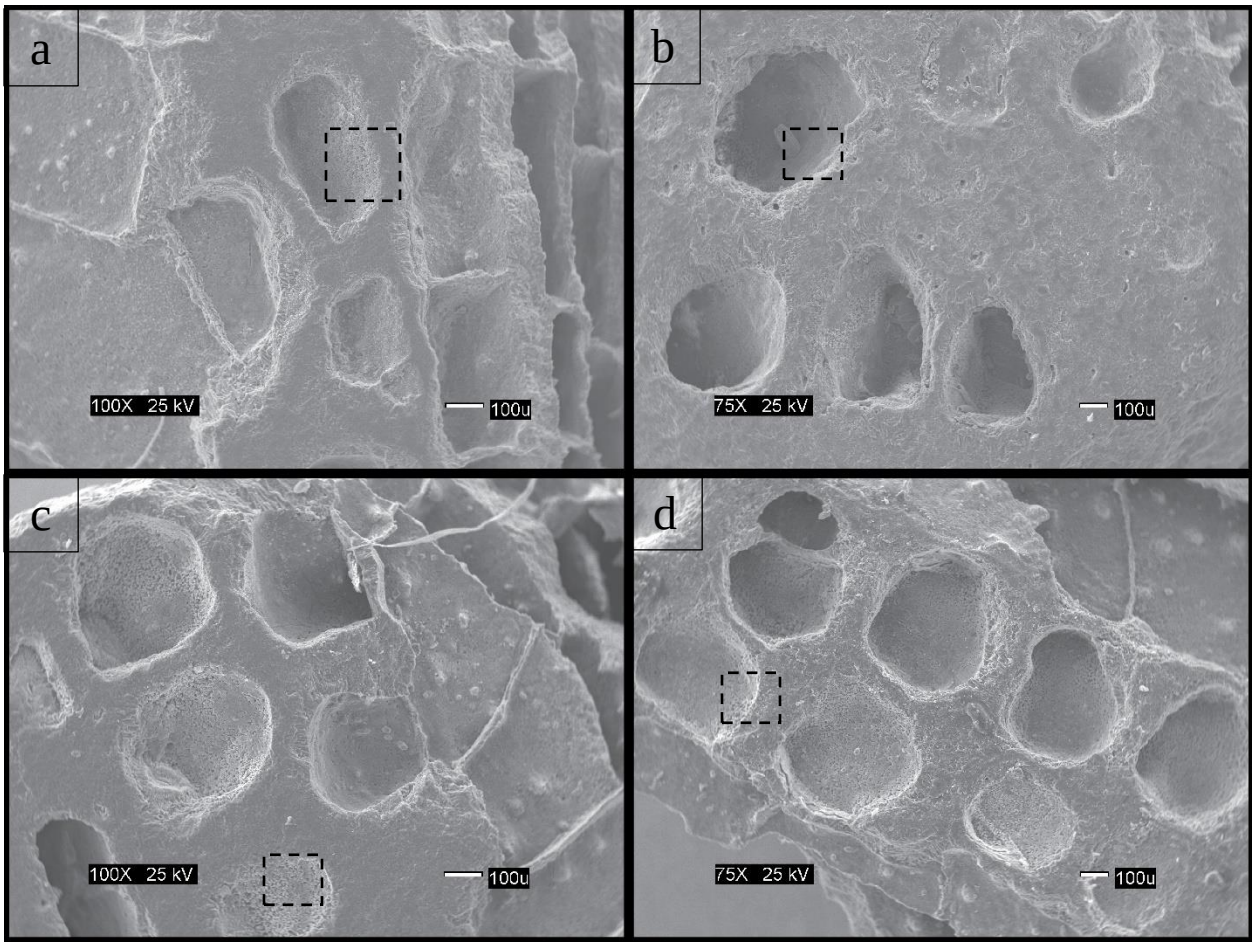

Figure 13. Continued below.

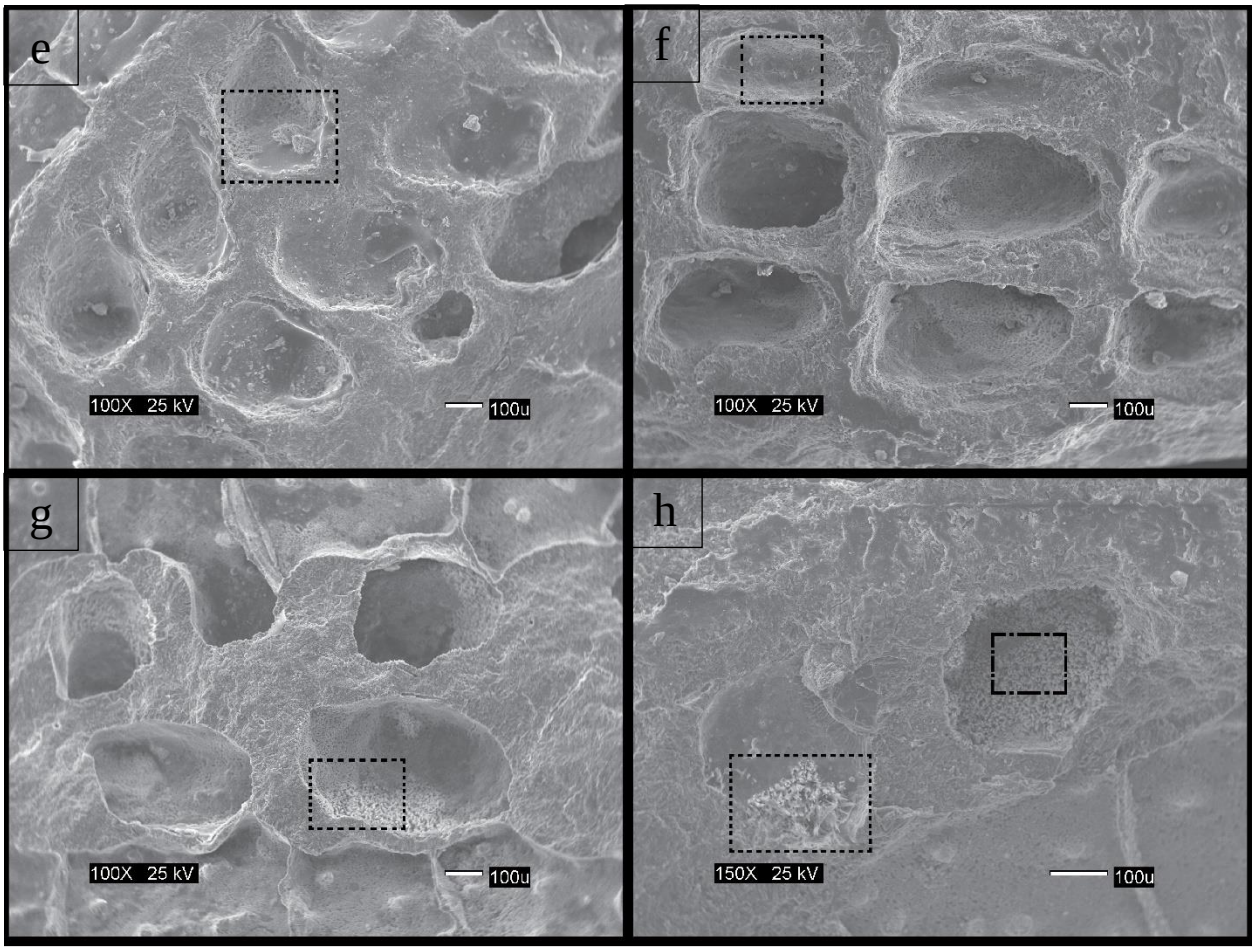

Figure 13. Coral thecal wall SEM images of corals (a) M2 140.7-0.7, (b) M2 150.7-1.3, (c) M2 140-0.8, (d) M2 136.3-1.1, (e) M2 145.7-3.1, (f) M2 144.8-3.1, (g) M2 120.4-1.5, and (h) M2 120.5-0.5C. Images suggest little presence of secondary aragonite precipitated over the previously formed coral surface (see h).

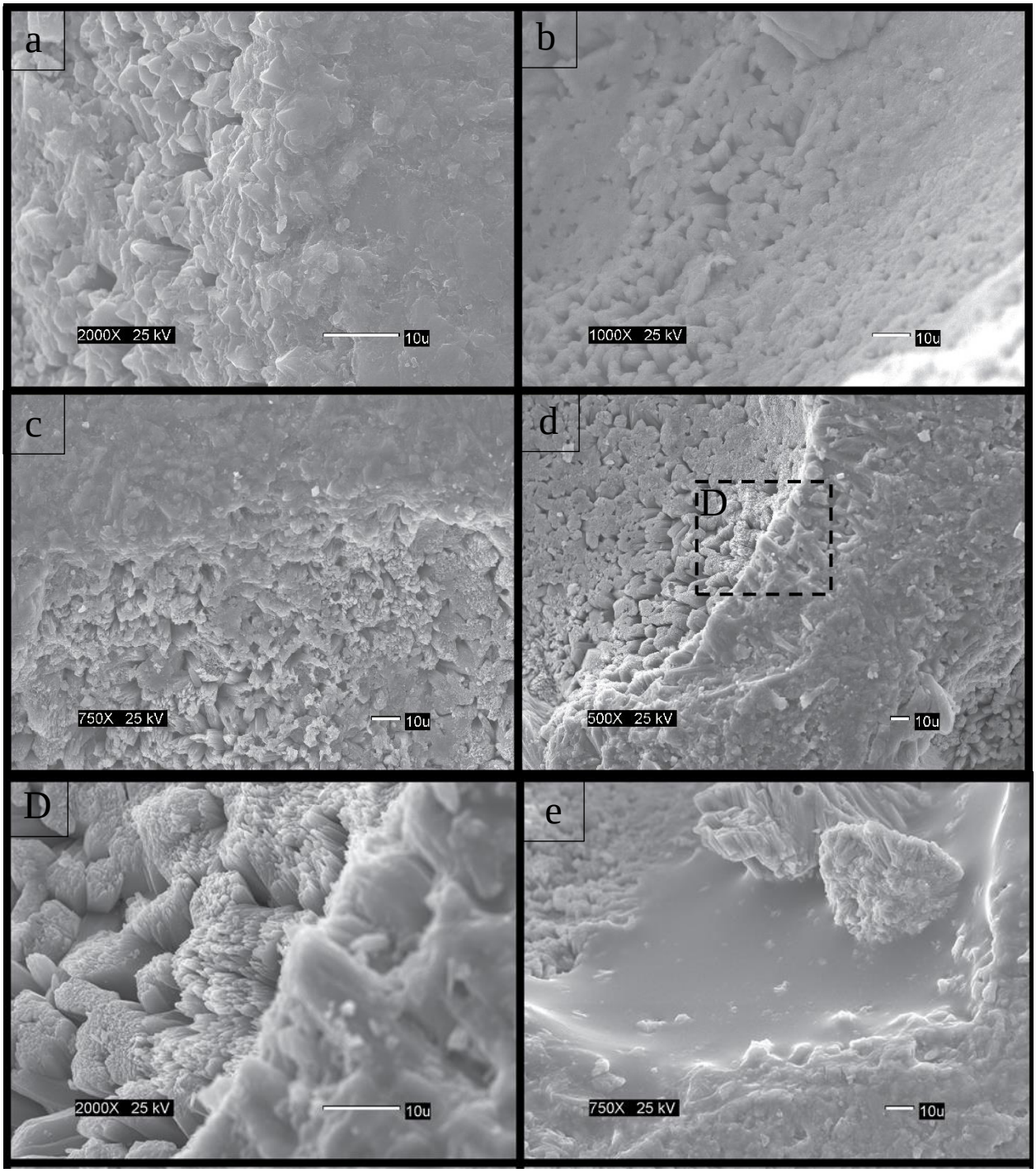

Figure 14. Continued below.

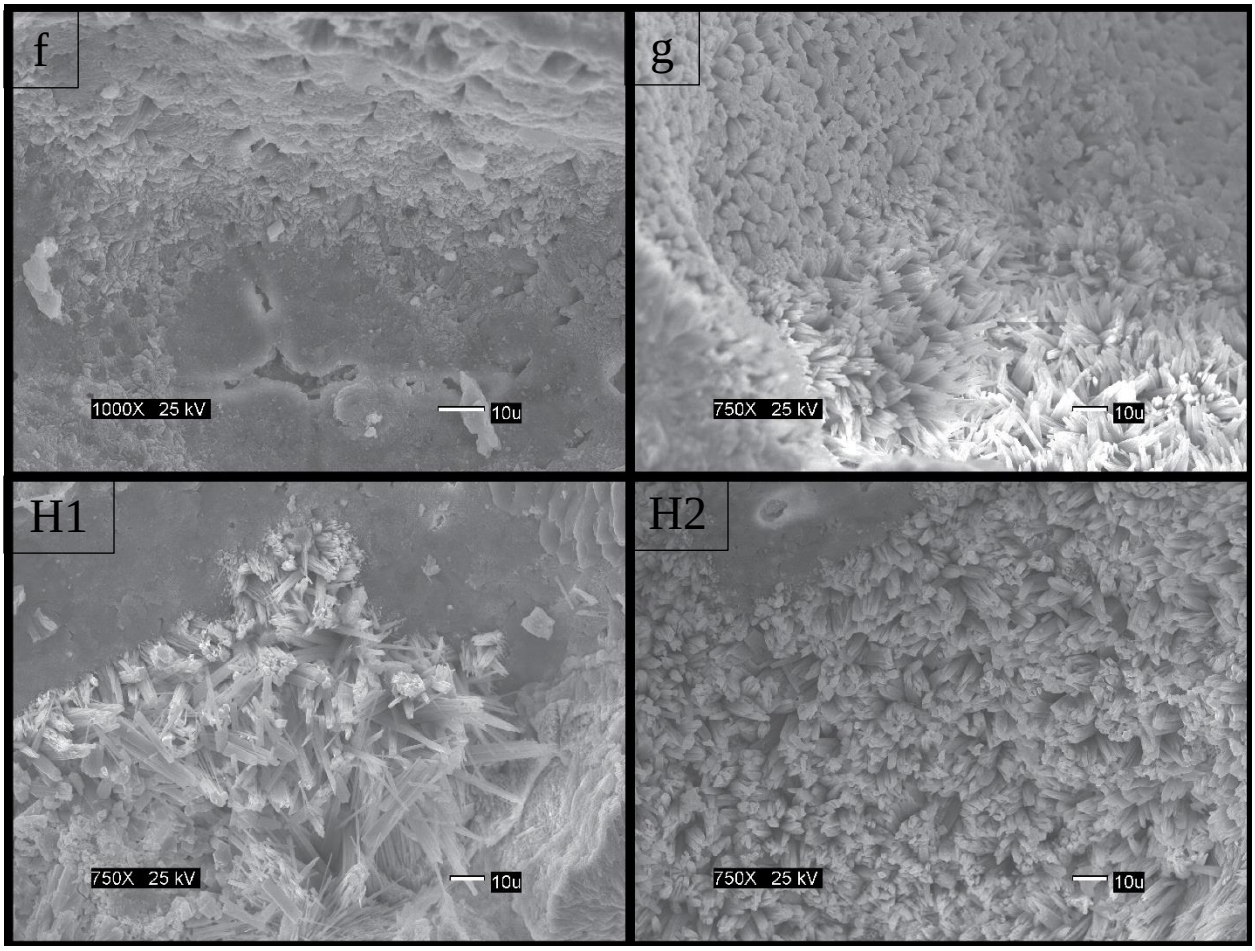

Figure 14. Amplified SEM images of corals corresponding to the plates in Figure 13. The following samples show an absence of secondary aragonite (long and thin needles or fibers) in the thecal wall, (a) M2 140.7-0.7, (b) M2 150.7-1.3, (c) M2 140-0.8, (d) M2 136.3-1.1, (D) is zoomed into the panel shown in (d) and shows the original aragonite precipitated by the coral, (e) M2 145.7-3.1, and (f) M2 144.8-3.1. Samples (g) M2 120.4-1.5, and (H1) M2 120.5-0.5C, show a small amount of secondary aragonite. Sample (H2) M2 120.5-0.5C shows short and blunt aragonite bundles precipitated by the coral.

3.1.3 Modern and Fossil Coral Stable Isotope Analysis

Another assessment to test for diagenetic alteration is the comparison of stable isotope analysis to values expected for modern corals. Milliman (1974) published stable isotope fields for Quaternary carbonate sediments. Oxygen and carbon isotope ratios from all corals analyzed in this study (M2 120.5-0.5, M2140.7-0.7a, M2 140.7-0.7b, M2 140.0-0.8, M2 136.3-1.1, M2134.4-1.2, M2 120.4-1.5, M2144.8-3.1, and M2 145.7-3.1) were plotted relative to these

published values (See Figure 15). The corals exhibit a similar range of $\delta^{13}C$ compared to modern corals. The $\delta^{18}O$ values of the Cañada Honda corals analyzed in this study are 1-2‰ heavier than the values expected for coral skeletons precipitated in open marine waters. Several explanations are possible to account for this 1-2‰ heavier $\delta^{18}O$ value relative to Milliman (1974) data and they will be evaluated in the discussion section.

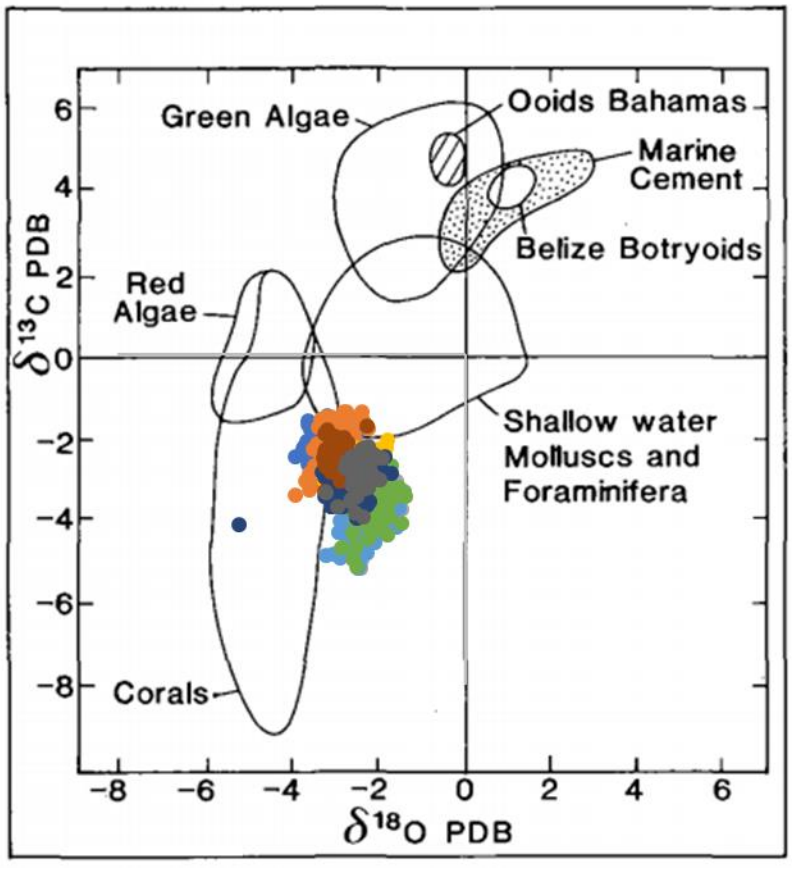

Figure 15. Oxygen and carbon isotope ratios from all corals analyzed in this study (M2 120.5-0.5, M2140.7-0.7a, M2 140.7-0.7b, M2 140.0-0.8, M2 136.3-1.1, M2134.4-1.2, M2 120.4-1.5, M2144.8-3.1, and M2 145.7-3.1) compared to Milliman (1974) compilation of oxygen and carbon isotope ratios of corals and other marine organisms in Quaternary carbonate sediments. Error bars not visible.

3.2 Coral Growth Rates

Coral growth rates were measured for M2 facies coral samples M2 148-0.6, M2140.7-0.7a, M2 140.7-0.7b, M2 150.7-1.3, M2 120.5-0.5, M2 140.0-0.8, M2134.4-1.2, M2 136.3-1.1, M2144.8-3.1, and M2 145.7-3.1. These results are presented as box plots (See Figure 16) to show the variability of the results. The average growth rates for all corals range from 2.38±0.3 to 5.44±0.43 mm/yr and the overall average coral growth rate was 4.53±0.2 mm/yr. Growth rates from corals in other studies at the Cañada Honda paleo-reef exposure and this study are plotted on Figure 17 and summarized on Table 6. The average growth rate for all corals from this and other studies of the M2 facies is 3.13±1.28 mm/yr and ranges from 5.44 to 1.30 mm/yr. Appendix 2 contains the coral growth rate transects from corals in this study. All coral growth rate data and sources from Cañada Honda Facies is in Appendix 3.

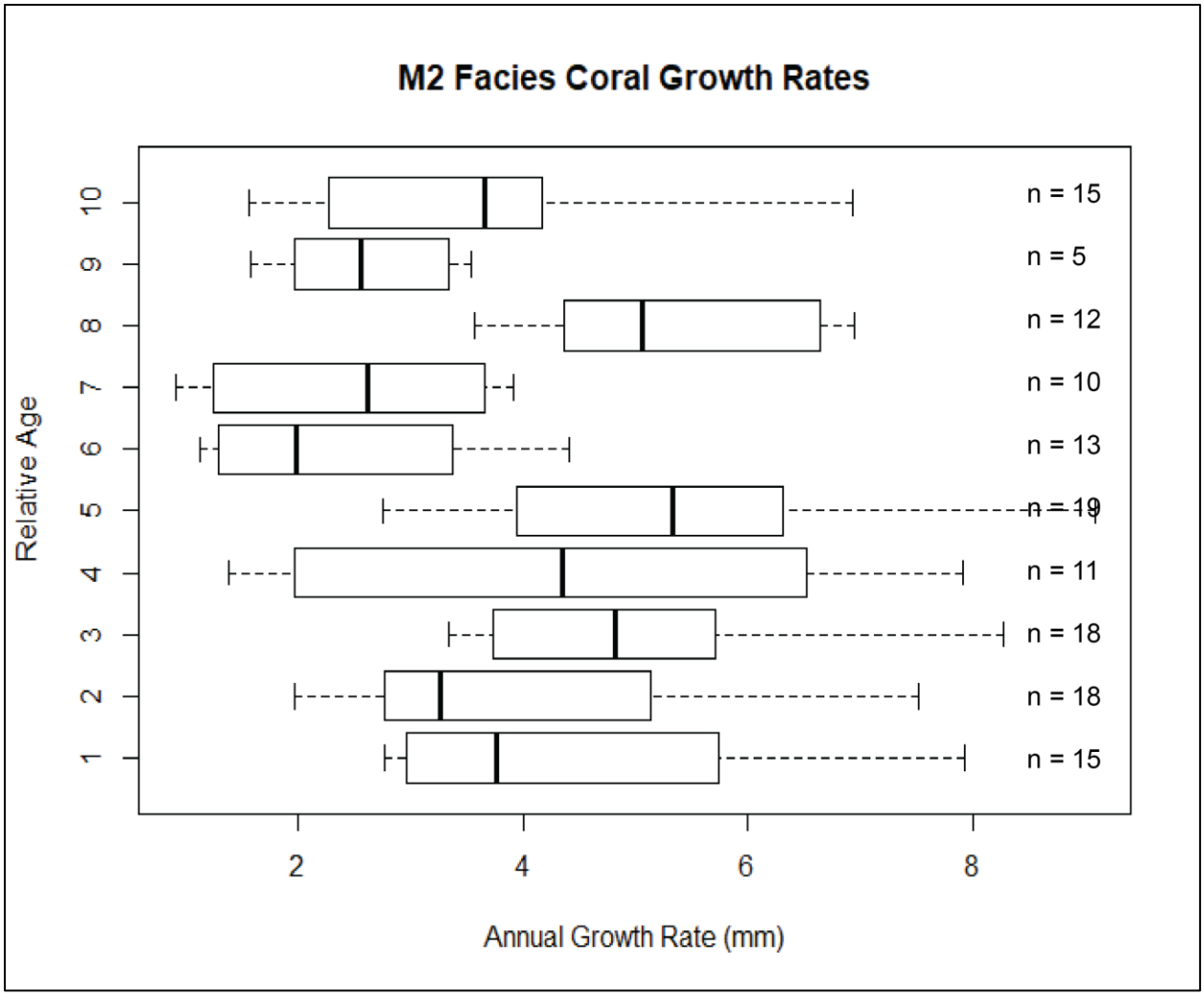

Figure 16. Coral growth rates versus relative age (relative age described in the methods section 2.2.3.1). Corals in order from 1 to 10: M2 148-0.6, M2140.7-0.7a, M2 140.7-0.7b, M2 150.7-1.3, M2 120.5-0.5, M2 140.0-0.8, M2134.4-1.2, M2 136.3-1.1, M2144.8-3.1, and M2 145.7-3.1. The number of samples (n=x) is equal to the number of years (HD and LD band couplets) measured in each coral to calculate growth rate quartile statistics displayed as boxplots. Coral growth rate data used in this chart is in Appendix 8.

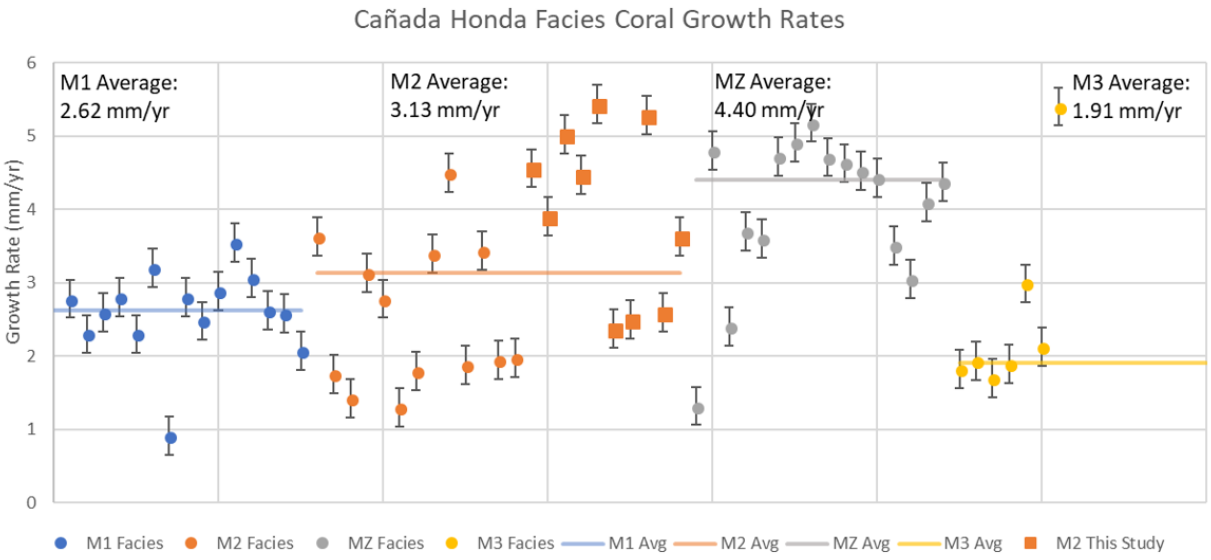

Figure 17. Compilation of average coral growth rates from all Cañada Honda facies. Lines for each facies represent the average for each facies. All coral growth rate data and sources used in this chart is in Appendix 3. Data collected from: Diaz (2005), Cuevas et al. (2005), Cuevas (2010), Morales (2015), Arana (2018), Jimenez (2018), Rodriguez (2018), and this study.

Table 6. Average coral growth rates available for each facies of Cañada Honda, including corals measured in this study. All data used to calculate these averages is in Appendix 3.

	Cañada Honda Average Coral Growth Rates by Facies			
All units are mm/yr	Average Growth Rate	Growth Rate Error (stdv)	Maximum Growth Rate	Minimum Growth Rate
M1 Facies	2.62	0.60	3.55	0.91
M2 Facies	3.13	1.28	5.44	1.30
MZ Facies	4.40	1.03	5.18	1.32
M3 Facies	1.91	0.47	5.40	1.70

3.3 Sedimentation Rates

Two of the corals (M2 140.7-0.7b and M2 136.3-1.1) for this study displayed exaggerated foliations that were used to calculate sedimentation rates. The average sedimentation rate from coral M2 140.7-0.7 is 0.59 mm/yr (n=1) and for coral M2 136.3-1.1is 0.99 mm/yr (n=2) therefore the average sedimentation rate produced by the two samples analyzed is 0.79± 0.2 mm/yr or 0.000218 cm/day. Most studies that work on this theme present sedimentation rates as mg/cm^2*d. Following the assumption that the sediment was 100% calcite, the sedimentation

rate (cm/d) is multiplied by the density of calcite (2.71mg/cm^3) and indicates the average sedimentation rate in the M2 facies was 0.6 mg/cm^2*d. See methods section 2.2.1 for a description of how sedimentation rates were derived. Figure 18 shows M2 140.7-0.7b an example of a coral foliation used to determine sedimentation rates and the resulting transect data. Appendix 4. contains the coral radiographies and transects worked for the sedimentation rate analysis from coral M2 136.3-1.1.

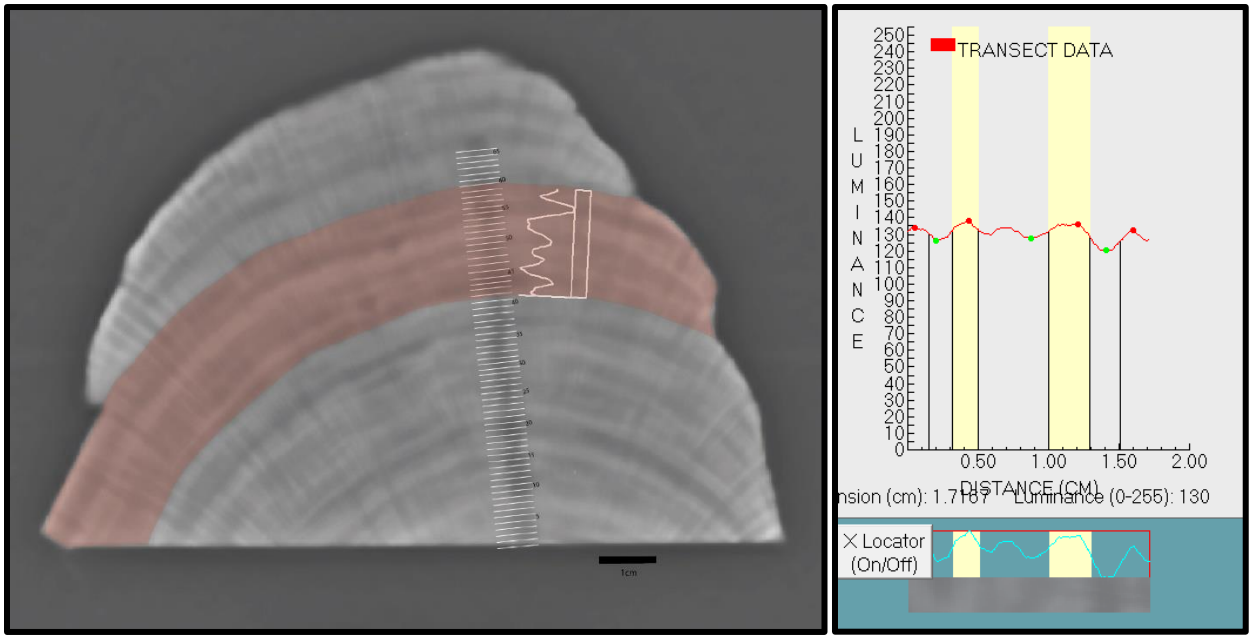

Figure 18. Radiography of the coral sample M2 140.7-0.7b showing coral foliation measured and the transect data. The red shadow shows the foliation used to calculate the sedimentation rate.

3.4 Coral U/Th Dates

Four corals were selected for U/Th geochronometry (M2-140.7-0.7, M2-120.5-0.5, M2-136.3-1.1, M2-145.7-3.1). Ages for the corals analyzed from the M2 facies are 7,518±46, 7,440±46, 7,047±57, and 5,944±28 ybp (See Table 7). Jimenez (2018) proposed the M2 facies is as old as 8,166±35 ybp based on coral M2 146.7-0.7. Corals M2 120.5-0.5 and M2 140.7-0.7

dated from this study are located at similar stratigraphic heights (See Figure 19) however they exhibit a trend where corals located towards the north of the exposure (towards the paleo shore) are older. Morales (2015) reported this trend in the massive 1 (M1) facies. Coral U/Th dates are younger in higher locations along the stratigraphy of the reef, as expected (See Table 8 that lists all the age data available for Cañada Honda facies). $\delta^{234}U$ values were also calculated in this study from 234U/238U activity ratios measured during the dating process. They have an average of 139.4 ± 2.2‰ (See Table 7). Coral ages and vertical distances were used to estimate reef accretion rates. The average accretion rate is 1.3 ± 0.2 m/ky (See Figure 19 and methods section 2.2.3.1). According to Figure 29 (See methods section 2.2.3.1), coral M2-140.7-0.7 (7,518±46) grew at a paleodepth of 17±1 meters below paleo-sea level, M2-120.5-0.5 (7440±46) grew at a paleodepth of 18±1 meters below paleo-sea level, M2-136.3-1.1 (7047±57) grew at a paleodepth of 19±1 meters below paleo-sea level, and M2-145.7-3.1(5944±28) grew at a paleodepth of 20±1 meters below paleo-sea level.

Table 7. Corals dated from the M2 Facies listed with corrected ages and 234U/238U listed with 95% confidence intervals. The $\delta^{234}U$ values are calculated with the formula $\delta^{234}U = ((234U/238U) - 1) * 1000$ (Himmler et al., 2016).

Sample Name	Corrected Age	± 95% CI	Activity ratio 234U/238U initial	± 95% CI	$\delta^{234}U$(‰) ±2.2
M2-120.5-0.5	7440	46	1.136038794	0.003	136.039
M2-136.3-1.1	7047	57	1.138666224	0.004	138.666
M2-140.7-0.7	7518	46	1.137090441	0.003	137.090
M2-145.7-3.1	5944	28	1.145595707	0.004	145.596

Table 8. Cañada Honda paleo-reef ages from all studies. Table includes the dating method, name of the coral specimen dated, age, and source.

Cañada Honda Paleo-Reef Ages				
Facies	Type of dating	Specimen dated	Age	Source
Massive-3	U/Th	*O. faveolata*	5199±26	Rodriguez 2018 (unpublished)
	U/Th	*O. faveolata*	6427±81	Rodriguez 2018 (unpublished)
	U/Th	*O. faveolata*	5690±29	Jimenez, 2018 (unpublished)
	U/Th	*O. faveolata*	5702±30	Jimenez, 2018 (unpublished)
Mixed	U/Th	*O. faveolata*	5152±30	Arana, 2018 (unpublished)
	U/Th	*O. faveolata*	5545±62	Arana, 2018 (unpublished)
	U/Th	*O. faveolata*	6694±48	Arana, 2018 (unpublished)
	U/Th	*O. faveolata*	6833±31	Arana, 2018 (unpublished)
	U/Th	*O. faveolata*	6521±32	Jimenez, 2018 (unpublished)
	U/Th	*O. faveolata*	6694±48	Jimenez, 2018 (unpublished)
	Radiocarbon	*O. faveolata*	7705±106	Cuevas, 2010
	Radiocarbon	*S. siderea*	7465±83	Cuevas, 2010
	Radiocarbon	*O. faveolata*	6736.5±94.5	Cuevas, 2010
	Radiocarbon	*Coral*	6200	Taylor et al., 1984
Massive 2	U/Th	*O. faveolata*	5944±28	This study
	U/Th	*O. faveolata*	7047±57	This study
	U/Th	*O. faveolata*	7440±46	This study
	U/Th	*O. faveolata*	7518±46	This study
	U/Th	*O. faveolata*	8166±35	Jimenez, 2018 (unpublished)
	Radiocarbon	Coral	6500	Taylor et al., 1984
	Radiocarbon	*S. siderea*	7846±97	Cuevas, 2010
	Radiocarbon	*O. faveolata*	7882.5±99.5	Cuevas, 2010
Mad. Layer	Radiocarbon	*Madracis sp.*	9400-9000	Hubbard, 2008
Massive 1	U/Th	*O. faveolata*	8233±24	Morales, 2015 (unpublished)
	U/Th	*O. faveolata*	8036±26	Morales, 2015 (unpublished)
	U/Th	*O. faveolata*	8047±27	Morales, 2015 (unpublished)
	U/Th	*O. faveolata*	8353±25	Morales, 2015 (unpublished)
	U/Th	*O. faveolata*	8365±24	Morales, 2015 (unpublished)
	U/Th	*O. faveolata*	8910±28	Morales, 2015 (unpublished)
	Radiocarbon	*S. siderea*	8628±165	Cuevas, 2010
	Radiocarbon	*O. faveolata*	9256±137	Cuevas, 2010
	Radiocarbon	Coral	8400	Hubbard et al., 2004
	Radiocarbon	Coral	8400	Hubbard et al., 2004
	Radiocarbon	Coral	8700	Hubbard et al., 2004
	Radiocarbon	Coral	8900	Hubbard et al., 2004
	Radiocarbon	Coral	8600	Taylor et al., 1984
Mollusk	Radiocarbon	Mollusk	9800	Taylor et al., 1984

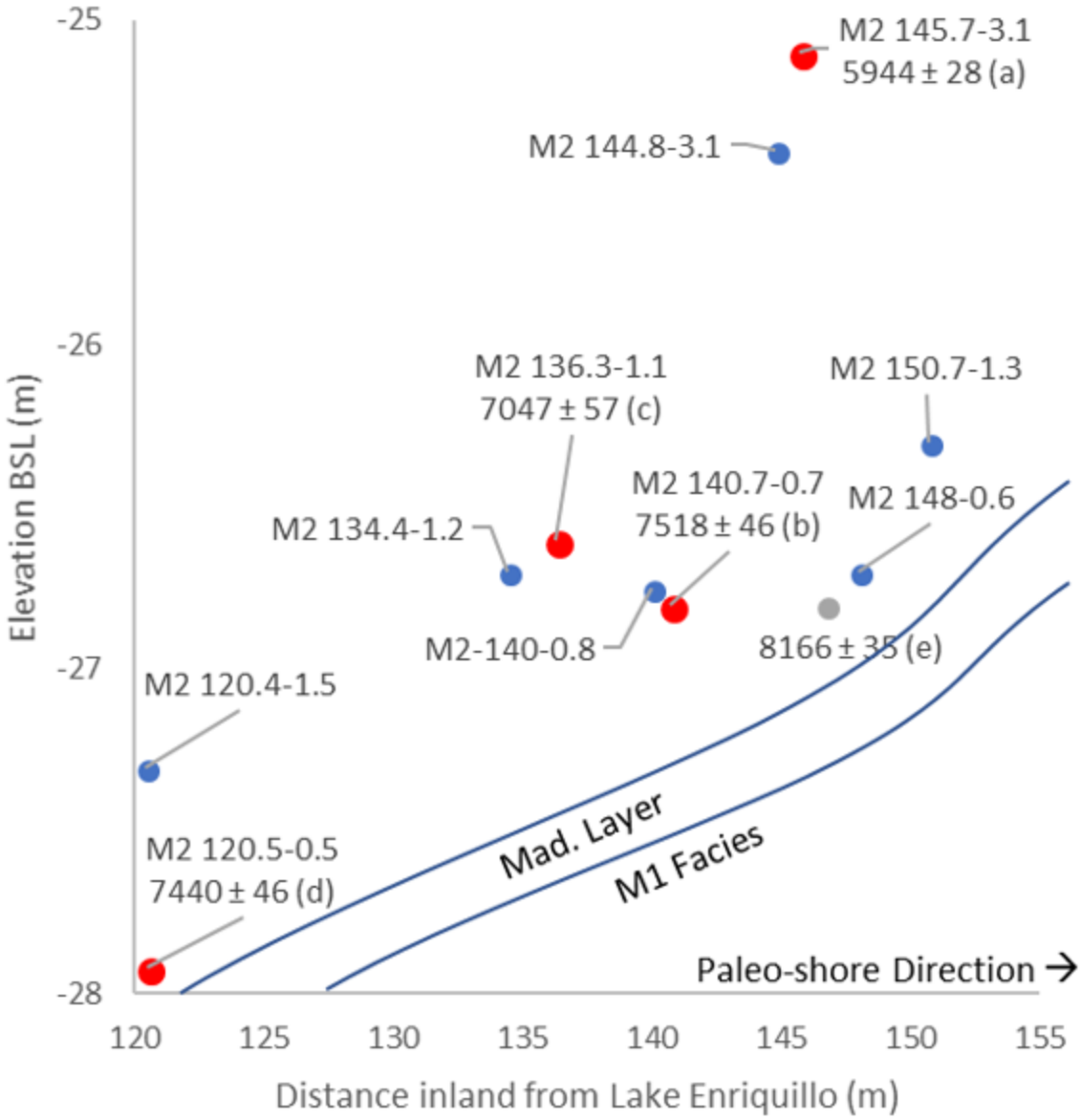

Figure 19. Corals and their stratigraphic positions and ages. The *Madracis* Layer is a storm layer composed primarily of *Madracis sp.* corals which separates the M1 and M2 facies. Corals with ages are (a) M2-145.7-3.1 (b) M2-140.7-0.7a (c) M2-136.3-1.1 (d) M2-120.5-0.5 (e) M2-146.7-0.7 (Jimenez, 2018). Corals that were not dated are labeled with their sample name. The Y-Axis is the elevation of the coral sample below modern sea level. The X-Axis is the distance in meters from the coast of Lake Enriquillo as of 2004. This figure was used to determine relative age of each coral sample (relative age described in the methods section 2.2.3.1).

3.5 Stable Isotope and Trace Element Analysis

Ten corals were sampled for stable isotope. Two of the corals were chosen for trace element analysis based on $\delta^{18}O$ results. Sr/Ca ratios, $\delta^{18}O$, and $\delta^{13}C$ values from the samples M2140.7-0.7b and M2145.7-3.1 are plotted with estimated ages in Figure 21. Table 9 lists the values, standard error, and range of the Sr/Ca ratios, $\delta^{18}O$, and $\delta^{13}C$ for each coral from youngest to oldest according to relative age (relative age described in the methods section 2.2.3.1). According to Swart et al. (2002), heavier $\delta^{18}O$ values and higher Sr/Ca ratios correspond to lower temperatures. The $\delta^{18}O$ values for all corals analyzed in this study range from -1.37 to -3.9‰ with an outlier of -5.19‰. The mean $\delta^{18}O$ value for all coral samples analyzed is -3.05±0.02‰. $\delta^{13}C$ values for all corals analyzed range from -1.41 to -5.18‰ with a mean of -2.29±0.01‰. The correlation coefficient between $\delta^{18}O$ and $\delta^{13}C$ values is r=0.47. Figure 20 shows the $\delta^{18}O$ and $\delta^{13}C$ values from all corals in order of their relative age with their individual correlation coefficients. Note the shift to higher $\delta^{13}C$ values and lower $\delta^{18}O$ values after coral M2 140.0-0.8. Sr/Ca ratios from corals M2140.7-0.7b and M2145.7-3.1 range from 9.13 to 9.60 mmol/mol with a mean of 9.36±0.02 mmol/mol.

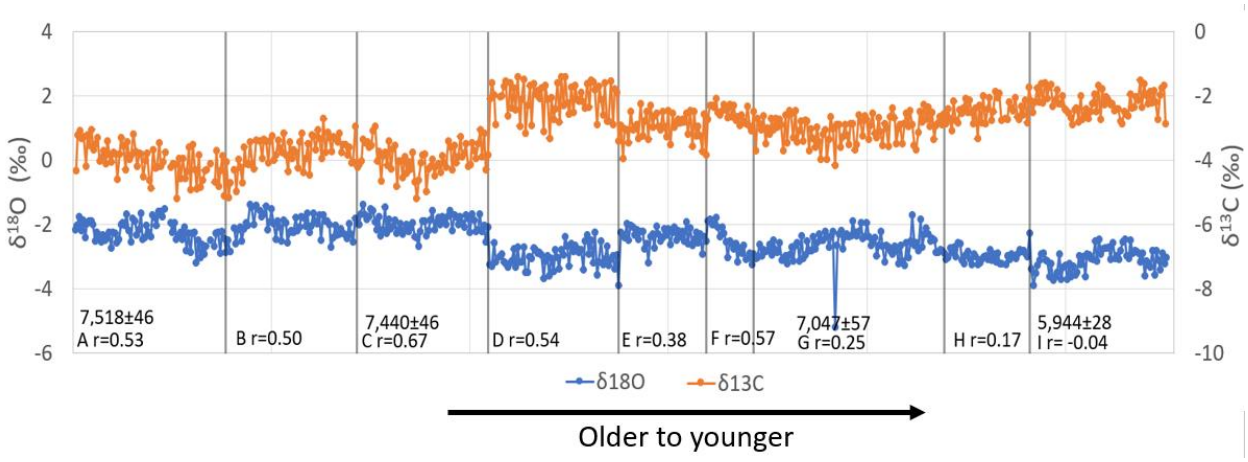

Figure 20. Coral $\delta^{18}O$ and $\delta^{13}C$ ratios based on their relative age (oldest to youngest) with their individual correlation coefficients (r=x). Relative age described in the methods section 2.2.3.1.

Letters indicate the coral sample (A) M2 140.7-0.7a, (B) M2 140.7-0.7b, (C) M2 120.5-0.5, (D) M2 140.0-0.8, (E) M2 120.4-1.5, (F) M2 134.4-1.2, (G) M2 136.3-1.1, (H) M2 144.8-3.1, and (I) M2 145.7-3.1. $\delta^{18}O$ values are plotted on the Y-axis to the left and $\delta^{13}C$ values are plotted on the Y-axis to the right. The grey lines separate each coral and thus is not a continuous record. Standard error for $\delta^{13}C$ is 0.013‰ and $\delta^{18}O$ is 0.019‰ (not visible on the chart).

Table 9. The $\delta^{18}O$, $\delta^{13}C$, and Sr/Ca ratios range, average and standard deviation of the geochemical analysis of every coral analyzed in this study.

Coral Sample	Geochem Analysis	Maximum	Minimum	Average	Standard deviation
M2 145.7-3.1	δ13C (‰)	-1.51	-2.88	-2.23	0.36
	δ18O (‰)	-2.46	-3.90	-3.11	0.34
	Sr/Ca (mmol/mol)	9.59	9.23	9.42	0.09
M2 144.8-3.1	δ13C (‰)	-1.74	-9.46	-2.93	1.75
	δ18O (‰)	-2.27	-5.07	-3.10	0.53
M2 136.3-1.1	δ13C (‰)	-2.26	-4.15	-3.03	0.40
	δ18O (‰)	-1.70	-5.19	-2.65	0.42
M2 134.4-1.2	δ13C (‰)	-2.08	-3.09	-2.56	0.25
	δ18O (‰)	-1.79	-3.24	-2.54	0.44
M2 120.4-1.5	δ13C (‰)	-2.25	-9.40	-3.36	1.62
	δ18O (‰)	-1.92	-5.03	-2.53	0.69
M2 140.0-0.8	δ13C (‰)	-1.41	-3.41	-2.14	0.53
	δ18O (‰)	-2.23	-3.90	-3.01	0.34
M2 120.5-0.5	δ13C (‰)	-2.95	-5.18	-3.93	0.46
	δ18O (‰)	-1.39	-2.67	-1.98	0.27
M2 140.7-0.7b	δ13C (‰)	-2.70	-5.17	-3.74	0.49
	δ18O (‰)	-1.37	-2.85	-2.05	0.33
	Sr/Ca (mmol/mol)	9.42	9.13	9.30	0.08
M2 140.7-0.7a	δ13C (‰)	-3.05	-5.18	-4.00	0.50
	δ18O (‰)	-1.52	-3.18	-2.25	0.36

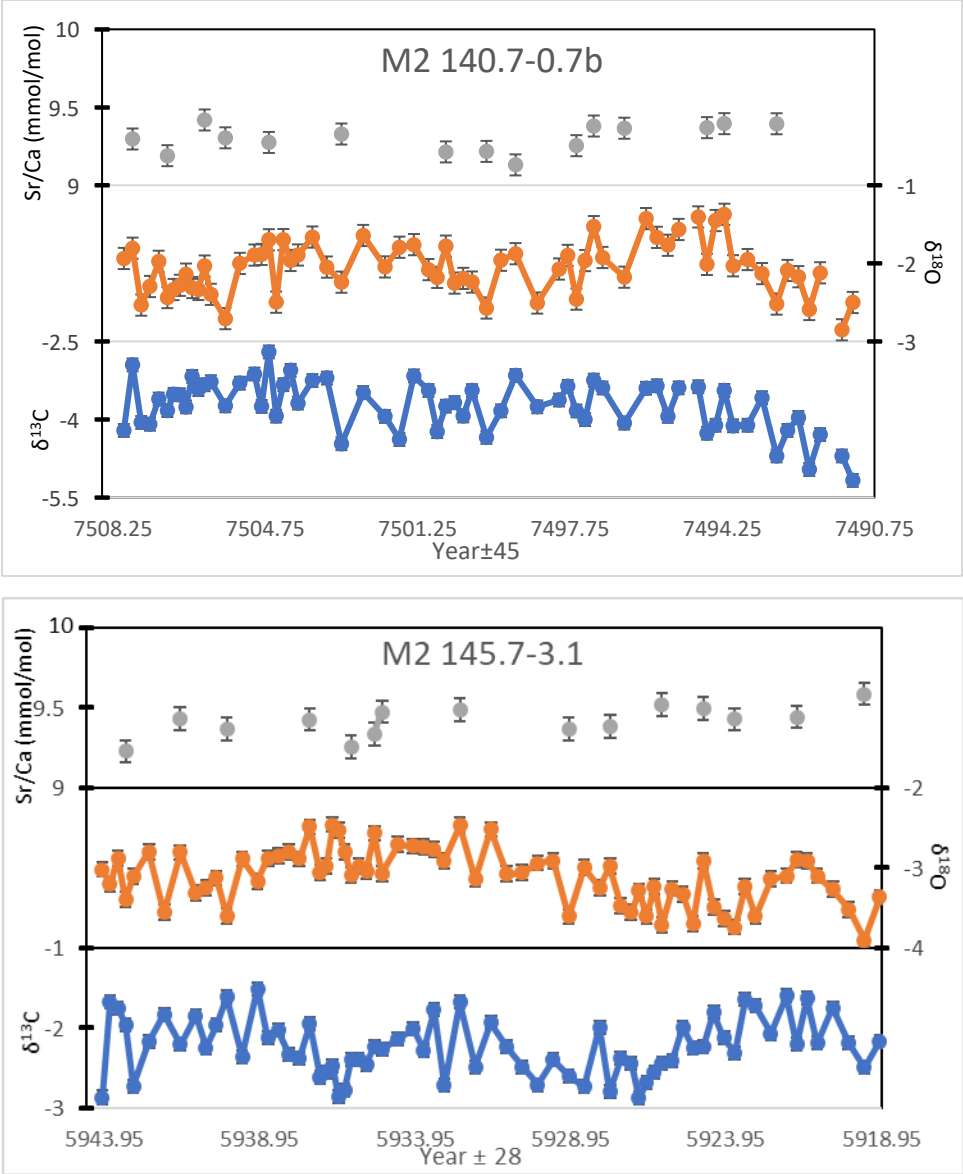

Figure 21. Sr/Ca ratios, $\delta^{18}O$, and $\delta^{13}C$ values from corals M2-140.7-0.7b (7508±46) and M2-145.7-3.1 (5944±28).

3.5.1 Oxygen Isotope Cyclicity

Oxygen isotope records and high low-density bands from four corals (M2-140.7-0.7, M2-120.5-0.5, M2-136.3-1.1, M2-145.7-3.1) were analyzed for cyclicity. One high and low-density band (HD-LD Bands) are equivalent to one year of growth. Plots of $\delta^{18}O$ over radiographies or charts showing HD-LD bands display the number of samples taken per year. Coral sample M2-

140.7-0.7 has 66 samples taken over 16 years. Thus, there is 4.13 samples per year. This information can also be used to measure cyclicity. The oxygen isotope records show annual and multi-annual variability. The length of multi-annual variability can be inferred by the number of years between two peaks. Cycles in coral sample M2-140.7-0.7 are approximately 8 years in length. Table 10 lists the cyclicity for each coral sample. Figures 22-25 show plots of HD-LD bands and $\delta^{18}O$ records used to determine cyclicity.

Table 10. Coral samples analyzed for cyclicity, their age, number of years sampled, number of samples taken for geochemical analysis, the number of samples that represent one year, and the length of cycles in each coral.

Sample Name	Corrected Age	± 95% CI	Years	Sample Count	Samples/yr	Cycle Length (yrs)
M2-140.7-0.7	7518	46	16	66	4.13	8
M2-120.5-0.5	7440	46	13	66	5.08	8
M2-136.3-1.1	7047	57	21	96	4.57	10
M2-145.7-3.1	5944	28	25	69	2.76	12

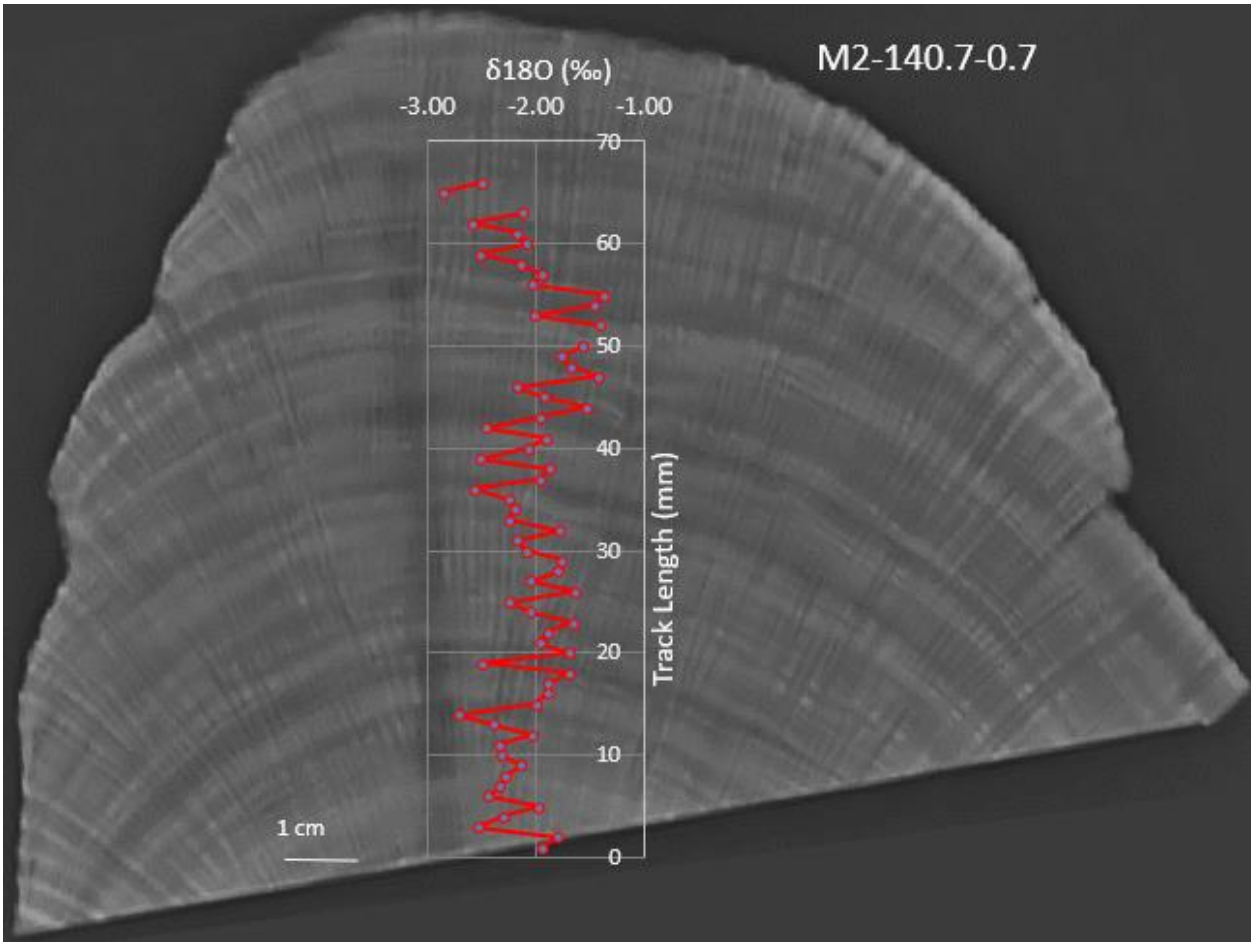

Figure 22. $\delta^{18}O$ and radiography of coral sample M2 140.7-0.7b (7508±46).

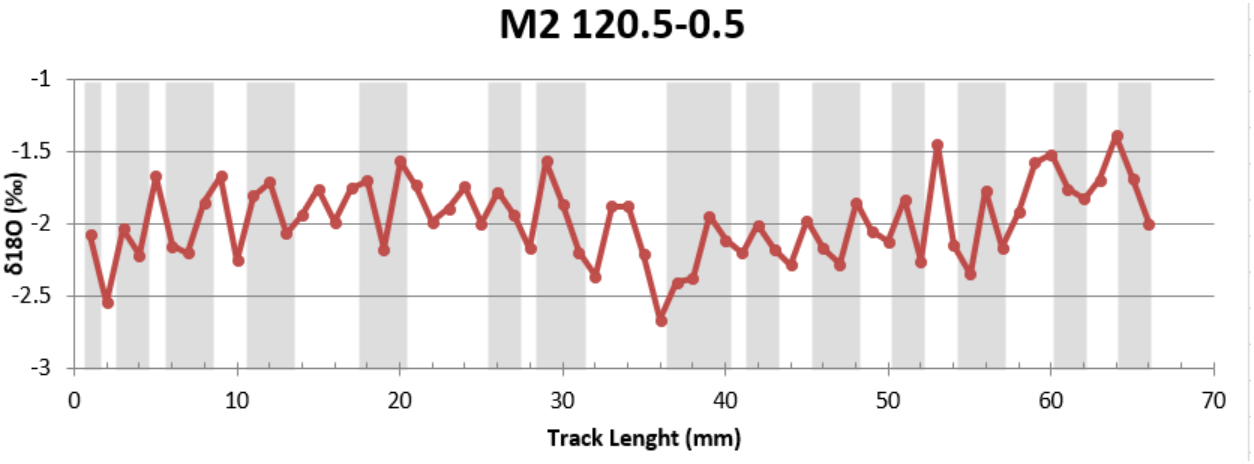

Figure 23. $\delta^{18}O$ and HD-LD bands of coral sample M2 120.5-0.5 (7440±46). Grey sections represent HD bands and white sections represent LD bands.

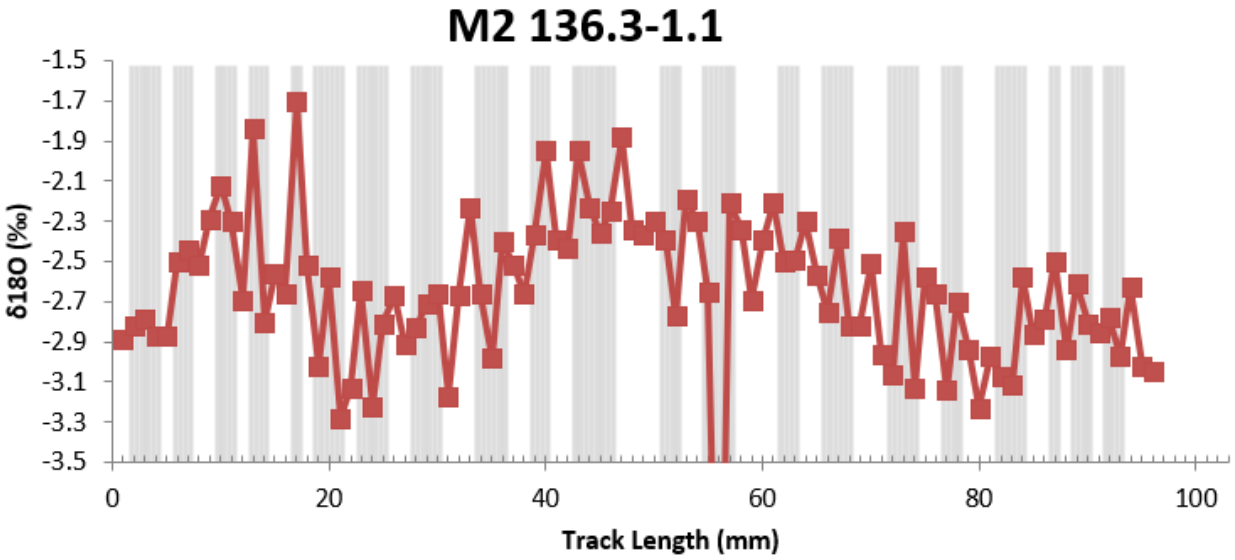

Figure 24. $\delta^{18}O$ and HD-LD bands of coral sample M2 136.3-1.1 (77047±57). Grey sections represent HD bands and white sections represent LD bands.

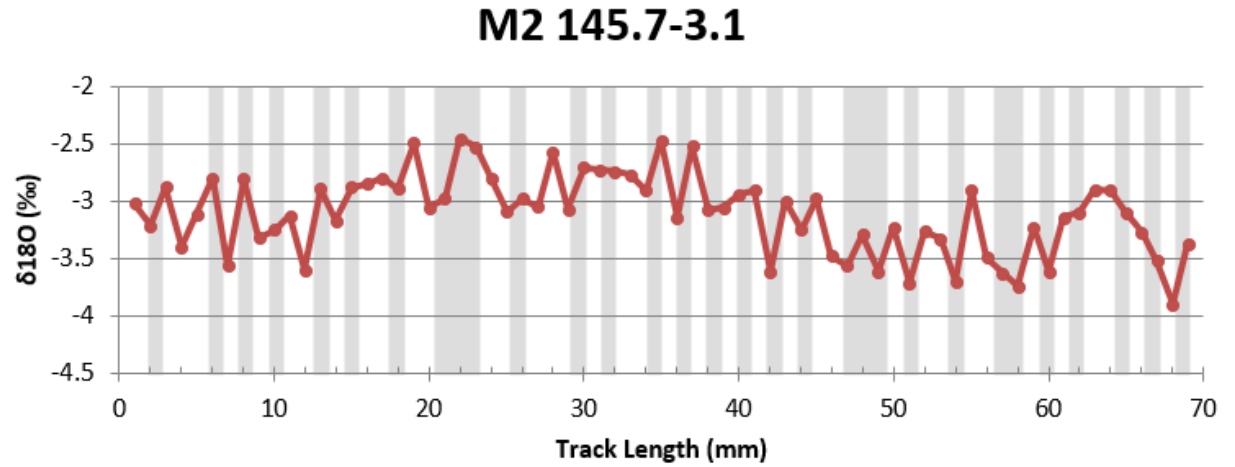

Figure 25. $\delta^{18}O$ and HD-LD bands of coral sample M2-145.7-3.1 (5944±28). Grey sections represent HD bands and white sections represent LD bands.

3.6 δ^{18}O-SST

Sea surface temperatures were calculated from both δ^{18}O and Sr/Ca values. The δ^{18}O derived SST were calculated using the equation derived by Leder et al. (1996) and are plotted in Figure 26. δ^{18}O derived sea surface temperatures (δ^{18}O-SST) from all the corals (M2 140.7-0.7a, M2 140.7-0.7b, M2 120.5-0.5, M2 140.0-0.8, M2 120.4-1.5, M2 134.4-1.2, M2 136.3-1.1, M2 144.8-3.1, and M2 145.7-3.1) in this study range from 7 to 28°C with an average of 16°C and standard deviation of 2.8. Table 11 shows the δ^{18}O-SST maximum, minimum, average, and standard deviation for corals M2 140.7-0.7 and M2 145.7-3.1. Sr/Ca-SSTs are also listed in Table 11 for comparison.

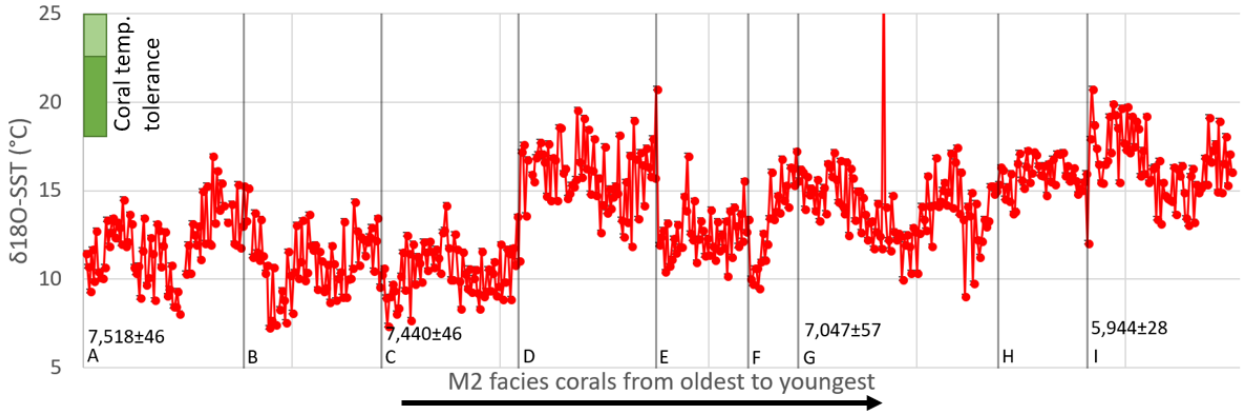

Figure 26. δ^{18}O derived SST of all corals in order of their relative age. Relative age described in the methods section 2.2.3.1. Note the relative rise in SST after coral (D) M2 140.0-0.8. Letters indicate the coral sample (A) M2 140.7-0.7a, (B) M2 140.7-0.7b, (C) M2 120.5-0.5, (D) M2 140.0-0.8, (E) M2 120.4-1.5, (F) M2 134.4-1.2, (G) M2 136.3-1.1, (H) M2 144.8-3.1, and (I) M2 145.7-3.1. Standard error for SSTs is 0.10°C.

3.7 Sr/Ca-SST

Sr/Ca values from corals M2 140.7-0.7 and M2 145.7-3.1 were used to derive SST values using six different calibration equations from different authors (See Table 11). The Sr/Ca-SSTs from Jimenez (2018) equation range from 18 to 24°C with an average of 21°C and standard

deviation of 1.6°C. This calibration was developed using a modern coral from Barahona Bay approximately 50 miles east of the Canãda Honda paleo-reef exposure. Table 11 shows the maximum, minimum, average, and standard deviation for the six Sr/Ca-SST calibrations and δ^{18}O-SST for corals M2 140.7-0.7 and M2 145.7-3.1. Sr/Ca-SST calculated with the six calibration equations and δ^{18}O-SST for corals M2 140.7-0.7 and M2 145.7-3.1 are plotted in Figure 27.

Table 11. Sr/Ca-SST and δ^{18}O-SST calculated from corals M2140.7-0.7 (7,518±46 ybp) and M2145.7-3.1 (5,944±28 ybp).

Coral Sample	SST Equation Source	Minimum (°C)	Maximum (°C)	Average (°C)	Standard deviation (°C)
M2 145.7-3.1	Jimenez, 2018	17.76	23.05	20.28	1.37
	Saenger et al. 2008 (1)	22.67	26.43	24.47	0.97
	Flannery and Poore, 2013	15.78	24.91	20.14	2.37
	Saenger et al. 2008 (2)	18.10	22.74	20.32	1.21
	Smith, 2006	13.32	26.00	19.38	3.29
	Swart et al., 2002	12.28	19.88	15.91	1.97
	δ18O-SST Leder et al., 1996	13.17	20.79	16.79	2.47
M2 140.7-0.7b	Jimenez (2018)	20.23	24.49	21.95	1.24
	Saenger et al. 2008 (1)	24.43	27.46	25.65	0.89
	Flannery and Poore, 2013	20.05	27.39	23.01	2.15
	Saenger et al. 2008 (2)	20.27	24.01	21.78	1.09
	Smith, 2006	19.25	29.45	23.37	2.98
	Swart et al., 2002	15.83	21.94	18.30	1.79
	δ18O-SST Leder et al., 1996	7.30	14.43	11.09	2.09

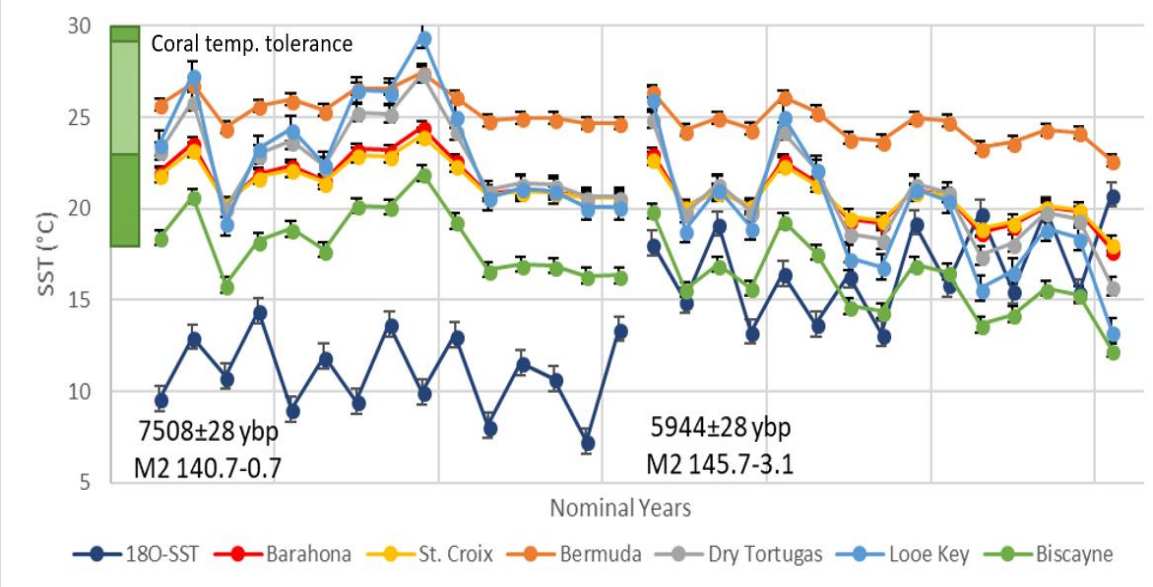

Figure 27. Sr/Ca ratio derived SST from corals M2140.7-0.7 and M2145.7-3.1 (Top). Each series corresponds to SST calculated from published Sr/Ca-SST equations: Barahona (Jimenez, 2018), St. Croix (Saenger et al. 2008 (2 Coral SC)), Bermuda (Saenger et al. 2008 (1 Coral BER), Dry Tortugas (Flannery and Poore., 2013), Looe Key (Smith, 2006), and Biscayne (Swart et al., 2002). The chart also includes the $\delta^{18}O$ derived SST using the equation published by Leder et al. (1996).

3.8 Residual $\delta^{18}O$ ($\Delta\delta^{18}O$)

Residual $\delta^{18}O$ ($\Delta\delta^{18}O$) was calculated using both $\delta^{18}O$-SST and Sr/Ca-SST and represent the deviation of $\delta^{18}Ow$ from mean modern seawater $\delta^{18}Ow$ (Yu et al., 2005). Figure 28 shows the $\Delta\delta^{18}O$ and $\delta^{18}O$-SST, and Sr/Ca-SST plotted versus age for corals M2140.7-0.7 and M2145.7-3.1. $\Delta\delta^{18}O$ results for both M2140.7-0.7 and M2145.7-3.1 range from -0.57 to 2.72±0.16‰ with an average of 1.35±0.16‰ (See Table 12).

Table 12. Residual $\delta^{18}O$ statistics from corals M2140.7-0.7 (7,518±46 ybp) and M2145.7-3.1 (5,944±28 ybp).

Residual $\delta^{18}O$ ($\Delta\delta^{18}O$) Statistics				
Coral Sample	Maximum (‰)	Minimum (‰)	Average (‰)	Standard deviation (‰)
M2-145.7-3.1	1.46	-0.57	0.66	0.55
M2-140.7-0.7b	2.72	1.34	2.04	0.42

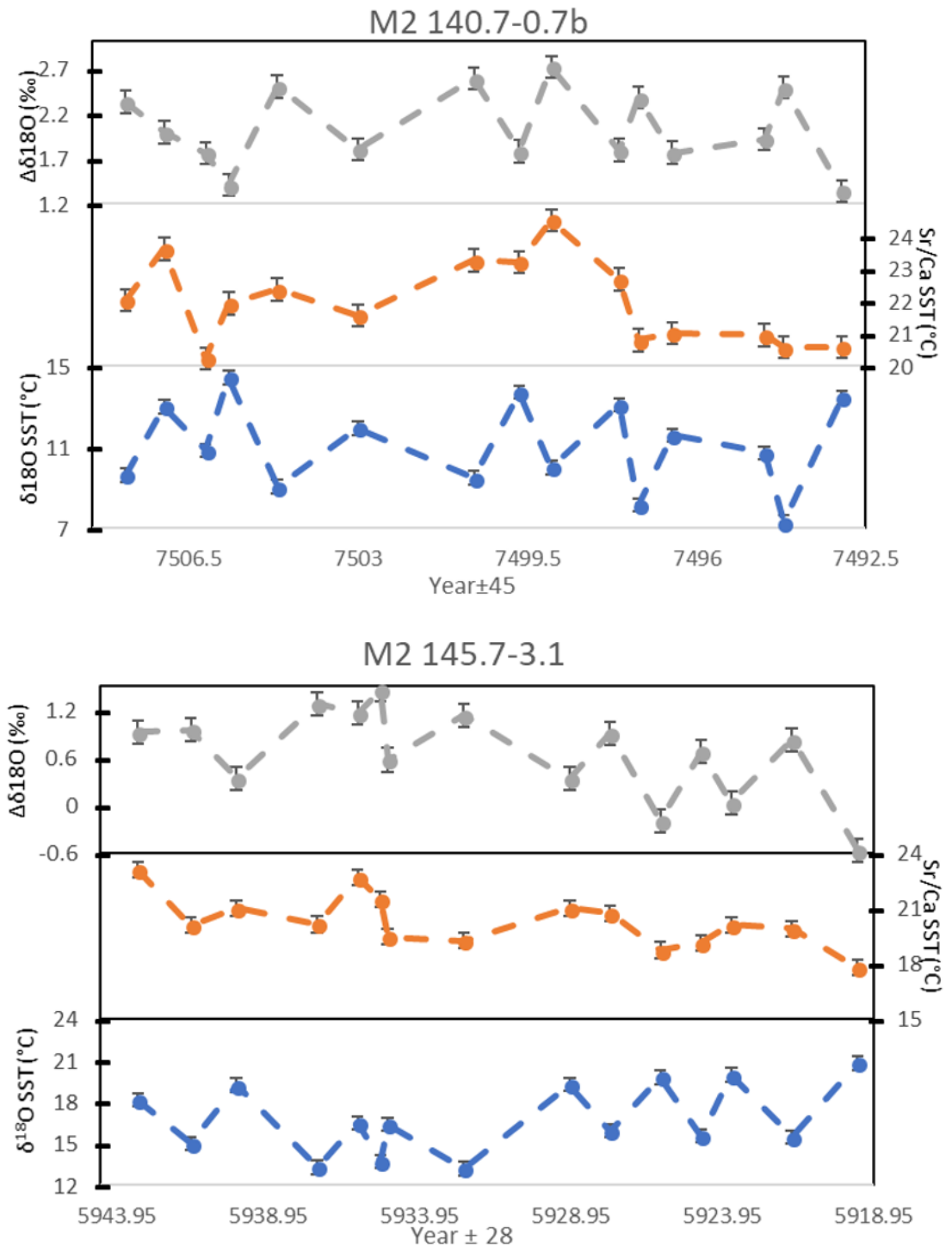

Figure 28. Residual $\delta^{18}O$ (‰), $\delta^{18}O$-SST (°C), and Sr/Ca-SST (°C) plotted versus estimate age for corals M2140.7-0.7b (7,508±46 ybp) and M2145.7-3.1 (5,944±28 ybp).

4 CHAPTER – DISCUSSION

4.1 Coral Skeleton Preservation Verification

XRD, SEM, and stable isotope analysis were used to verify the integrity of the coral skeletons used in this study. XRD results indicate the corals analyzed in this study are pure aragonite in composition. The diffractograms obtained were comparable to published aragonite powder diffraction data from the American Mineralogist Crystal Structure database. XRD results are consistent with the spectra obtained from aragonite precipitates published by Sepulcre et al. (2009) and DeCarlo et al. (2015).

Enmar et al. (2000) and Muller et al. (2001) documented the presence of secondary aragonite in corals used for paleoclimate studies. Both studies reported significant shifts to higher $\delta^{18}O$ and Sr/Ca values which result in lower SST values. Quinn and Taylor (2006) studied the influence of secondary aragonite on the skeletal geochemistry of *Porites* coral. This study found that secondary aragonite presence not only produced a cooling effect on SSTs but also resulted in a significantly higher correlation of coral Sr/Ca, Mg/Ca, $\delta^{18}O$, and $\delta^{13}C$ values (Quinn and Taylor, 2006). These studies highlight the importance of inspecting corals for secondary aragonite. SEM images of four corals in this study verify the absence of secondary aragonite diagenesis in the corals used in this study (See Figures 13 and 14). Greer and Swart (2006) also concluded that secondary aragonite is absent in mid-Holocene corals from the Enriquillo Valley.

Stable isotope analyses from coral samples in this study were compared to published stable isotope fields of Quaternary carbonate sediments by Milliman (1974). Milliman (1974) states that stable isotope values for modern corals range from 2.0 to -9.0‰ for $\delta^{13}C$ and -6.0 to -3.0‰ for $\delta^{18}O$. The $\delta^{18}O$ values from corals in this study are 1-2‰ heavier than the values expected for

modern corals while $\delta^{13}C$ values fall within the expected values of modern corals. This could be interpreted as either diagenetic alteration from secondary aragonite or a result of changes in salinity and SST in the Enriquillo paleo-embayment. The higher $\delta^{18}O$ values could be explained by secondary aragonite (Quinn and Taylor, 2006) but as stated before only two SEM images from coral samples (M2 120.4-1.5 and M2 120.5-0.5C) show some presence of secondary aragonite. The correlation coefficient of $\delta^{18}O$ and $\delta^{13}C$ values from corals in this study range from -0.04 to 0.67 for individual corals (see Figure 19), and 0.47 for all corals in this study. Table 13 compares the correlation coefficient of Sr/Ca, $\delta^{18}O$, and $\delta^{13}C$ values for corals samples M2140.7-0.7b and M2145.7-3.1 to unaltered and secondary aragonite altered coral correlation coefficients published by Quinn and Taylor (2006). $\delta^{18}O$-Sr/Ca and $\delta^{13}C$-Sr/Ca correlation coefficients from this study are low relative to both unaltered and altered coral values published by Quinn and Taylor (2006). The correlation coefficient of $\delta^{18}O$ and $\delta^{13}C$ (0.47) lies between the published values for an unaltered (0.37) and altered coral (0.74). According to Greer and Swart (2006), positive correlation between $\delta^{18}O$ and $\delta^{13}C$ could be due to local precipitation and/or freshwater flooding patterns. Since SEM images show sparse signs of secondary aragonite and $\delta^{18}O$-Sr/Ca and $\delta^{13}C$-Sr/Ca correlation coefficients are low, the positive $\delta^{18}O$ values of corals in this study relative to the fields published by Milliman (1974) can be attributed to changes in salinity and SST in the Enriquillo paleo-embayment, not diagenetic alteration from secondary aragonite.

Table 13. The correlation coefficient of Sr/Ca values, $\delta^{18}O$, and $\delta^{13}C$ for corals samples M2 140.7-0.7 (7,518±46 ybp) and M2 145.7-3.1 (5,944±28 ybp). Unaltered and altered correlation coefficients for Sr/Ca values, $\delta^{18}O$, and $\delta^{13}C$ were published by Quinn and Taylor (2006).

Coral Sample	$\delta^{13}C$ - $\delta^{18}O$	$\delta^{13}C$ -Sr/Ca	$\delta^{18}O$ -Sr/Ca
M2-145.7-3.1	0.31	-0.11	-0.11
M2-140.7-0.7b	0.65	-0.17	0.19
Unaltered	0.37	0.27	0.51
Altered	0.74	0.74	0.91

4.2 Coral Growth Rates

Coral growth rates in samples from the M2 facies in Cañada Honda range from 2.5 to 5.3±0.2 mm/yr on average. These values are within the range of previously reported growth rates for Cañada Honda corals by other authors (See Table 6). For the M2 facies specifically, growth rates were previously measured to vary from 1.42±0.14 to 3.63±0.24 mm/yr by Cuevas (2010). Coral growth rates in this study vary within each coral skeleton as well, and individual HD/LD couplets range from 0.5 to 8.6mm/yr. Longer individual couplets suggest coral stress. Stress bands are anomalously thick, bright, high density bands that correlate to mass bleaching and cold-water events (Hudson et al, 1976). Corals near the base of the M2 facies above the *Madracis* layer had a high occurrence of sediment incorporated into the growth bands (See corals M2 148-0.6 and M2 120.5-0.4 in Figure 9). Average growth rates are lower towards the top of the facies (See Figure 16).

Hubbard and Scaturo (1985) measured growth rates of 95 *Orbicella annularis* specimen and determined that primary controls in coral growth rates include water depth, light level, turbidity, and sedimentation rate. According to Cuevas (2010), corals in the M2 facies grew at 12±1 meters below paleo-sea level. Cuevas (2010) determined the paleodepth using the correlation of radiocarbon ages from two corals in the M2 facies in Canada Honda with the corrected Holocene sea-level curve by Toscano and Macintyre (2003). The vertical difference

between the elevation of the sample and sea level at the time it was alive yields the paleodepth of the coral. This same method was applied to the four corals dated in this study (M2-140.7-0.7, M2-120.5-0.5, M2-136.3-1.1, M2-145.7-3.1) to determine paleodepth using the corrected Lighty et al. (1982) sea level curve by Hubbard et al., (2005) (See Figure 29 and 31). According to Figure 29, corals in this study grew at a paleodepth of 17 and 20±1 meters below paleo-sea level. Therefore, the range of *Orbicella sp.* complex growth rates in this study could have been responding to changes in depth. Where corals with growth rates near 2.5±0.2 mm/yr grew at approximately 20 meters depth and corals with growth rates near 5.3±0.2 mm/yr grew at approximately 17 meters depth.

A high sedimentation environment is inferred by the corals highly foliated and columnar morphology abundant in the specimen along the M2 facies (Hubbard et al., 2008). Also, as previously mentioned, this and other studies reported sediment incorporated into the coral growth bands (See Figure 9). High sedimentation rates are associated with turbidity that presumably blocks light contributing to the low growth rates. However, according to Te (1997), fine-grained carbonate sediment has greater light scattering optical properties compared to fine-grained siliciclastic sediment. This results in greater light penetration and coral photosynthesis for a reef with high carbonate sediment influx, as Cañada Honda, versus a reef with high siliciclastic sediment influx (Te, 1997). Therefore, depth may have had a greater affect on coral growth rates in the M2 facies than sedimentation.

The relationship between growth rates and sea level change can also be observed by the increase of the average growth rates from the M1 (2.62 mm/yr) to the MZ facies (4.4 mm/yr) and the drop in the M3 facies (1.91 mm/yr) see in Figure 17. Figure 31 shows how sea level rose relatively rapidly from 8000 ybp to 7000 ybp then slowed from 6000 to 5000 ybp. This implies

that conditions in the paleo-embayment became closer to open ocean conditions from the M1 to the MZ facies then became more restricted as sea level rise fell and allowed deltaic deposits from the Rio Yaque del Sur to accumulate (Mann et al., 1984, Cuevas, 2010, and others). The M1, M2, and M3 are characterized by low diversity massive corals, the MZ facies is characterized by higher coral diversity (See section 1.1.2 and Cuevas et al., 2005). Changing diversity in the coral reef also seem to respond to sea level changes. Increasingly stressed conditions towards the end of coral reef accretion is also suggested by Cuevas et al., 2005.

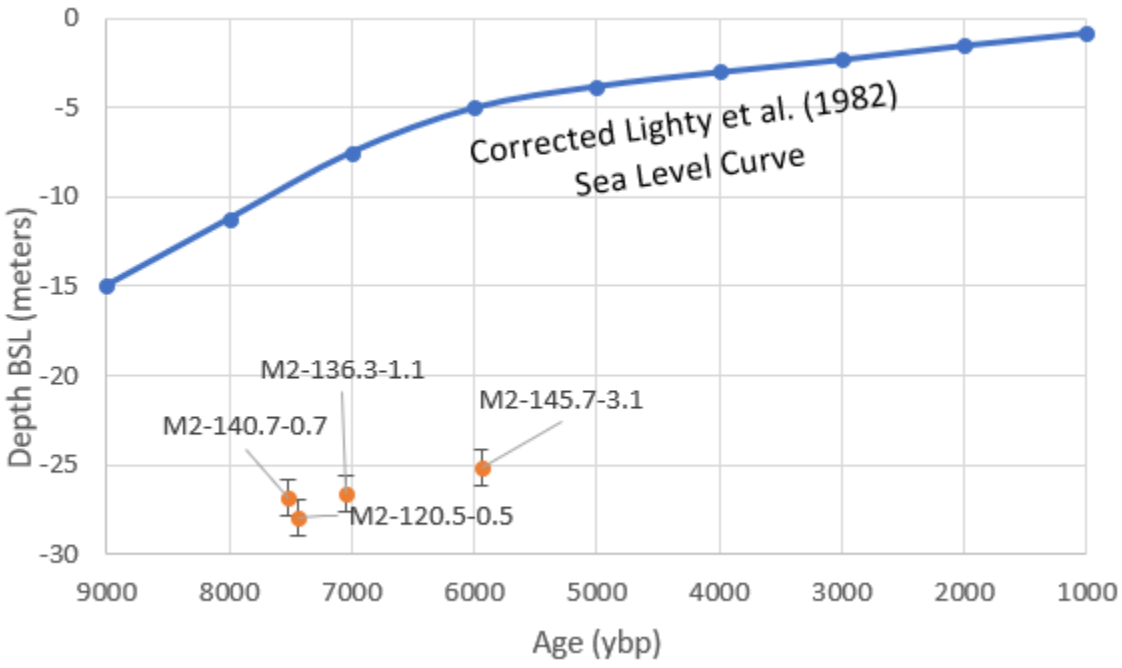

Figure 29. Coral samples M2-140.7-0.7, M2-120.5-0.5, M2-136.3-1.1 and M2-145.7-3.1 plotted based on their age and elevation relative sea level. to the vertical difference between the elevation of the sample and sea level at the time it was alive yields the paleodepth of the coral.

4.3 Sedimentation Rates

Sedimentation rates estimated from the M2 facies corals range from 0.59 to 0.99 mm/yr with an average of 0.79 ± 0.20mm/yr (See Figure 18). Assuming the sediment in the M2 facies was 100% calcite the sedimentation rate, accounting for sediment density, was 0.6 mg/cm^2*d

(See methods section 2.2.1). Sediment in the Cañada Honda paleo-reef was estimated to be less than 10% non-carbonate material by Cuevas et al. 2005. The sedimentation rates calculated by this study are about half the sedimentation rates estimated from *Orbicella sp*. complex corals (1.67 ± 0.05mm/yr) in the M2 facies by Hubbard et al. (2004). Sedimentation rates from this study are lower than those reported by Morales (2015) for the M1 facies (2.06 ± 0.30mm/yr). Growth rates in the M1 facies are lower (2.62 ± 0.60mm/yr) than the growth rates from this study (3.13 ± 1.28 mm/yr) (See Figure 17). This difference could be attributed to lower sedimentation rates of the M2 facies.

4.4 Coral Ages, δ234U, and Reef Accretion

U/Th dates were obtained from four coral specimens (M2-140.7-0.7, M2-120.5-0.5, M2-136.3-1.1, M2-145.7-3.1) and their ages range from 7,518±46 to 5,944±28 ybp. These coral ages represent the middle Holocene (8,200 to 4,200 ybp) proposed by Walker et al. (2012). In his MS Thesis Jimenez (2018) reported a U/Th date from coral M2 146.7-0.7 (M2 facies) of 8166±35 ybp. Radiocarbon dates of corals in the M2 facies were published by previous studies and report ages of 8,600 ybp (Taylor et al., 1984), 6,500 ybp (Hubbard et al., 2004), and 7,882.5±99.5. Ages obtained from corals in this study are consistent with those previously published. U/Th dates reported for the M1 facies are 8,036 ± 26 to 8,910 ± 28 ybp (Morales, 2015), which is located below the M2 facies and *Madracis* layer (See Figure 4). Figure 19 shows a trend were corals at the same stratigraphic location (M2 120.5-0.5 and M2 140.7-0.7) are older (7440±46 and 7518±46, respectively) towards the north of the exposure (i.e. towards the paleo-shore). This trend is also reported for the massive 1 (M1) facies by Morales (2015). As expected corals are younger in higher vertical locations within a stratigraphic column (See Figure 19).

Ages and vertical locations were also used to estimate reef accretion rates. The average accretion rate is 1.3±0.2 m/kyr and ranges from 0.7 to 1.88 m/kyr (See Figure 19). Edwards (1988) used mid-Holocene corals (8294±44 ybp) from a gully 1km east of Cañada Honda and obtained a reef accretion rate of 1.7 m/kyr. Hubbard et al. (2008) studied the accretion rates of Holocene Caribbean reefs (St. Croix and Puerto Rico) and proposed that regardless of dominant coral type and/or water depth, the majority reefs accrete at rates between 3 and 5 m/ka. The fact that the Cañada Honda paleo-reef accretion rates are much lower than published accretion rates for Caribbean coral reefs, at similar time frames, suggest the reef accreted in less than ideal conditions. However, regardless of its low accretion rate, the Cañada Honda reef was able to keep up with the Holocene (8,000–6,000 ybp) sea-level rise (1 m/ka) proposed by Lighty et al. (1982).

Uranium isotopes ($\delta^{234}U$) were obtained from corals in the M2 facies. $\delta^{234}U$ for corals M2-140.7-0.7 (137.1±2.2‰), M2-120.5-0.5 (136.0±2.2‰), and M2-136.3-1.1 (138.7±2.2‰) are lower than those expected from open seawater in the Atlantic (Figure 30). A low $\delta^{234}U$ value (82±4‰) was also obtained by Edwards (1988) in a coral sample (8294±44 ybp) from Cañada Honda. The $\delta^{234}U$ value (145.6±2.2‰) from coral sample M2-145.7-3.1 was within the range expected from open seawater in the Atlantic. Edwards (1988) proposed that $\delta^{234}U$ of open ocean water ranges from 140.0±5 to 150.0±5‰ and suggests that low $\delta^{234}U$ values correlate to freshwater influx. Figure 30 shows the increase of $\delta^{234}U$ over time in the Enriquillo paleo-embayment (Morales, 2015, Arana, 2018, Jimenez, 2018, and Rodriguez, 2018). The increase of $\delta^{234}U$ in the Enriquillo paleo-embayment correspond to rise in sea level during the accretion of the Cañada Honda paleo-reef. This implies that rising sea level weakened the influence of fresh water in the Enriquillo paleo-embayment.

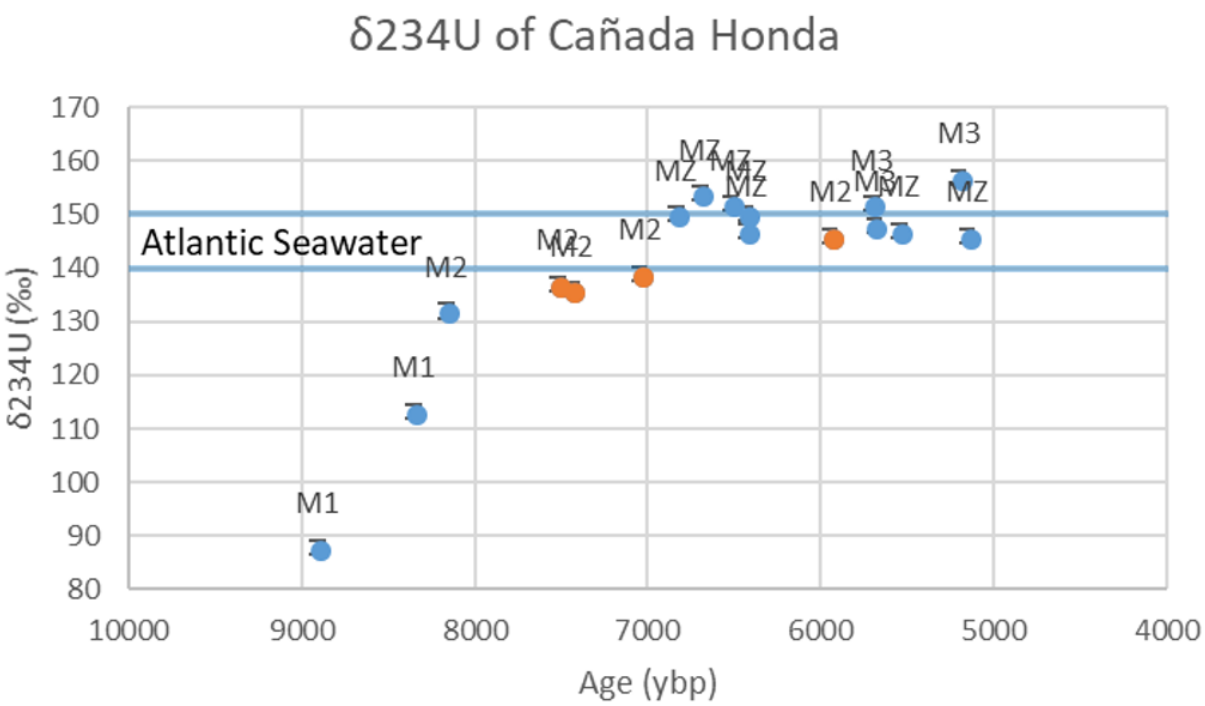

Figure 30. $\delta^{234}U$ values of corals in Cañada Honda over time. Labels indicate the facies corresponding to each coral. Orange dots correspond to M2 corals from this study. Blue dots correspond to data from Morales, 2015, Arana, 2018, Jimenez, 2018, and Rodriguez, 2018. The blue lines correspond to the $\delta^{234}U$ of open ocean water (140.0±5 to 150.0±5) proposed by Edwards (1988).

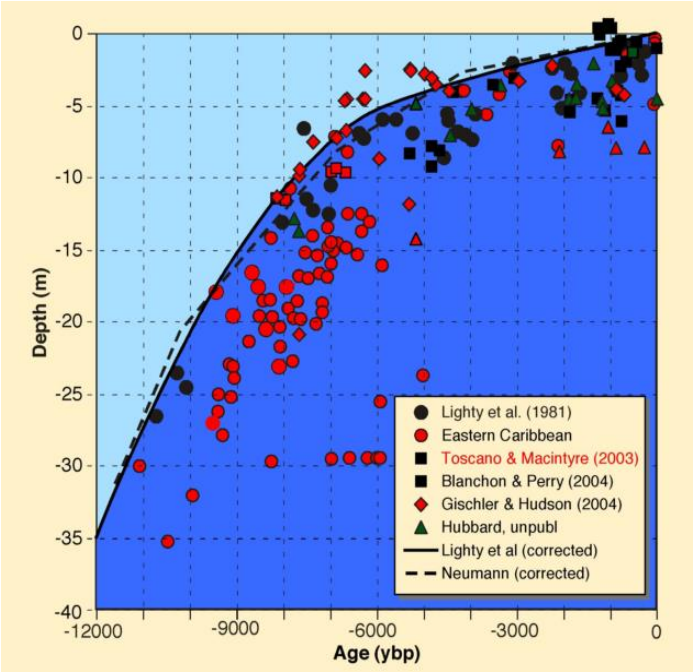

Figure 31. Corrected Lighty et al. (1982) sea level curve by Hubbard et al., (2005).

4.5 Stable Isotope and Trace Element Analysis

4.5.1 Stable Isotope Analysis

Stable isotope values from *Orbicella sp.* complex corals in this study range from -1.37 to -3.9‰ for $\delta^{18}O$ and -1.41 to -5.18‰ for $\delta^{13}C$ (See Figure 20). Greer and Swart (2006), reported *Orbicella annularis* stable isotopes ranging from -4.94 to -1.94‰ for $\delta^{18}O$ and -4.77 to -2.33‰ for $\delta^{13}C$ on early to mid-Holocene fossil corals from the Enriquillo Valley. Morales (2015) studied corals in the M1 facies of Cañada Honda and found *Orbicella sp.* complex stable isotopes range from -0.69 to -2.41‰ for $\delta^{18}O$ and -5.96 to -2.43‰ for $\delta^{13}C$.

Overall, $\delta^{18}O$ of most corals in the Enriquillo Valley have relatively heavy or ^{18}O enriched oxygen isotopes compared to Quaternary corals that range from approximately from -3.0 to -6.0‰ according to Milliman (1974). Based on similar results to the ones obtained in this study, Greer and Swart (2006) suggested the oxygen isotope enrichment of the Enriquillo Valley Holocene corals relative to modern values is a result of the corals being exposed to a high salinity environment. Increases in temperature and precipitation deplete $\delta^{18}O$ values of marine waters. Therefore, the lowest $\delta^{18}O$ values of mid-Holocene coral skeletons (relative to modern corals in open water conditions) are assumed to occur when temperature and precipitation is high. Therefore, Figure 20 shows how conditions in the Enriquillo paleo-embayment became warmer and wetter from 7518±46 to 5944±62 ybp.

4.5.1.1 Oxygen Isotope Cyclicity

Fossil corals (*Orbicella annularis and Siderastrea sp.*) from the Enriquillo paleo-embayment studied by Greer and Swart (2006) displayed patterns in $\delta^{13}C$ and $\delta^{18}O$ of the corals to suggest oscillations on a roughly decadal to multidecadal scale with an approximate frequency of 15–20 years. Corals used by Greer and Swart (2006) range in age from 7.2 to 5.2 kyr which

overlap with the ages from this study (7518 to 5944 ybp). Greer and Swart (2006) suggest the oscillations may represent cyclic fluctuations in mid-Holocene migration of the Intertropical Convergence Zone (ITCZ) or in the hydrogeology of the region as governed by fluctuations in the passage of tropical storms and hurricanes. Giry et al. (2012) studied Sr-Ca-SSTs fossil corals from the mid-Holocene in Bonaire and found that the southern Caribbean Sea during the mid- to late Holocene SST was characterized by clear seasonal cycles, persistent quasi-biennial and prominent interannual as well as inter- to multidecadal-scale variability. Giry et al. (2012) found 8.2 year variability in modern and 6220 ybp summer SST. Giry et al. (2012) connected the 8.2 variability to the meridional movement of Walker circulation and the norther location of the Intertropical Convergence Zone (ITCZ). Similar oscillations are expected for the stable isotope records from the corals in this study. Oscillations in this study range from 8 to 12 years in length, and therefore decadal to sub-decadal (See Table 10) and are also possibly responding to the migration of the ITCZ.

4.5.1.2 Oxygen Isotope Salinity

Fossil corals from the Enriquillo paleo-embayment were deposited during the mid-Holocene as sea level rose and flooded the Enriquillo Valley. Therefore, the coral oxygen isotope records were influenced by rising sea level, temperature, and salinity. The $\delta^{18}O$ record from all corals used in this study (M2 140.7-0.7a, M2 140.7-0.7b, M2 120.5-0.5, M2 140.0-0.8, M2 120.4-1.5, M2 134.4-1.2, M2 136.3-1.1, M2 144.8-3.1, and M2 145.7-3.1) vary from -1.37 to -3.9‰ which is a range of 2.53‰. The fossil corals used in this study grew when sea level was approximately 7 meters below present level, therefore 0.07‰ of the oxygen isotope range can be explained by sea level (Chappell and Shackleton, 1986). Greer (2001) found that regional COADS temperature data near the Enriquillo Valley had an annual range of about 4°C over the

last century. Assuming that the annual temperature range was similar during the mid-Holocene, 1.0‰ of the oxygen isotope range from corals in this study can be explained by the 4°C annual range (Dansgaard, 1964, Leder et al., 1996). The remaining 1.46‰ corresponds to salinity. According to Craig (1966) a 1.0‰ change in δ18O corresponds to a 4‰ (PSU) change in salinity. Thus, salinity in the Enriquillo paleo-embayment could have been as high as 41 PSU.

Similarly, salinity can be inferred from the average δ^{18}O-SST and Sr-U derived SST. Two mid-Holocene corals from the Enriquillo Valley were analyzed for SSTs using the Sr-U paleothermometer by Rodriguez (2018). Rodriguez found an average SST of 26.3°C. The average δ^{18}O-SST of all corals used in this study is 13.6°C. The difference of δ^{18}O-SST and Sr-U derived SST is 12.8°C which corresponds to a 3.2‰ δ^{18}O difference. Using the same assumptions previously mentioned, 0.07‰ of the δ^{18}O range corresponds to sea level and 1.0‰ by the 4°C temperature range. Therefore, the remaining 2.13‰ corresponds to salinity changes. This suggests salinity in the Enriquillo paleo-embayment could have been as high as 43 PSU. Thus, we can infer that the coral reefs accreted in the mid-Holocene Enriquillo paleo-embayment were subject to the upper limit of coral salinity tolerance.

4.5.1.3 Residual δ^{18}O ($\Delta\delta^{18}$O)

Residual δ^{18}O ($\Delta\delta^{18}$O) values were calculated using both δ^{18}O-SST and Sr/Ca-SST (using Sr/Ca-SST equation from Jimenez 2018). They represent the deviation of δ^{18}Ow from mean modern seawater δ^{18}Ow (Yu et al., 2005). For this proxy higher or more positive $\Delta\delta^{18}$O corresponds to relatively cold and dry conditions and vice versa (Gagan et al., 1998). $\Delta\delta^{18}$O was calculated for corals M2140.7-0.7 and M2145.7-3.1. $\Delta\delta^{18}$O for coral M2140.7-0.7 (7518±46 ybp) range from 1.34 to 2.72±0.42‰ with an average of 2.04±0.42‰. $\Delta\delta^{18}$O for coral M2145.7-3.1 (5944±28 ybp) range from -0.57 to 1.46±0.55‰ with an average of 0.66±0.55‰. This

suggests that seawater conditions 5,944±28 ybp were closer to open conditions than 7,518±46 ypb. $\Delta\delta^{18}O$ shows similar trends towards open ocean conditions as $\delta^{18}O$ trends shown in Figure 20. This proxy also suggests climate conditions in the Enriquillo paleo-embayment were warmer and wetter 5944±62 ybp than 7518±46 ybp. $\Delta\delta^{18}O$ were also calculated for the M1 and MZ facies. $\Delta\delta^{18}O$ from M1, M2, and MZ suggest seawater conditions became closer to open ocean conditions from ~ 8000 to 6000 ybp and then became restricted again towards 5500 ybp (See Figure 32). The $\Delta\delta^{18}O$ could be responding to the change in rate of sea level rise and subsequent restriction of the Enriquillo paleo-embayment.

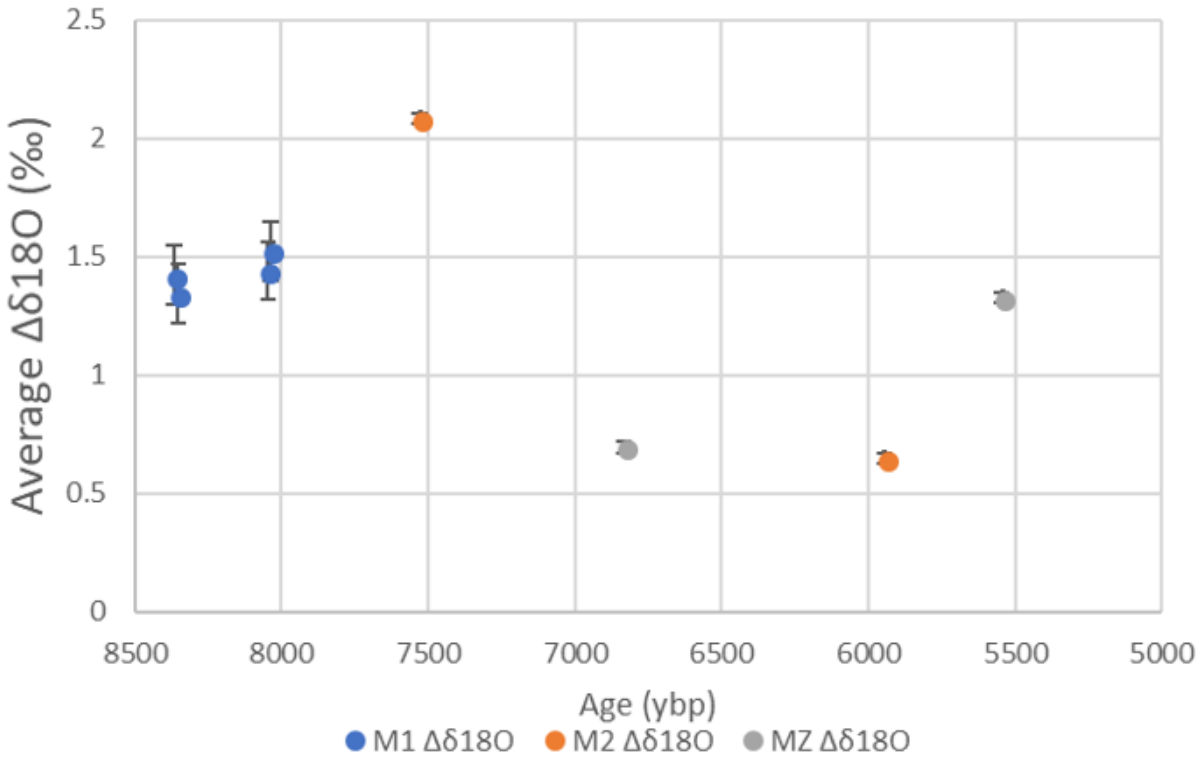

Figure 32. Residual $\delta^{18}O$ ($\Delta\delta^{18}O$) values for corals in the M1 (Morales, 2015), M2, and MZ (Arana, 2018) facies over time. Corals from the M2 facies are M2-140.7-0.7b (7508±46) and M2-145.7-3.1 (5944±28).

4.5.2 Trace Element Analysis

Analyzed coral Sr/Ca values in this study range from 9.13 to 9.60 mmol/mol and are relatively higher than Sr/Ca values reported for modern corals from the Florida Straights (8.624 to 9.085 mmol/mol) by Swart et al. (2002), however are similar to those reported by Smith (2006) (9.193 to 9.230 mmol/mol) for modern corals. Both Swart et al. (2002) and Smith (2006), found positive correlations between Sr/Ca and $\delta^{18}O$ values which is not the case for Enriquillo corals in this study (See Table 13). The reason for higher average Sr/Ca values, relative to modern corals from open ocean waters, and low correlations between Sr/Ca and $\delta^{18}O$ values could be the result of local environmental factors. High correlation coefficients between $\delta^{13}C$ and $\delta^{18}O$ were found in this study (See Table 13) as well as in Greer and Swart (2006). Greer and Swart (2006) proposed that covariance of $\delta^{13}C$ and $\delta^{18}O$ are related to changes in precipitation.

4.6 Sea Surface Temperature Calculations

4.6.1 $\delta^{18}O$ derived Sea Surface Temperature

$\delta^{18}O$ derived SSTs ($\delta^{18}O$-SST) were calculated for studied samples using the equation by Leder et al. (1996) and are plotted in Figure 26. $\delta^{18}O$-SSTs from corals in this study range from 7 to 28°C with an average of 16°C. The temperature ranges that support living Scleractinian corals is 18 to 30°C (Felis and Pätzold, 2004). Average temperatures of 16°C are not expected to have occurred in the paleo-Enriquillo embayment (Greer and Swart, 2006). Greer and Swart (2006) obtained even lower average coral temperature of 12°C mean annual temperature from their $\delta^{18}O$-SST. It is known that $\delta^{18}O$ values of coral skeletons respond to both the temperature and salinity of seawater surrounding the coral (Leder et al.,1996). $\delta^{18}O$-SSTs obtained from this study as well as, Greer and Swart (2006) suggest that $\delta^{18}O$ values in the coral skeletons of the Enriquillo paleo-embayment were not primarily controlled by temperature of the marine water

surrounding the corals. $\delta^{18}O$ values in the paleo-Enriquillo embayment were dominated changes in salinity. $\delta^{18}O$-SSTs from the M1 (Morales, 2015) and MZ (Arana, 2018) facies also exhibit SSTs that fall outside of coral temperature tolerance (See Figure 33). $\delta^{18}O$-SSTs from younger corals exhibit slightly higher temperatures implying younger corals grew in conditions closer to open ocean conditions (less influenced by salinity). A similar trend can be seen for all M2 corals $\delta^{18}O$-SSTs (See Figure 26).

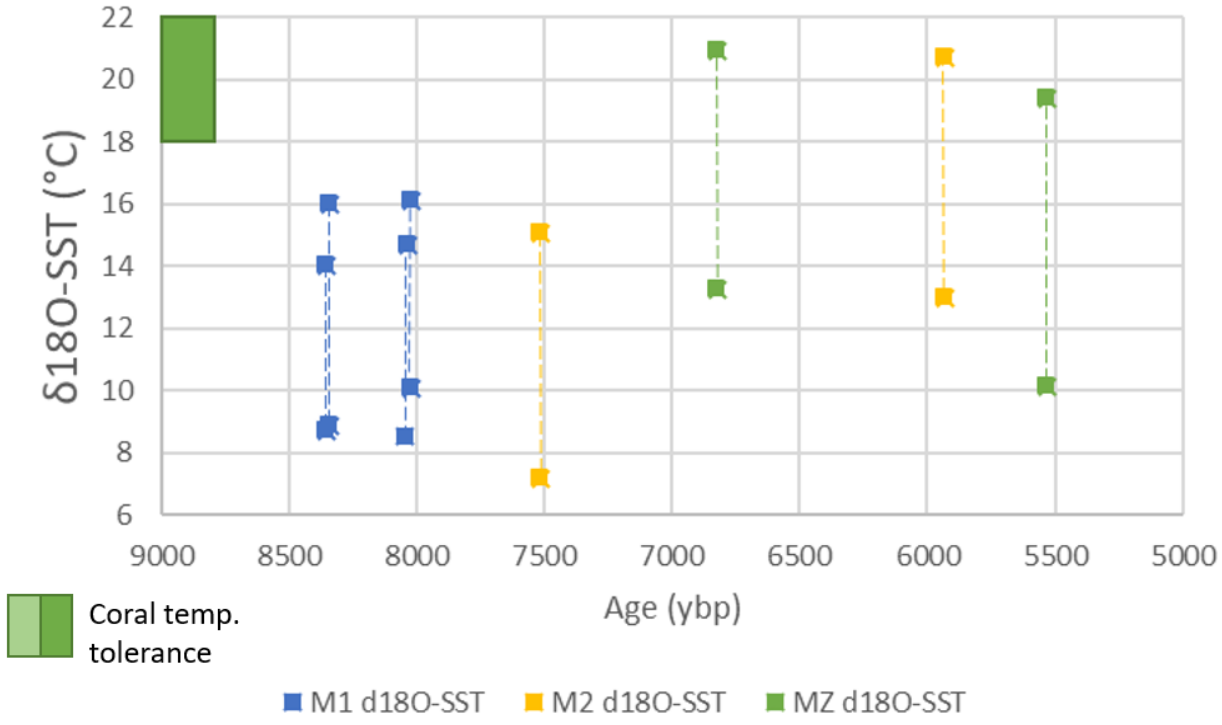

Figure 33. Range of $\delta^{18}O$ derived SST for corals in the M1 (Morales, 2015), M2, and MZ (Arana, 2018) facies over time. Corals from the M2 facies are M2-140.7-0.7b (7508±46) and M2-145.7-3.1 (5944±28).

4.6.2 Sr/Ca derived Sea Surface Temperature

Maximum and minimums $\delta^{18}O$ values from corals M2140.7-0.7 and M2145.7-3.1 were used to choose samples for Sr/Ca ratio analysis. Sr/Ca ratio derived SST (Sr/Ca-SST) requires the precipitation of aragonite by a living coral and the values of water temperature as it

precipitate. Sr/Ca-SSTs were calculated using calibration equations from six studies (See Table 11 and Figure 27). Saenger et al. (2008) analyzed the Sr/Ca values of four *Orbicella sp.* colonies in the Atlantic with growth rates ranging from 2.3 to 12.6 mm/yr and determined that temperatures calculated from SST-Sr/Ca are highly dependent on the location and growth rate. Table 14 shows average growth rates, coral type, location, and range of calculated Sr/Ca-SSTs from Sr/Ca values in this study. Non-growth rate dependent Sr/Ca-SSTs were calculated using equations derived from corals located in Looe Key, Florida (Smith, 2006), Biscayne National Park, Florida (Swart et al., 2002), Dry Tortugas, Florida (Flannery and Poore, 2013), Bermuda (Saenger et al., 2008 (1)), St. Croix, U.S. Virgin Islands (Saenger et al., 2008 (2)), and Baharaona Bay, Dominican Republic (Jimenez, 2018). The Sr/Ca-SST calibration that most closely resembles the Enriquillo paleo-embayment is the one reported by Jimenez (2018). The Sr/Ca-SST calibration equations that most closely resemble the growth rates in this study coral's is from Saenger et al. (2008 (1)) and Swart (2002). Sr/Ca-SSTs from Saenger et al. (2008 (1)) return relatively high temperatures (23-27°C) and Swart (2002) Sr/Ca-SSTs returns relatively low temperatures (12-22°C) relative to the values produced by other equations. Jimenez (2008) and Saenger et al. (2008(2)) Sr/Ca-SST equations return temperatures within 0.5°C of each other (See Figure 27). Considering the importance of location in Sr/Ca-SSTs; the equation used as representative for the paleo-embayment and in residual calculations in the next section is from Jimenez (2018). If the Sr/Ca-SST equation proposed by Jimenez (2018) is used, SSTs range from 18° to 25°C. This is consistent with the proposal that $\delta^{18}O$ ratios in the paleo-Enriquillo embayment were primarily controlled by salinity and not temperature, given that $\delta^{18}O$-SST results reflect a range in temperature of 7-28°C.

Sr/Ca-SSTs from the M2 and MZ (Arana, 2018) facies using the calibration reported by Jimenez (2018) exhibit SSTs that fall inside of coral temperature tolerance. Sr/Ca-SSTs from the M1 (Morales, 2015) facies using the calibration reported by Jimenez (2018) exhibit SSTs that do not completely fall inside of coral temperature tolerance (See Figure 34). This implies that the Sr/Ca-SST calibration reported by Jimenez (2018) is not the best representative for the M1 facies.

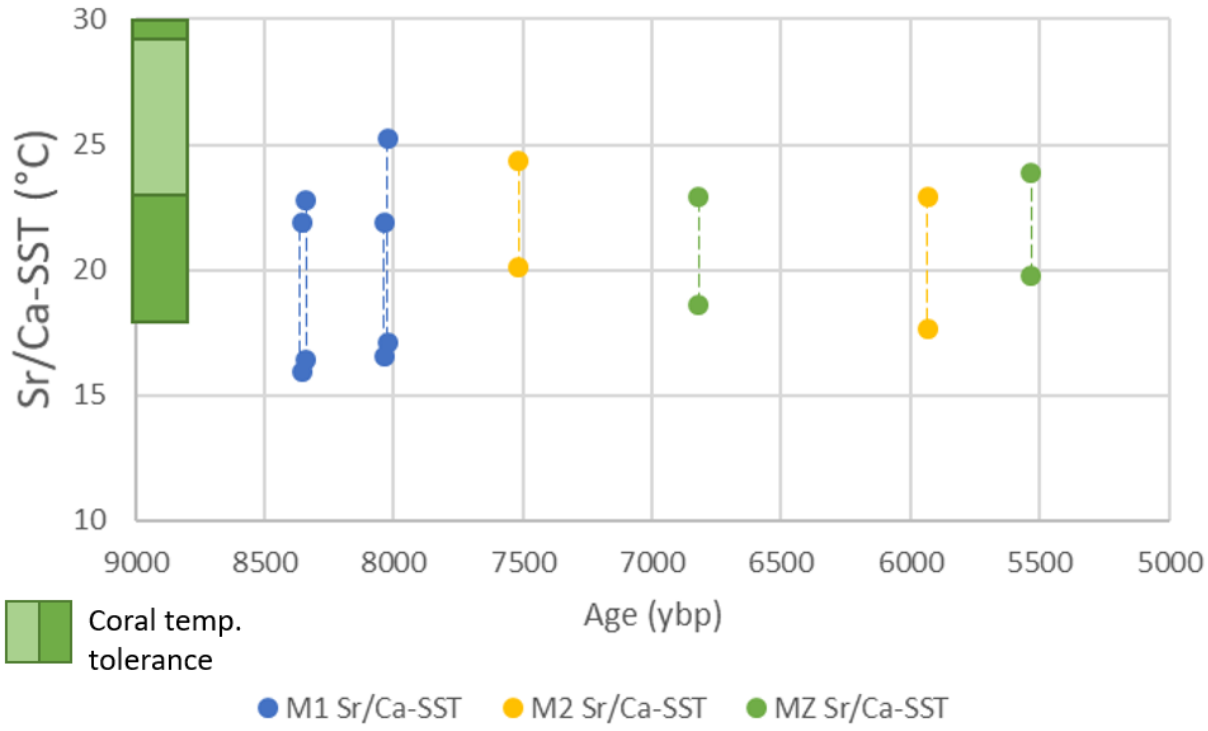

Figure 34. Range of Sr/Ca derived SST for corals in the M1 (Morales, 2015), M2, and MZ (Arana, 2018) facies over time. Corals from the M2 facies are M2-140.7-0.7b (7508±46) and M2-145.7-3.1 (5944±28).

Table 14. List of the Sr/Ca-SST equation sources and their average growth rates, coral type, location, and standard deviation of calculated Sr/Ca-SSTs from Sr/Ca values in this study.

SST Equation Source	Avg. growth rate (mm/yr)	Coral Type	Location	SST Range (°C)
Jimenez, 2018	7.34	*Orbicella sp.* complex	Baharaona Bay, Dominican Republic	18 - 25
Saenger et al. 2008 (2)	8	*Orbicella faveolata*	St. Croix, U.S. Virgin Islands	18 - 23
Saenger et al. 2008 (1)	2.3	*Orbicella franksi*	South shore reef, Bermuda	23 - 27
Flannery and Poore, 2013	8.1	*Orbicella faveolata*	Dry Tortugas, Florida	16 - 27
Smith, 2006	6.5	*Orbicella faveolata*	Looe Key, Florida	13 - 29
Swart et al., 2002	4.0 - 8.0	*Orbicella annularis*	Biscayne National Park, Florida	12 – 22
This Study	2.5 – 5.3	*Orbicella faveolata*	Enriquillo paleo-embayment, Dominican Republic	M2 140.7-0.7 and M2 145.7-3.1

4.7 Holocene Climate Proxies

Global mean SST has risen over the past 150 years with a trend of 0.04 °C/decade (Chollete et al., 2012). Sr/Ca-SST from Cañada Honda corals was compared to other Caribbean climate proxies. Ruhlemann et al. (1999) produced a high-temporal-resolution record of sea surface temperatures from the western tropical North Atlantic Ocean (spanning the past 29,000 years) derived from measurements of temperature-sensitive alkenone unsaturation in sedimentary organic matter. This record shows a gentle warming trend during the mid-Holocene (See Figure 35). Giry et al. (2012), used Sr/Ca ratio records from a modern *Diploria strigosa* to derive a Sr/Ca-SST calibration equation and applied the calibration to Holocene fossil *Diploria*

strigosa corals from Bonaire in the south Caribbean. Sr/Ca-SST from fossil Bonaire corals report temperatures within 1-2°C of the Ruhlemann et al. (1999) alkenone record. Rodriguez (2018) used two mid-Holocene corals from Cañada Honda to derive SSTs using the Sr-U paleothermometer. Sr-U derived SSTs reported by Rodriguez (2018) are within 0.5 C of the Ruhlemann et al. (1999) alkenone record. Sr/Ca-SSTs from the M1, M2, and MZ facies are within 5.5 to 8°C of the afore mentioned Caribbean SST proxies. This suggests that the Sr/Ca-SST calibration by Jimenez (2018) does not represent absolute temperatures for Cañada Honda corals. However, Sr/Ca-SSTs from the M1, M2, and MZ facies suggest warming over time in the mid-Holocene like other Caribbean SST proxies.

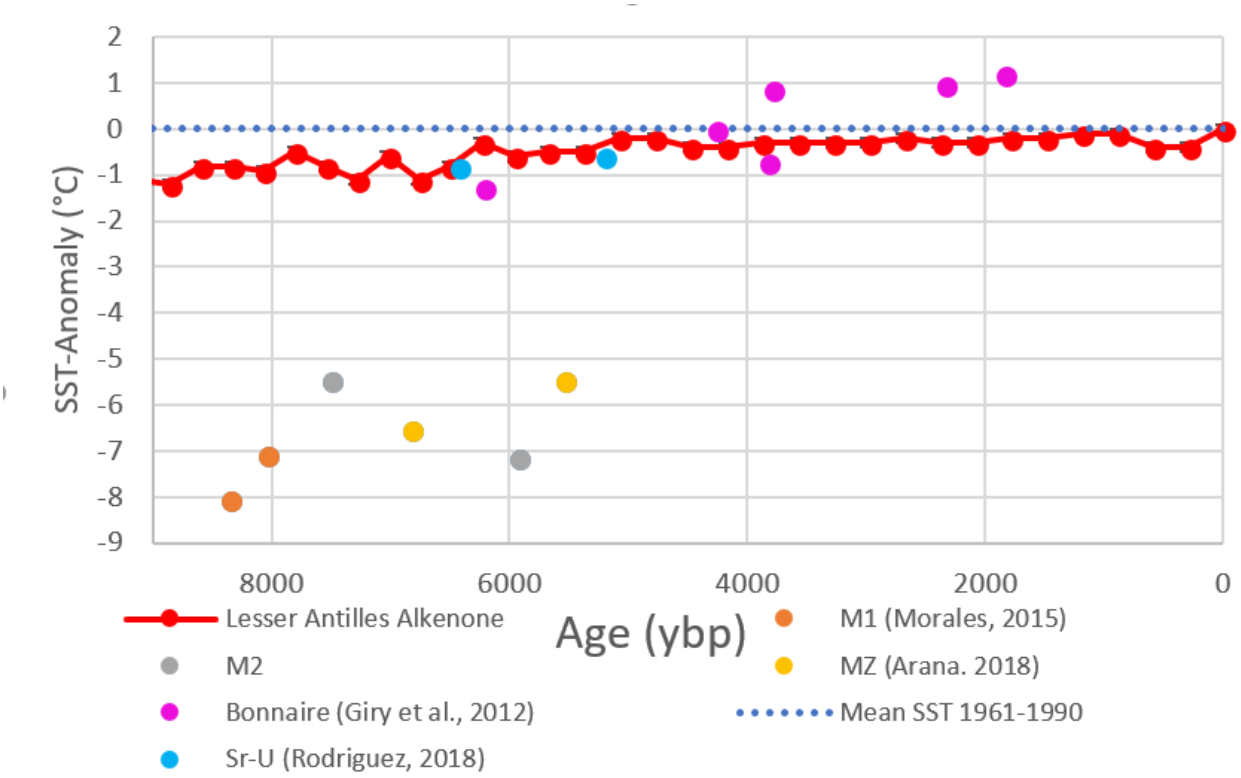

Figure 35. Sr/Ca-SSTs from the M1 (Morales, 2015), M2, and MZ (Arana, 2018) facies. Samples from M2 are M2-140.7-0.7b (7508±46) and M2-145.7-3.1 (5944±28) (grey dots). Blue dots correspond to Sr-U derived SSTs from Cañada Honda corals (Rodriguez, 2018). Pink dots correspond to Sr/Ca-SSTs from Bonaire corals (Giry et al., 2012). Lesser Antilles alkenone record (in red) from Ruhlemann et al. (1999). Anomaly for each record based on HADI-SST from 1961-1990 for each site.

5 CHAPTER – CONCLUSIONS

5.1 Conclusions

(1) This study confirms the pristine preservation of the coral skeletons present in Massive coral facies two (M2) of the Cañada Honda paleo-reef exposure in the Enriquillo Valley, Dominican Republic. XRD analysis of corals studied affirm corals are 98 to 100% aragonite. SEM images show sparse evidence of secondary aragonite indicating corals in this study experienced little diagenetic alteration. Preservation of these corals was made possible by the arid climate of the region combined with high carbonate sediment influx during reef accretion.

(2) *Orbicella sp.* complex colonies from the M2 facies had average growth rates that decrease with age. Older corals had growth rates near 5.3±0.2 mm/yr grew at approximately 17 meters depth. Younger corals had growth rates near 2.5±0.2 mm/yr grew at approximately 20 meters depth. Growth rates in the M2 facies are on average within the range of values previously published for the M2 Facies. Corals in the M2 facies show adapted foliated and columnar morphologies used to cope with high sediment influx. Growth rates of the corals in this study support findings from previous studies that suggest depth and high sedimentation affected the corals directly and indirectly by causing water turbidity, although the nature of the carbonate sediment suggests depth may have had a greater effect on coral growth rates than sedimentation.

(3) Growth rates collected from all Cañada Honda coral facies suggest that growth rates also responded to sea level change through out the accretion of the Cañada Honda reef. The rise and fall of growth rates over time correlate to rapid sea level rise followed by slower sea level rise. Conditions in the paleo-embayment became closer to open ocean conditions from the M1 to the MZ facies then became more restricted as sea level rise fell around the deposition of the M3

facies. Slower sea level rise may have allowed deltaic deposits from the Rio Yaque del Sur to accumulate thus creating restricted conditions. This response to changing oceanic conditions can also be observed by the increases of coral diversity from the M1 to MZ facies followed by a decrease in diversity in the M3 facies.

(4) Sedimentation rates derived from corals with exaggerated foliated morphology for corals in this study (0.59 to 0.99 mm/yr) are lower than previously published sedimentation rate values for the M2 facies. Sedimentation rates are lower than those reports for the M1 facies (2.06 ± 0.30mm/yr). Higher growth rates in the M2 facies (3.13 ± 1.28 mm/yr) compared to the M1 facies (2.62± 0.06 mm/yr) could be a result of the lower sedimentation rates in the M2 facies. Sedimentation rates are low relative to growth rates in the M2 facies suggesting that corals were able to thrive despite the sediment influx. Additional calculation of sedimentation rates is required to verify conclusions based on sedimentation rates.

(5) U/Th dating of corals analyzed in this study indicate the M2 facies was formed between 7518±46 to 5944±28 ybp. The U/Th date from a M2 coral analyzed by Jimenez (2018) indicates the M2 facies is as old as 8,166 ±35 ybp. Therefore, the corals in the M2 Facies were formed in the mid-Holocene. U/Th dates of the M2 facies are consistent with previously published radiocarbon dates which range from 8,600 to 6,500 ybp (Taylor et al., 1984; Hubbard et al., 2004). U/Th ages and stratigraphic positions were used to calculate reef accretion rates for the M2 facies. M2 facies average accretion rate is 1.3±0.2 m/kyr which is low compared to early-Holocene shelf edge reefs from Puerto Rico and the US Virgin Islands which had accretion rates between 3 and 5 m/kyr (Hubbard et al., 2008). Sea-level rise from 8,000 to 6,000 ybp was 1 m/ka (Lighty et al., 1982), meaning coral in the M2 facies were able to keep up with sea level rise regardless of less than optimal growth conditions.

(6) $\delta^{234}U$ obtained from corals in the M2 facies range from 136.0±2.2 to 145.6±2.2‰. Edwards (1988) proposed that $\delta^{234}U$ of open ocean water ranges from 140.0±5 to 150.0±5. Low $\delta^{234}U$ values suggest freshwater influx. $\delta^{234}U$ obtained from corals in the M1, M2, MZ, and M3 facies show an increase of $\delta^{234}U$ over time in the Enriquillo paleo-embayment. The increase of $\delta^{234}U$ in the Enriquillo paleo-embayment correspond to rise in sea level during the accretion of the Cañada Honda paleo-reef suggesting that rising sea level weakened the influence of fresh water in the Enriquillo paleo-embayment.

(7) Stable isotope values from *Orbicella sp.* complex corals in this study range from -1.37 to -3.9‰ for $\delta^{18}O$ and -1.41 to -5.18‰ for $\delta^{13}C$. Overall, stables isotopes in the M2 facies on average are within the range of values previously published for mid-Holocene corals from the Enriquillo paleo-embayment. $\delta^{18}O$ of mid-Holocene corals in the Enriquillo Valley from this and other studies are relatively heavy or ^{18}O enriched oxygen isotopes compared to Quaternary corals that range from approximately from -3.0 to -6.0‰ according to Milliman (1974).

(8) Previous studies of mid-Holocene Caribbean corals have found $\delta^{18}O$ oscillations on a roughly decadal to multidecadal scale (Giry et al., 2012 and Greer and Swart, 2006). $\delta^{18}O$ cyclicity in this study range from 8 to 12 years in length. The decadal to sub-decadal cyclicity found in M2 corals are possibly responding to the migration of the ITCZ.

(9) Both residual $\delta^{18}O$ ($\Delta\delta^{18}O$) and $\delta^{18}O$ derived salinity values suggest that that the coral reefs accreted in the mid-Holocene Enriquillo paleo-embayment were subject to the upper limit of coral salinity tolerance.

(10) Residual $\delta^{18}O$ ($\Delta\delta^{18}O$) has not been previously studied in the Cañada Honda paleo-reef. Average $\Delta\delta^{18}O$ for coral M2 140.7-0.7 (7518±46 ybp) and coral M2145.7-3.1 (5944±28

ybp) are 2.04‰ and 0.66‰., respectively. $\Delta\delta^{18}O$ suggest conditions in the Enriquillo paleo-embayment became warmer and wetter from 7518±46 to 5944±62 ybp. $\Delta\delta^{18}O$ shows also imply seawater conditions 5,944±28 ybp were closer to modern values than 7,518±46 ypb. $\Delta\delta^{18}O$ trends of the M1, M2, and MZ facies suggest seawater conditions became closer to open ocean conditions from ~ 8000 to 6000 ybp and then became restricted towards 5500 ybp and beyond.

(11) $\delta^{18}O$-SST were calculated for corals samples in this study using the equation derived by Leder et al. (1996). Resulting $\delta^{18}O$-SSTs are low compared to SSTs tolerated by Scleractinian corals (18 to 30°C). $\delta^{18}O$-SSTs for coral M2 140.7-0.7b (7518±46 ybp) average 11.09±2.09°C. $\delta^{18}O$-SSTs for coral M2 145.7-3.1 (5944±28 ybp) average 16.79±2.47°C. Greer and Swart (2006) determined there is no theoretical evidence for low temperature ranges in the Enriquillo paleo-embayment meaning $\delta^{18}O$ values of coral skeletons in the M2 facies reflect a blend of SST and the $\delta^{18}O$ of the seawater surrounding the coral. Therefore, $\delta^{18}O$ values in fossil corals from the M2 facies cannot be used to calculate SST records. $\delta^{18}O$-SST of the M1 and MZ facies also report SSTs that fall outside of coral temperature tolerance. $\delta^{18}O$-SSTs from younger corals exhibit slightly higher temperatures implying younger corals grew in conditions closer to open ocean conditions (less influenced by salinity). A similar trend can be seen for all M2 corals $\delta^{18}O$-SSTs where the three older corals used in this study report an average SST of 11.2°C and the six younger corals used in this study report average SST of 15.0°C.

(12) Sr/Ca-SSTs were calculated calibration equations from six studies. Sr/Ca-SST calibrations are dependent on location, therefore of the six calibration equations the equation used as representative for the paleo-embayment is from Jimenez (2018), which used a coral from Baharaona Bay, Dominican Republic. Sr/Ca-SSTs for coral M2 140.7-0.7b (7518±46 ybp) and

coral M2 145.7-3.1 (5944±28 ybp) have similar averages 21.95±1.24°C and 20.28±1.37 °C, respectively. Sr/Ca-SSTs from the M2 and MZ facies using the calibration reported by Jimenez (2018) exhibit SSTs that fall inside of coral temperature tolerance. However, the Sr/Ca-SSTs from M2 and MZ may not show the full range of temperatures because the corals from these studies were not continuously sampled. Sr/Ca-SSTs from the M1 facies using the calibration reported by Jimenez (2018) exhibit SSTs that do not completely fall inside of coral temperature tolerance suggesting that the Sr/Ca-SST calibration reported by Jimenez (2018) is not the best representative for the M1 facies.

(13) Sr/Ca-SST from Cañada Honda corals was compared to other Caribbean climate proxies including alkenone unsaturation derived SSTs from a sediment core the Lesser Antilles (Ruhlemann et al., 1999), Sr/Ca-SST record from mid-Holocene corals in Bonaire (Giry et al., 2012), and Sr-U derived SSTs from two mid-Holocene from Cañada Honda (Rodriguez, 2018). Sr/Ca-SSTs from the M1, M2, and MZ facies are 5.5 to 8°C cooler than other Caribbean SST proxies suggesting that the Sr/Ca-SST calibration by Jimenez (2018) does not represent absolute temperatures for Cañada Honda. Regardless, Sr/Ca-SSTs from the M1, M2, and MZ facies show a warming trend in the mid-Holocene also seen other Caribbean SST proxies.

(14) Future studies of Cañada Honda corals should experiment with different methods to obtain longer coral records to be able to calculate statistically significant cyclicity patterns of $\delta^{18}O$ and Sr/Ca values. $\delta^{18}O$ records should no longer be used to choose maxima and minima for Sr/Ca analysis, because $\delta^{18}O$ records are dominated by salinity changes not temperature changes. Sr/Ca analysis of coral samples in this study should be completed to calculate continuous Sr/Ca-SST and $\Delta\delta^{18}O$ records. Continuous $\Delta\delta^{18}O$ and $\delta^{18}O$ derived salinity records should provide a

greater understanding of how precipitation patterns and sea level rise influenced environmental conditions in the Enriquillo paleo-embayment.

References

Ainsworth, Tracy D., et al. Climate change disables coral bleaching protection on the Great Barrier Reef. Science 352.6283 (2016): 338-342.

Arana, A., Middle Holocene SST record (6,200±80 to 4,760±90 yrB.P.)based on corals from Cañada Honda, Dominican Republic, 2018. Thesis, University of Puerto Rico at Mayaguez.

Beck, J.W., Edwards, L.R., Ito, E., Taylor, F.W., Recy, J., Rougerie, F., Joannot, P., Henin, C., 1992, Sea-surface temperature from coral skeletal stronrium/calcium rations, Science, 257, 644-647.

Benway, H.M. and Mix, A.C., 2004. Oxygen isotopes, upper-ocean salinity, and precipitation sources in the eastern tropical Pacific. Earth and Planetary Science Letters, 224(3-4), pp.493-507.

Bigg, G.R. and Rohling, E.J., 2000. An oxygen isotope data set for marine waters. Journal of Geophysical Research: Oceans, 105(C4), pp.8527-8535.

Brachert, T. C., M. Reuter, K. F. Kroeger, and J. M. Lough, 2006, Coral growth bands: A new and easy to use paleothermometer in paleoenvironment analysis and paleoceanography (late Miocene, Greece), Paleoceanography, 21, PA4217, doi:10.1029/2006PA001288.

Birgmark, D., 2014, El Niño-Southern Oscillation and North Atlantic Oscillation induced sea surface temperature variability in the Caribbean Sea [M.S. thesis]: University of Gothenburg, 27 p.

Budd, A.F., Fukami, H., Smith, N.D. and Knowlton, N., 2012. Taxonomic classification of the reef coral family Mussidae (Cnidaria: Anthozoa: Scleractinia). Zoological Journal of the Linnean Society, 166(3), pp.465-529.

Chappell, J. and Shackleton, N., 1986. Oxygen isotopes and sea level. Nature, 324(6093), p.137.

Charlery, J., Nurse, L., Whitehall, K., 2006, Exploring the relationship between the North Atlantic Oscillation and rainfall patterns in Barbados, Int. J. Climatol., 26, 819-827, doi: 10.1002/joc.1334.

Cobb, K.M., Westphal, N., Sayani, H.R., Watson, J.T., Di Lorenzo, E., Cheng, H., Edwards, R.L. and Charles, C.D., 2013. Highly variable El Niño–Southern Oscillation throughout the Holocene. Science, 339(6115), pp.67-70.

Corrège, T., 2006. Sea surface temperature and salinity reconstruction from coral geochemical tracers. Palaeogeography, Palaeoclimatology, Palaeoecology, 232(2-4), pp.408-428.

Craig, H., 1966. Isotopic composition and origin of the Red Sea and Salton Sea geothermal brines. Science, 154(3756), pp.1544-1548.

Cuevas, D., Sherman, C.E., Ramirez, W., Díaz, V., Hubbard, D.K., Development of Mid-Holocene Cañada Honda fossil reef, Dominican Republic: Preliminary results and implications to modern trends of reef degradation in high sedimentation environments, 17th Caribbean Geological Conference in San Juan, Puerto Rico, 2005

Cuevas D., Development of The Holocene Canada Honda Fossil Reef, Dominican Republic: Short And Long-Term Responses To High Sedimentation, 2010. Dissertation, University of Puerto Rico at Mayaguez.

Cuevas D., Sherman C. and Ramírez-Martínez W.R. (2013) Evidence of coral reef accretion under unique environmental conditions: The mid-Holocene fossil reefs in the Enriquillo Valley of the southwestern Dominican Republic, *abstract in*: Southeastern GSA Section Meeting 2013 Abstracts with Programs, Vol. 45, No. 2, ISSN 0016-7592, p. 79.

Dansgaard, W., 1964. Stable isotopes in precipitation. Tellus, 16(4), pp.436-468.

DeCarlo, T.M., Gaetani, G.A., Holcomb, M. and Cohen, A.L., 2015. Experimental determination of factors controlling U/Ca of aragonite precipitated from seawater: Implications for interpreting coral skeleton. Geochimica et cosmochimica acta, 162, pp.151-165.

Diaz, V.D., 2005, The effects of terrigenous sedimentation on the growth rate and morphology of the Holocene fossil corals of Cañada Honda in Enriquillo Valley, Southwestern Dominican Republic. Undergraduate Thesis, University of Puerto Rico at Mayaguez.

Dodge, R.E., Szmant-Froelich, A., Garcia, R., Swart, P.K., Forester, A. and Leder, J.J., 1993. Skeletal structural basis of density banding in the reef coral Montastrea annularis.

Donders, T.H., 2005, Reconstruction of El Niño-Southern Oscillation variability during the Holocene [Ph.D. thesis]: Utrecht University, 176p.

Druffel, E. R. (1997). Geochemistry of corals: Proxies of past ocean chemistry, ocean circulation, and climate. Proceedings of the National Academy of Sciences, 94(16), 8354-8361.

Edwards, R.L., 1988. High precision thorium-230 ages of corals and the timing of sea level fluctuations in the late Quaternary (Doctoral dissertation, California Institute of Technology).

Enmar, R., Stein, M., Bar-Matthews, M., Sass, E., Katz, A. and Lazar, B., 2000. Diagenesis in live corals from the Gulf of Aqaba. I. The effect on paleo-oceanography tracers. Geochimica et Cosmochimica Acta, 64(18), pp.3123-3132.

Felis, T. and Pätzold, J., 2004. Climate reconstructions from annually banded corals. Global environmental change in the ocean and on land, pp.205-227.

Flannery, J.A., Poore, R.Z., 2013, Sr/Ca proxy sea-surface temperature reconstructions from modern and Holocene Montastraea faveolata specimens from the Dry Tortugas National Parl, Florida, U.S.A., Journal of coastal Research, 63, 20-31. Karl, Thomas R., and Kevin E. Trenberth. "Modern global climate change." science 302.5651 (2013): 1719-1723.

Gagan, M.K., Ayliffe, L.K., Beck, J.W., Cole, J.E., Druffel, E.R.M., Dunbar, R.B. and Schrag, D.P., 2000. New views of tropical paleoclimates from corals. Quaternary Science Reviews, 19(1-5), pp.45-64.

Gagan, M.K., Ayliffe, L.K., Hopley, D., Cali, J.A., Mortimer, G.E., Chappell, J., McCulloch, M.T. and Head, M.J., 1998. Temperature and surface-ocean water balance of the mid-Holocene tropical western Pacific. Science, 279(5353), pp.1014-1018.

Geister, J., 1977. The influence of wave exposure on the ecological zonation of Caribbean coral reefs. In Proceedings of the 3rd International Coral Reef Symposium, 1977 (Vol. 1, pp. 23-29).

Giannini A., Cane, M.A., Kushnir, Y., 2001, Interdecadal changes in the ENSO teleconnection to the Caribbean region and the North Atlantic Oscillation, Journal of Climate, 14, 2867-

2879.

Gill, I., Olson, J.J. and Hubbard, D.K., 1995. Corals, paleotemperature records, and the aragonite-calcite transformation. Geology, 23(4), pp.333-336.

Giry, C., Felis, T., Kölling, M., Scholz, D., Wei, W., Lohmann, G., Scheffers, S., 2012, Mid- to late Holocene changes in tropical Atlantic temperature seasonality and interannual to muldidecadal variability documented in southern Caribbean corals, Earth and Planetary Science Letters, 331-332, 187-200.

Greer, M.L., 2001. Seasonal to centennial holocene and modern climate variability in the Dominican Republic. Dissertation, University of Miami.

Greer, L. and Swart, P.K., 2006, Decadal cyclicity of regional mid-Holocene precipitation: Evidence from Dominican coral proxies, Paleoceanography., 21, PA2020, doi:10.1029/2005PA001166.

Grottoli, A.G, 2001, Climate: Past Climate From Corals, in: Encyclopedia of Ocean Sciences [eds. Steele, J., Thorpe, S., Turekian, K.], Academic Press, London p. 2098-2107.

Guzmán Rodríguez, G., 2017, Survey of Coral Populations in the Barahona Bay, Dominican Republic. Undergraduate Thesis, University of Puerto Rico at Mayaguez.

Haigh, J., 2011, Solar influences on climate, Grantham Institute for Climate Change, Biefing paper No. 5, 20 p.

Helmle, K.P., Kohler, K.E. and Dodge, R.E., 2002. Relative optical densitometry and the coral X-radiograph densitometry system: CoralXDS. In International Society of Reef Studies European Meeting, Cambridge, England.

Hendy, E.J., Gagan, M.K., Lough, J.M., McCulloch, M. and DeMenocal, P.B., 2007. Impact of skeletal dissolution and secondary aragonite on trace element and isotopic climate proxies in Porites corals. Paleoceanography, 22(4).

Himmler, T., Bayon, G., Wangner, D., Enzmann, F., Peckmann, J. and Bohrmann, G., 2016. Seep-carbonate lamination controlled by cyclic particle flux. Scientific reports, 6, p.37439.

Hubbard, D.K., Ramirez, W., Cuevas, D., 2004, A preliminary model of Holocene coral-reef

development in the Enriquillo Valley, SW Dominican Republic. Abstract. GSA Abstracts with Programs, 36, No. 5, 291 p.

Hubbard, D.K., Ramirez, W., Cuevas D., Erickson, T., Estep, A., 2008, Holocene reef accretion along the north side of Bahia Enriquillo (western Dominican Republic): unique insights into patterns of reef development in response to sea-level rise, Proceedings of the 11th International Coral Reef Symposium, Ft. Lauderdale, Florida, 43-47.

Hubbard, D.K. and Scaturo, D., 1985. Growth rates of seven species of scleractinean corals from Cane Bay and Salt River, St. Croix, USVI. Bulletin of Marine Science, 36(2), pp.325-338.

Hudson, J.H., Shinn, E.A., Halley, R.B. and Lidz, B., 1976. Sclerochronology: a tool for interpreting past environments. Geology, 4(6), pp.361-364.

Jimenez, A.L., Sea Surface Temperature Reconstruction (Sr/Ca) from Modern and Fossil Caribbean Holocene Corals, 2018. Thesis, University of Puerto Rico at Mayaguez.

Karl, T.R. and Trenberth, K.E., 2003. Modern global climate change. science, 302(5651), pp.1719-1723.

Kobashi, T., Severinghaus, J.P., Brook, E.J., Barnola, J.M., Grachev, A.M., 2007, Precise timing and characterization of abrupt climate change 8200 years ago from air trapped in polar ice, Quaternary Science Reviews, 26, 1212-1222.

Leder, J.J., Swart, P.K., Szmant, A.M. and Dodge, R.E., 1996. The origin of variations in the isotopic record of scleractinian corals: I. Oxygen. Geochimica et Cosmochimica Acta, 60(15), pp.2857-2870.

Lighty, R. G., Ian G. Macintyre, and Robert Stuckenrath. "Acropora palmata reef framework: a reliable indicator of sea level in the western Atlantic for the past 10,000 years." Coral reefs 1.2, 1982,: 125-130.

Mann, P., Lawrence, S., 1991, Petroleum potential of Southern Hispaniola: Journal of Petroleum Geology, 14, No. 3, 291-308.

Mann, P., Taylor F.W., Burke, B., Kulstad, R., 1984, Subaerially exposed Holocene coral reef, Enqiruillo Valley, Dominican Republic: Geological Society of America Bulletin, 95, 1084-1092.

Mann, Paul; Hernaiz Pedro, and Ramírez, Wilson R., 2008, Stratigraphy, tectonics and subsurface petroleum geology of the Ocoa, Azua, and Enriquillo Basins, Dominican Republic 18th Caribbean Geologic Conference, Santo Domingo, Dominican Republic. *in:* Hydrocarbons, Stratigraphy and Tectonics, Field Guide, p.127. PDF 48 Mbytes

Martin, G.D., Wilkinson, B.H. and Lohmann, K.C., 1986, The role of skeletal porosity in aragonite neomorphism--Strombus and Montastrea from the Pleistocene Key Largo Limestone, Florida. Journal of Sedimentary Research, 56(2).

Maslin, M., Stickley, C., & Ettwein, V., 2001, Holocene climate variability. Marine Policy & Economics: A Derivative of the Encyclopedia of Ocean Sciences, 479.

Mayewski, P.A., Rohling, E.E., Stager J.C., Karlé, W., Maasch, K.A., Meeker L.D., Meyerson, E.A., Gasse, F., van Kreveld, S., Holmgren, K., Lee-Thorp, J., Rosqvist, G., Rack, F., Staubwasser, M., Schneider R.R., Steig, E.J., 2004, Holocene climate variability, Quaternary Research, 62, 243-255.

McGregor, H. V., & Gagan, M. K., 2003, Diagenesis and geochemistry of Porites corals from Papua New Guinea: implications for paleoclimate reconstruction. Geochimica et Cosmochimica Acta, 67(12), 2147-2156.

Milliman, J. D., 1974, Marine carbonate. Part I: Recent sedimentary carbonates: Berlin, Springer-Verlag,379 p

Morales Collazo, J. A., Reconstructing sea surface temperatures in the Caribbean during the early-mid Holocene from a reef exposure in Cañada Honda , Enriquillo Valley , Dominican Republic, 2015, Masters Thesis, University of Puerto Rico at Mayaguez.

Müller, A., Gagan, M.K. and McCulloch, M.T., 2001, Early marine diagenesis in corals and geochemical consequences for paleoceanographic reconstructions. Geophysical Research Letters, 28(23), pp.4471-4474.

Myhre, G., D. Shindell, F.-M. Bréon, W. Collins, J. Fuglestvedt, J. Huang, D. Koch, J.-F. Lamarque, D. Lee, B. Mendoza, T. Nakajima, A. Robock, G. Stephens, T. Takemura and H. Zhang, 2013, Anthropogenic and Natural Radiative Forcing. In: Climate Change 2013: The Physical Science Basis. Contribution of Working Group I to the Fifth Assessment Report of the Intergovernmental Panel on Climate Change [Stocker, T.F., D. Qin, G.-K. Plattner, M. Tignor, S.K. Allen, J. Boschung, A. Nauels, Y. Xia, V. Bex and P.M. Midgley (eds.)]. Cambridge University Press, Cambridge, United Kingdom and New York, NY, USA.

Quinn, T. M., and F. W. Taylor, 2006, SST artifacts in coral proxy records produced by early marine diagenesis in a modern coral from Rabaul, Papua New Guinea, Geophys. Res. Lett., 33, L04601, doi:10.1029/2005GL024972.

Reuter, M., Brachert, T.C. and Kroeger, K.F., 2005. Diagenesis of growth bands in fossil scleractinian corals: identification and modes of preservation. Facies, 51(1-4), pp.146-159.

Rodriguez, L., Application of the Sr-U coral paleo-thermometer to reconstruct sea surface temperatures during the Mid-Holocene using corals from Cañada Honda, Dominican Republic, 2018, Thesis, University of Puerto Rico at Mayaguez.

Rogers, C.S., 1983, Sublethal and lethal effects of sediments applied to common Caribbean reef corals in the field. Marine Pollution Bulletin, 14(10), pp.378-382.

Rogers, C.S., 1990, Responses of coral reefs and reef organisms to sedimentation. Marine ecology progress series, pp.185-202.

Saenger, C., Cohen, A. L., Oppo, D. W., & Hubbard, D., 2008, Interpreting sea surface temperature from strontium/calcium ratios in Montastrea corals: Link with growth rate and implications for proxy reconstructions. Paleoceanography, 23(3).

Sayani, H.R., Cobb, K.M., Cohen, A.L., Crawford, E.W., Nurhati, I.S., Dunbar, D.B., Rose, K.A., Zaunbrecher, L.K., 2011, Effect of diagenesis on paleoclimate reconstructions from modern and young fossil corals, Geochimica et Cosmochimica Acta, 75, 6361-6373.

Sepulcre, S., Durand, N. and Bard, E., 2009, Mineralogical determination of reef and periplatform carbonates: calibration and implications for paleoceanography and radiochronology. Global and Planetary Change, 66(1-2), pp.1-9.

Siegel, F.R., 1960, The effect of strontium on the aragonite-calcite ratios of Pleistocene corals. Journal of Sedimentary Research, 30(2).

Smith, J.M., 2006, Geochemical signatures in the Coral Montastraea: Modern and mid-Holocene perspectives. Dissertation, University of South Florida.

Stein, M., Wasserburg, G.J., Aharon, P., Chen, J.H., Zhu, Z.R., Bloom, A. and Chappell, J., 1993, TIMS U-series dating and stable isotopes of the last interglacial event in Papua New Guinea. Geochimica et Cosmochimica Acta, 57(11), pp.2541-2554.

Stemann, T. A., & Johnson, K. G., 1992, Coral assemblages, biofacies, and ecological zones in the mid-Holocene reef deDosits of the Enriquillo Valley, Dominican Republic. Lethaia, 25(3), 231-241.

Swart, P.K., Elderfield, H. and Greaves, M.J., 2002, A high-resolution calibration of Sr/Ca thermometry using the Caribbean coral Montastraea annularis. Geochemistry, Geophysics, Geosystems, 3(11), pp.1-11.

Taylor, F.W., Mann, P., Valastro, S., Burke, K., 1985, Stratigraphy and radiocarbon chronology of a subaerially exposed Holocene coral reef, Dominican Republic, The Journal of Geology, 93, No. 3, 311-332.

Te, F.T., 1997. Turbidity and its effects on corals: a model using the extinction coefficient (k) of photosynthetic active radiance (PAR). In Proceedings of the 8th International Coral Reef Symposium, Panama (Vol. 2, pp. 1899-1904).

Watanabe, T., Winter, A. and Oba, T., 2001, Seasonal changes in sea surface temperature and salinity during the Little Ice Age in the Caribbean Sea deduced from Mg/Ca and 18O/16O ratios in corals. Marine Geology, 173(1-4), pp.21-35.

Walker, M.J.C., Berkelhammer, M., Björck, Cwynar, L.C., Fisher, D.A., Long, A.J., Lowe, J.J., 69 Newnham, R.M., Rasmusen, S.O., Weiss, H., 2012, Formal subdivision of the Holocene Series/Epoch; a Discussion Paper by a Working Group of INTIMATE

(Integration of ice-core, marine and terrestrial records) and the Subcommission on Quaternary Stratigraphy (International Commission on Stratigraphy), Journal of Quaternary Science, 27 (7), 649-659, doi: 10.1002/jqs.2565.

Wei, G., Yu, J., Gui, X., Yu, F., Chen, Y. and Liu, D., 1998, Paleoclimate implication of oxygen and carbon isotopic composition from diagenesis coral. Science in China Series D: Earth Sciences, 41(6), pp.609-615.

Winter, A., Ishioroshi, H., Watanabe, T., Oba, T., Christy, J., 2000, Caribbean sea surface temperatures: two-to-three degrees cooler than present during the Little Ice Age, Geophysical Research Letters, 27, No. 20, 3365-3368.

Winter, A., Vieten, R., Miller, T., Mangini, A., Scholz, D., 2013, 8.2ky event associated with high precipitation in the eastern Caribbean, American Geophysical Union, Fall Meeting 2013, abstract #PP31B-1870.

Yu, K.F., Zhao, J.X., Wei, G.J., Cheng, X.R., Chen, T.G., Felis, T., Wang, P.X. and Liu, T.S., 2005, δ18O, Sr/Ca and Mg/Ca records of Porites lutea corals from Leizhou Peninsula, northern South China Sea, and their applicability as paleoclimatic indicators. Palaeogeography, Palaeoclimatology, Palaeoecology, 218(1-2), pp.57-73.

Zhu, Z.R., Marshall, J. and Chappell, J., 1988, Diagenetic sequences of reef-corals in the late Quaternary raised coral reefs of the Huon Peninsula, New Guinea. In 6th International Coral Reef Symposium, Australia (pp. 565-573).

Zhu, Z., 1990, Diagenesis of the late quaternary raised coral reefs of the Huon Peninsula, Papua New Guinea.

Zhu, Z., Marshall, J.F. and Chappell, J., 1994, Effects of differential tectonic uplift on Late Quaternary coral reef diagenesis, Huon Peninsula, Papua New Guinea. Australian Journal of Earth Sciences, 41(5), pp.463-474.

Middle Holocene SST record (7518 to 5944 ybp) based on corals from the Enriquillo Valley, Dominican Republic:

Appendices

Appendix 1: XRD Analyses

In all XRD analysis green (aragonite) and red(calcite) lines were added using excel to add the powder diffraction data peak locations of aragonite and calcite from the American Mineralogist Crystal Structure database (ID 0006302 and 0000098, respectively). XRD results output show intensity counts in the Y-axis versus 2theta in the X-axis.

Coral M2 120.4-0.5 has seven XRD analyses. Numbers 1, 3, 5, and 7 were from sections of coral M2 120.4-0.5 with sediment infilling the interstices of the corals and 2, 4, and 6 did not. Two XRD samples were taken from coral sample M2 148-0.6, sample 1 was taken from pristine coral and sample 2 was taken from a section with sediment and dissolution features. Two XRD analyses were also conducted on coral M2 150.7-1.3, sample 1 was taken from a pristine section and sample 2 was taken from a surface where growth stopped and was later recolonized. XRD analysis powders for coral samples M2 145.7-3.1, M2 144.8-3.1, M2 120.5-0.5C, M2 134.4-1.2, M2140.7-0.7, M2136.3-1.1, M2140-0.8, and M2 120.4-1.5 were taken from pristine coral.

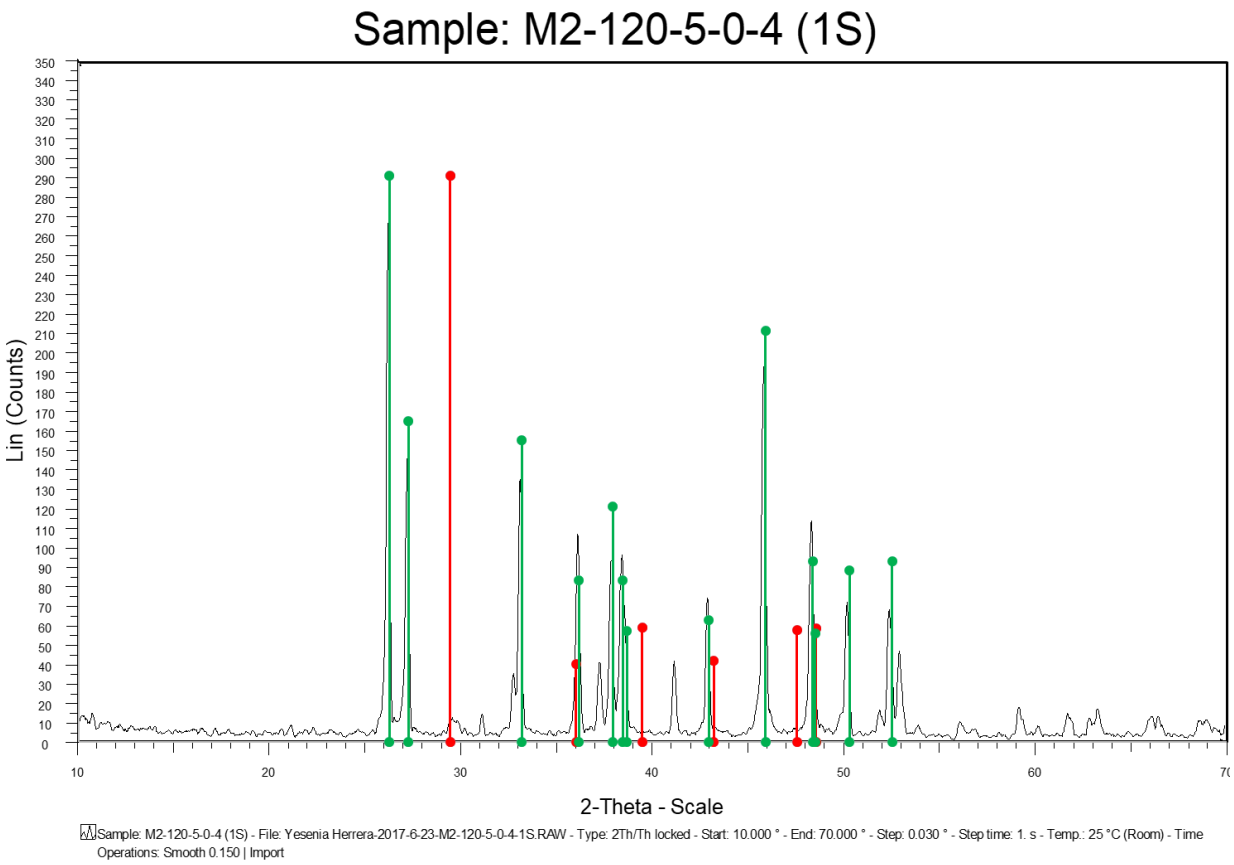
Sample: M2-120-5-0-4 (1S)
Lin (Counts)
2-Theta - Scale
Sample: M2-120-5-0-4 (1S) - File: Yesenia Herrera-2017-6-23-M2-120-5-0-4-1S.RAW - Type: 2Th/Th locked - Start: 10.000 ° - End: 70.000 ° - Step: 0.030 ° - Step time: 1. s - Temp.: 25 °C (Room) - Time
Operations: Smooth 0.150 | Import

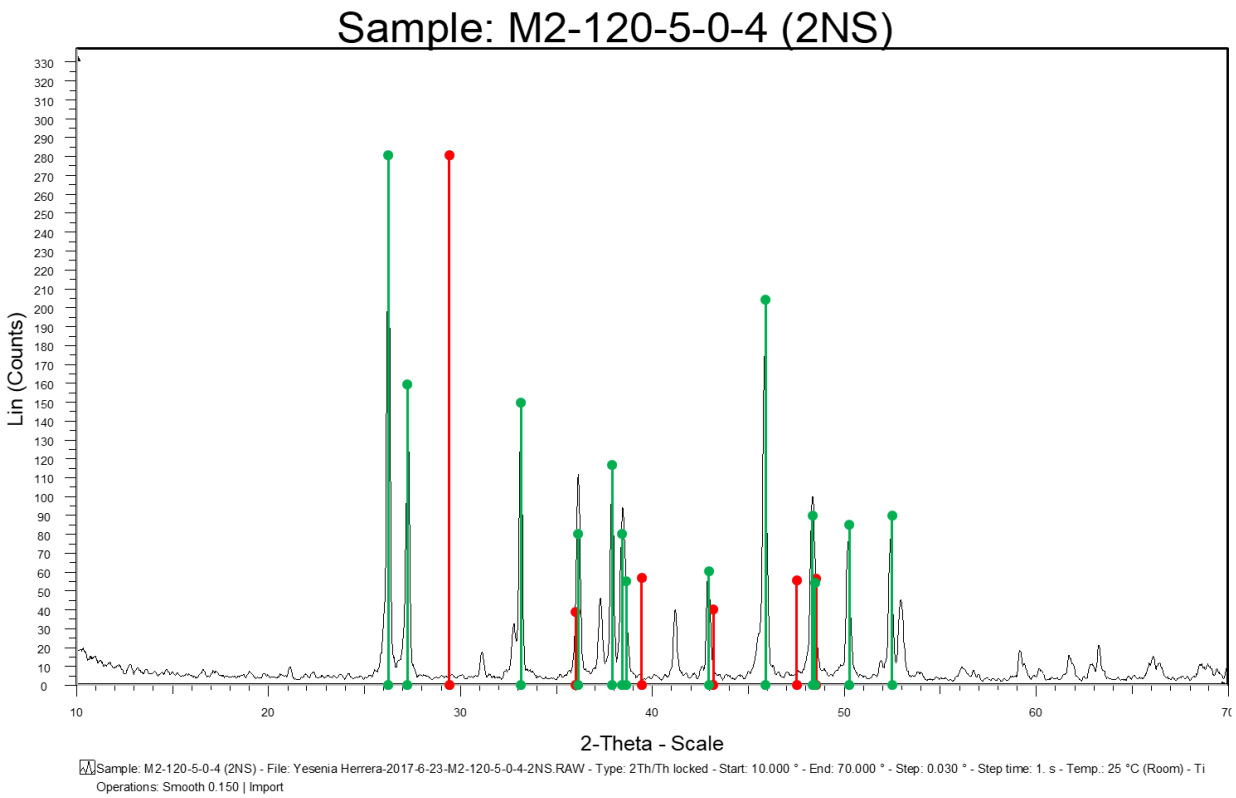
Sample: M2-120-5-0-4 (2NS)
Lin (Counts)
2-Theta - Scale
Sample: M2-120-5-0-4 (2NS) - File: Yesenia Herrera-2017-6-23-M2-120-5-0-4-2NS.RAW - Type: 2Th/Th locked - Start: 10.000 ° - End: 70.000 ° - Step: 0.030 ° - Step time: 1. s - Temp.: 25 °C (Room) - Ti
Operations: Smooth 0.150 | Import

Sample: M2-120-5-0-4 (3S)

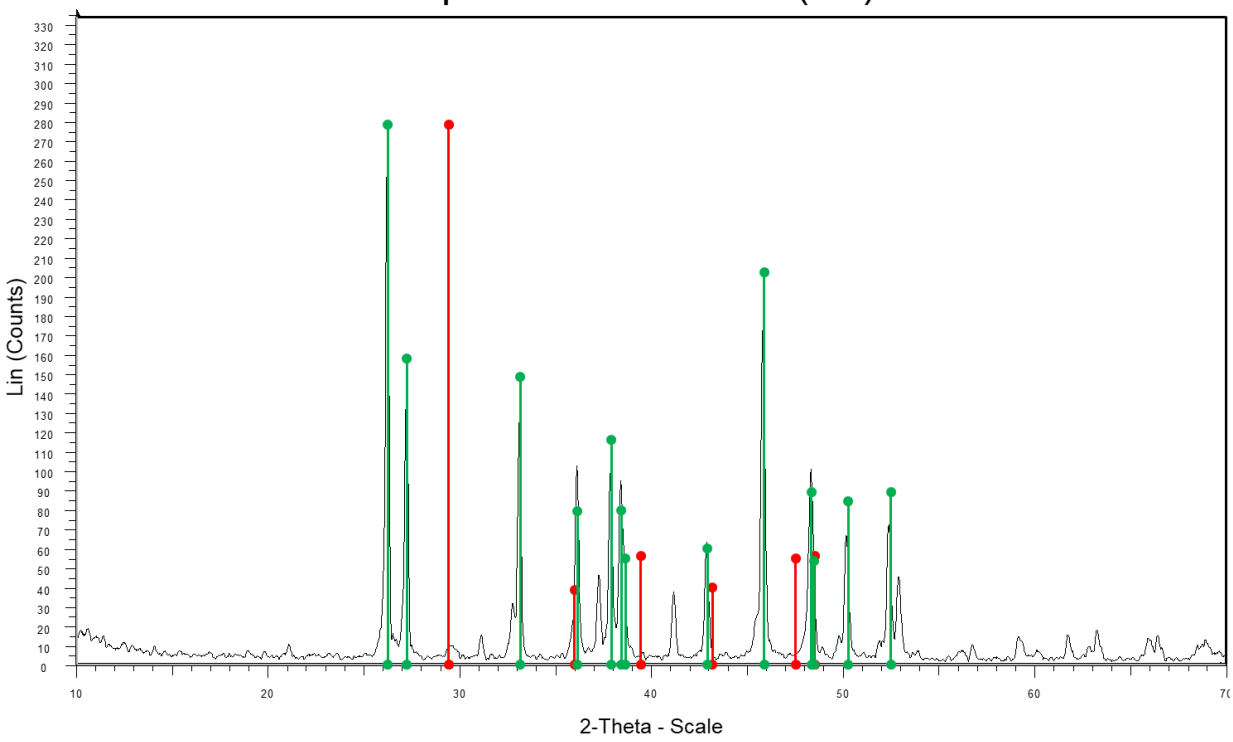

Sample: M2-120-5-0-4 (3S) - File: Yesenia Herrera-2017-6-23-M2-120-5-0-4-3S.RAW - Type: 2Th/Th locked - Start: 10.000 ° - End: 70.000 ° - Step: 0.030 ° - Step time: 1. s - Temp.: 25 °C (Room) - Time
Operations: Smooth 0.150 | Import

Sample: M2-120-5-0-4 (4NS)

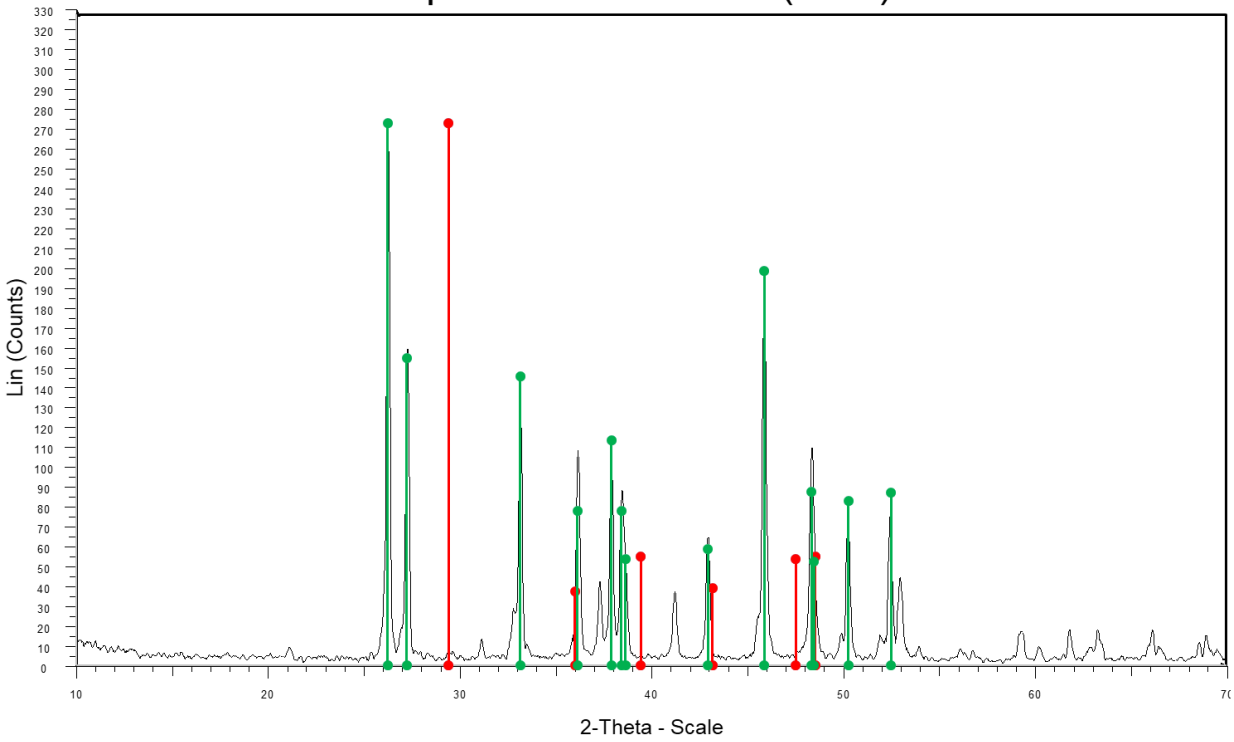

Sample: M2-120-5-0-4 (4NS) - File: Yesenia Herrera-2017-6-23-M2-120-5-0-4-4NS.RAW - Type: 2Th/Th locked - Start: 10.000 ° - End: 70.000 ° - Step: 0.030 ° - Step time: 1. s - Temp.: 25 °C (Room) - Ti
Operations: Smooth 0.150 | Import

Sample: M2-120-5-0-4 (5S)

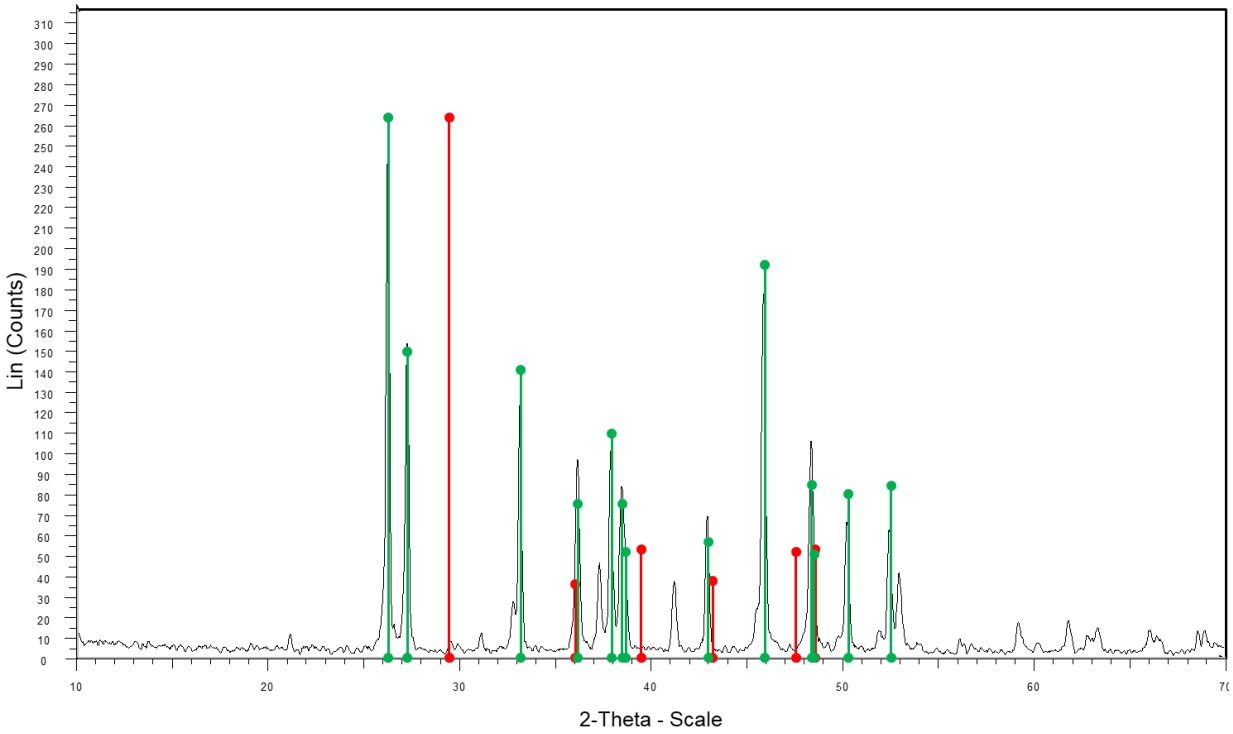

Sample: M2-120-5-0-4 (5S) - File: Yesenia Herrera-2017-6-23-M2-120-5-0-4-5S.RAW - Type: 2Th/Th locked - Start: 10.000 ° - End: 70.000 ° - Step: 0.030 ° - Step time: 1. s - Temp.: 25 °C (Room) - Time
Operations: Smooth 0.150 | Import

Sample: M2-120-5-0-4 (6NS)

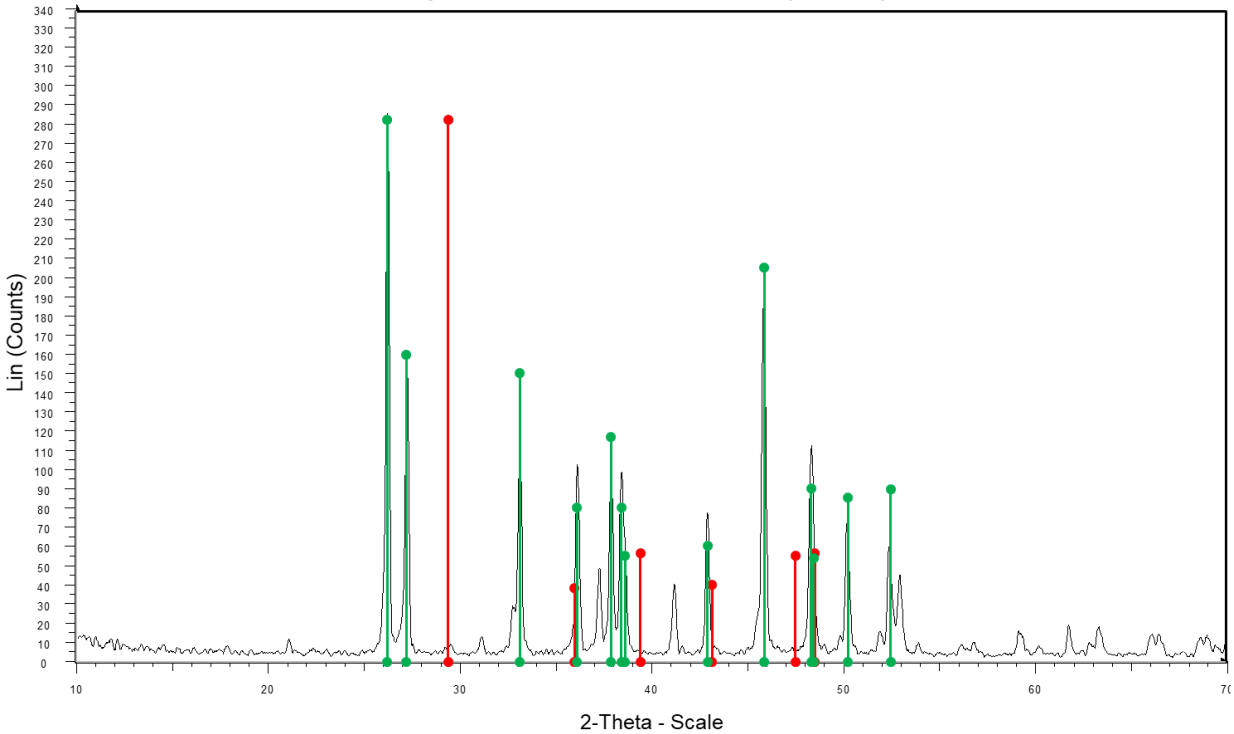

Sample: M2-120-5-0-4 (6NS) - File: Yesenia Herrera-2017-6-23-M2-120-5-0-4-6NS.RAW - Type: 2Th/Th locked - Start: 10.000 ° - End: 70.000 ° - Step: 0.030 ° - Step time: 1. s - Temp.: 25 °C (Room) - Ti
Operations: Smooth 0.150 | Import

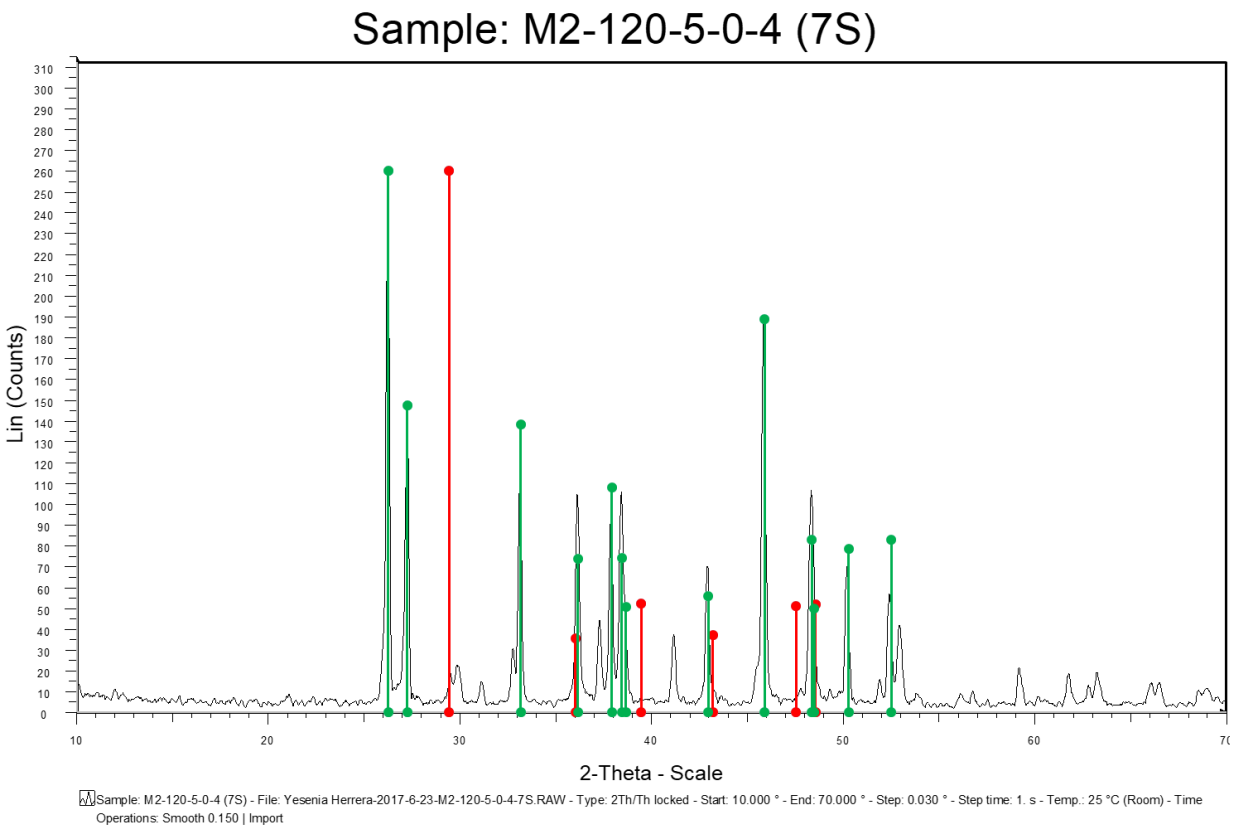
Sample: M2-120-5-0-4 (7S)
Lin (Counts)
2-Theta - Scale
Sample: M2-120-5-0-4 (7S) - File: Yesenia Herrera-2017-6-23-M2-120-5-0-4-7S.RAW - Type: 2Th/Th locked - Start: 10.000 ° - End: 70.000 ° - Step: 0.030 ° - Step time: 1. s - Temp.: 25 °C (Room) - Time
Operations: Smooth 0.150 | Import

Sample: M2-148-0-6 (1)

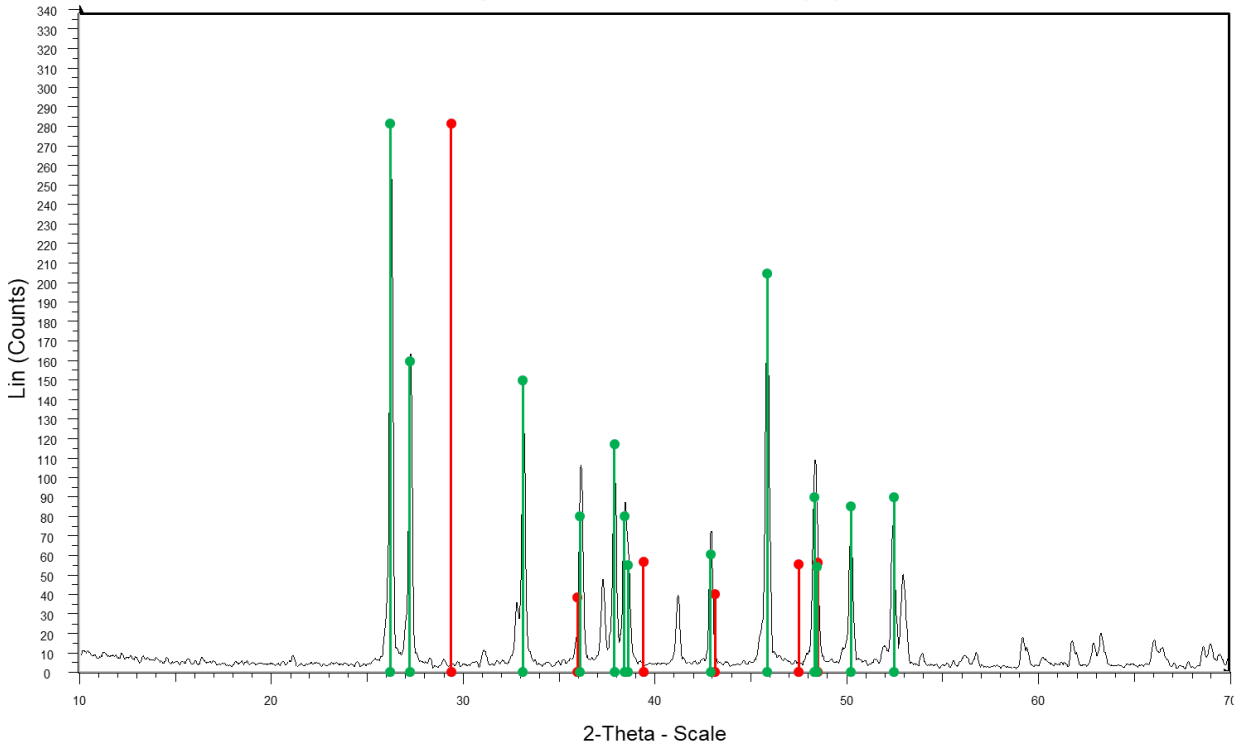

Sample: M2-148-0-6 (1) - File: Yesenia Herrera-2017-6-23-M2-148-0-6-1.RAW - Type: 2Th/Th locked - Start: 10.000 ° - End: 70.000 ° - Step: 0.030 ° - Step time: 1. s - Temp.: 25 °C (Room) - Time Starte
Operations: Smooth 0.150 | Import

Sample: M2-148-0-6 (2)

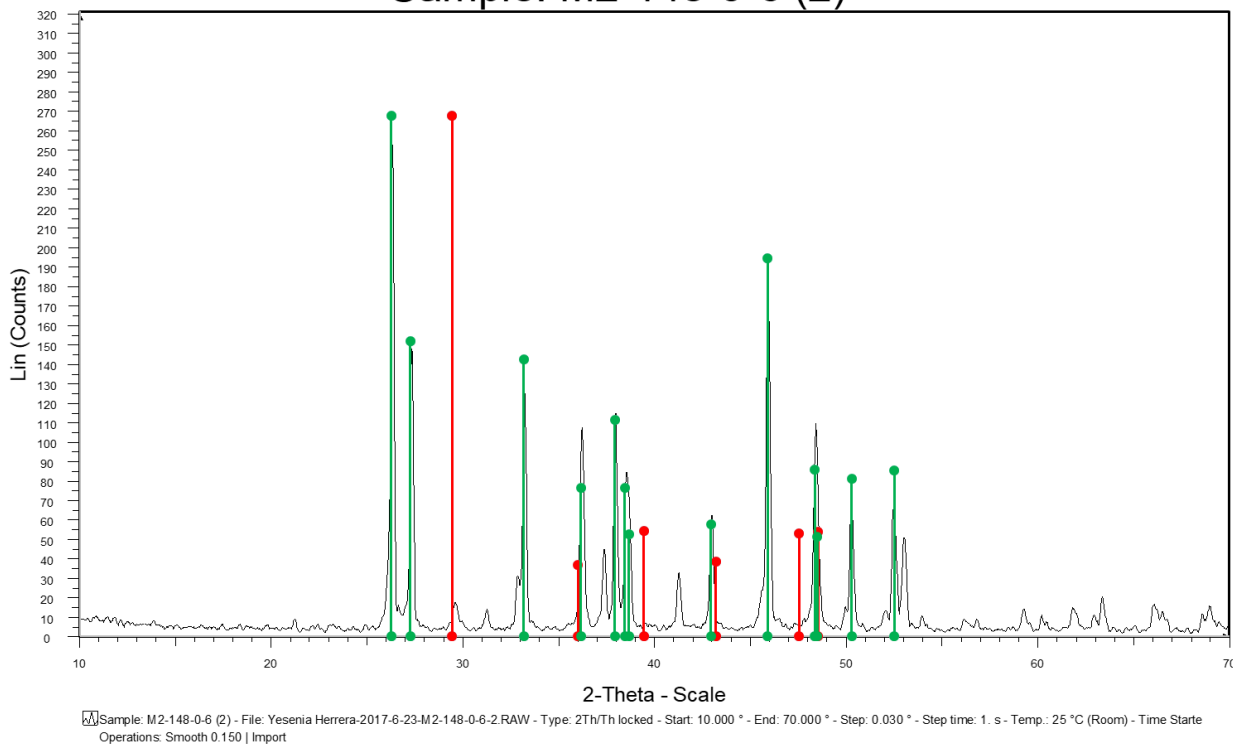

Sample: M2-148-0-6 (2) - File: Yesenia Herrera-2017-6-23-M2-148-0-6-2.RAW - Type: 2Th/Th locked - Start: 10.000 ° - End: 70.000 ° - Step: 0.030 ° - Step time: 1. s - Temp.: 25 °C (Room) - Time Starte
Operations: Smooth 0.150 | Import

Sample: M2-150-7-1-4-(1)

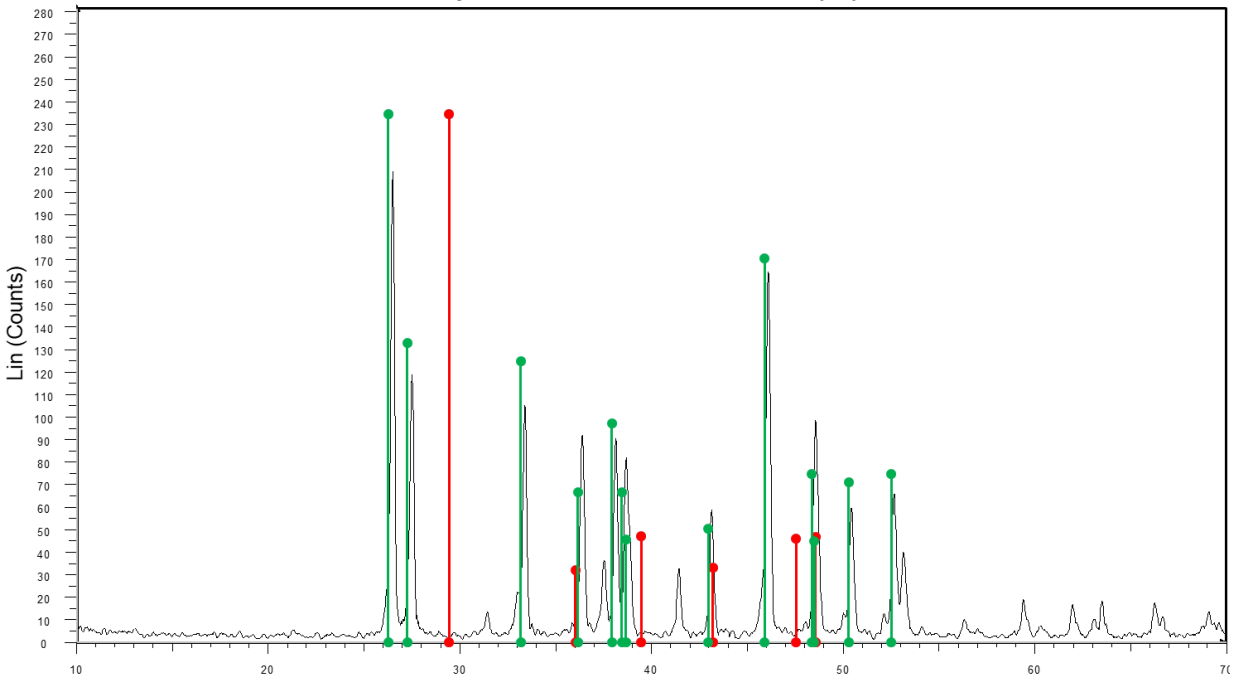

Sample: M2-150-7-1-4-(1) - File: Yesenia Herrera-2017-6-23-M2-150-7-1-4-1.RAW - Type: 2Th/Th locked - Start: 10.000 ° - End: 70.000 ° - Step: 0.030 ° - Step time: 1. s - Temp.: 25 °C (Room) - Time St
Operations: Smooth 0.150 | Import

Sample: M2-150-7-1-4-(2)

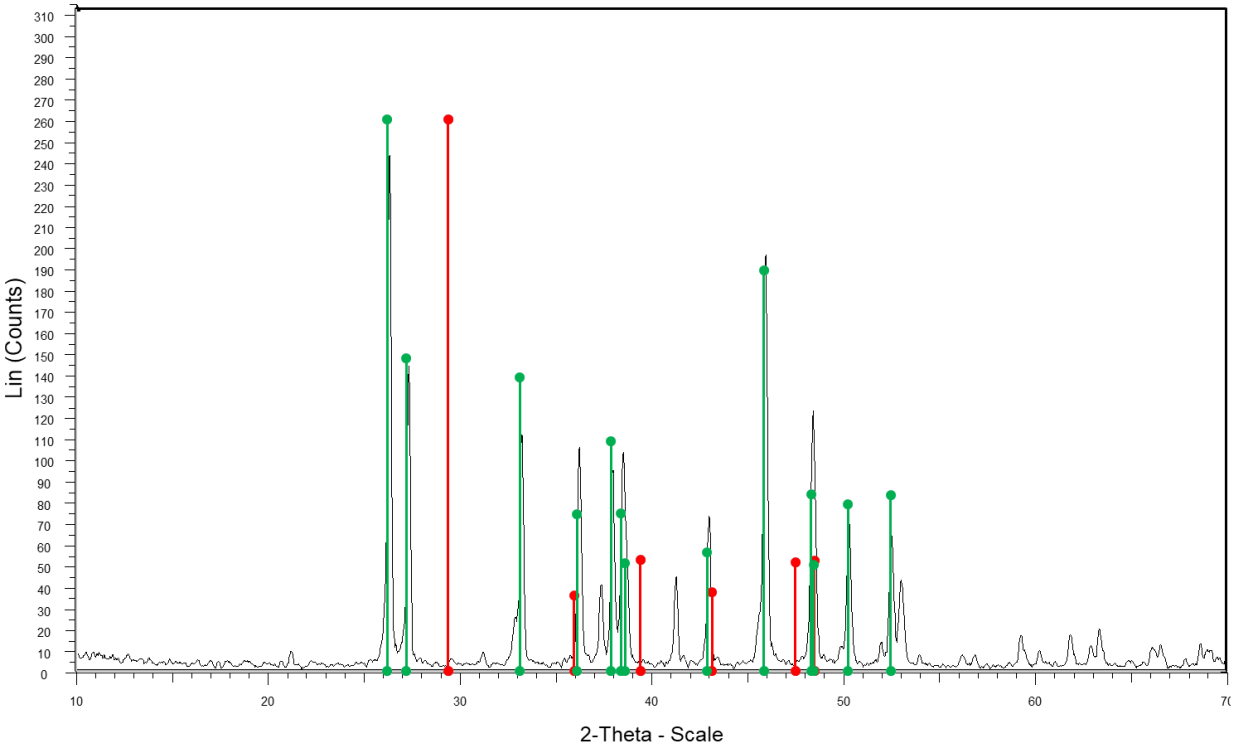

Sample: M2-150-7-1-4-(2) - File: Yesenia Herrera-2017-6-23-M2-150-7-1-4-2.RAW - Type: 2Th/Th locked - Start: 10.000 ° - End: 70.000 ° - Step: 0.030 ° - Step time: 1. s - Temp.: 25 °C (Room) - Time St
Operations: Smooth 0.150 | Import

Sample: M2-145-7-3-1

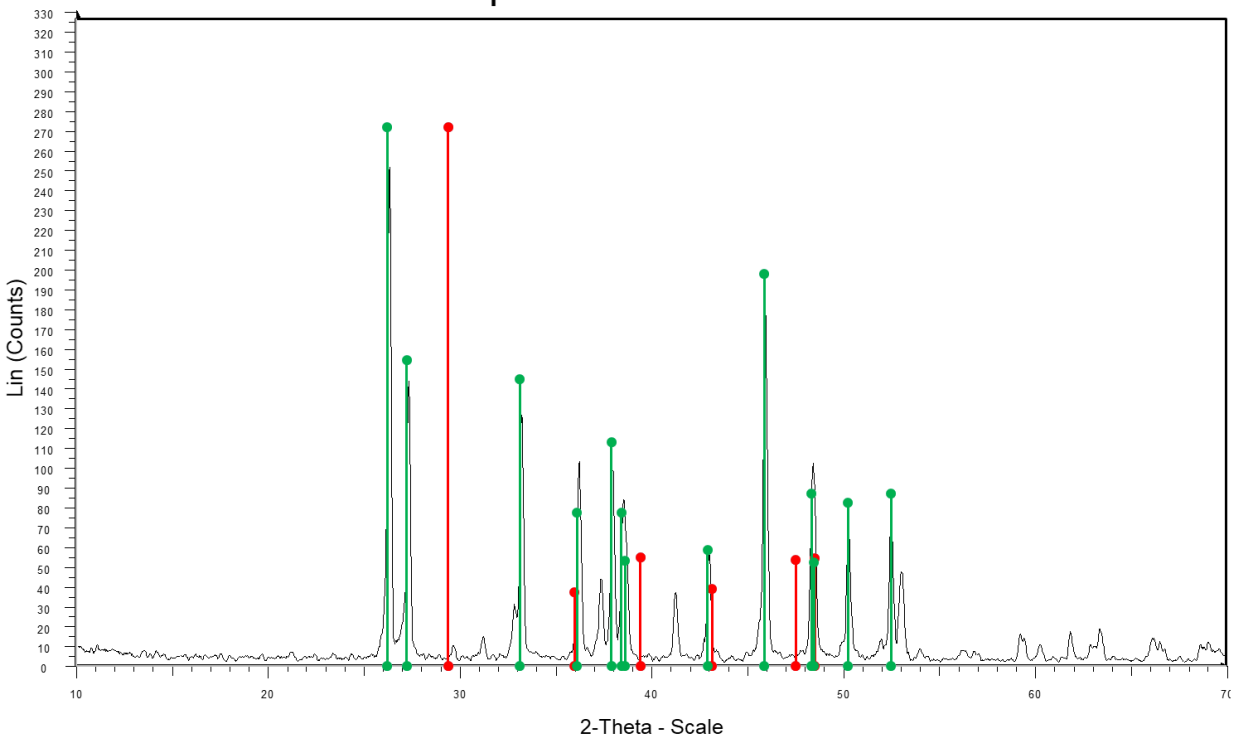

Sample: M2-145-7-3-1 - File: Yesenia Herrera-2017-6-23-M2-145-7-3-1.RAW - Type: 2Th/Th locked - Start: 10.000 ° - End: 70.000 ° - Step: 0.030 ° - Step time: 1. s - Temp.: 25 °C (Room) - Time Started:
Operations: Smooth 0.150 | Import

Sample: M2-144-8-3-1

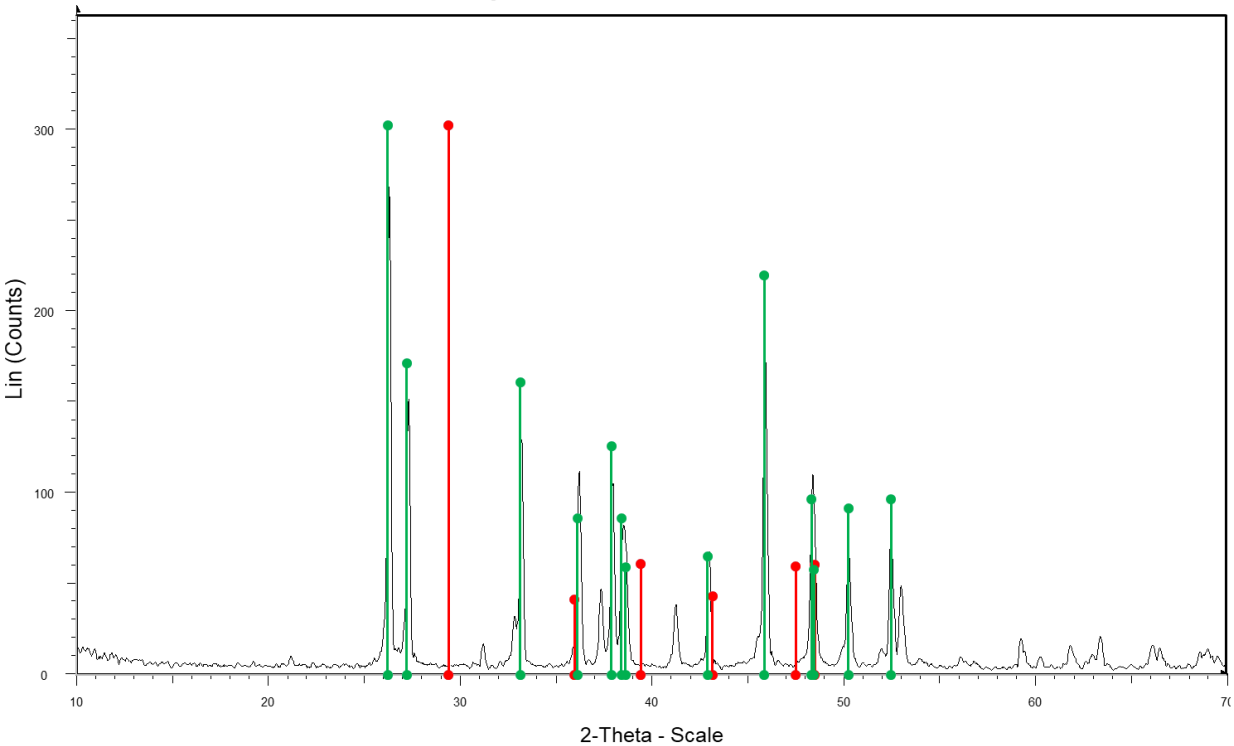

Sample: M2-144-8-3-1 - File: Yesenia Herrera-2017-6-23-M2-144-8-3-1.RAW - Type: 2Th/Th locked - Start: 10.000 ° - End: 70.000 ° - Step: 0.030 ° - Step time: 1. s - Temp.: 25 °C (Room) - Time Started:
Operations: Smooth 0.150 | Import

Sample: M2-120-5-0-5C

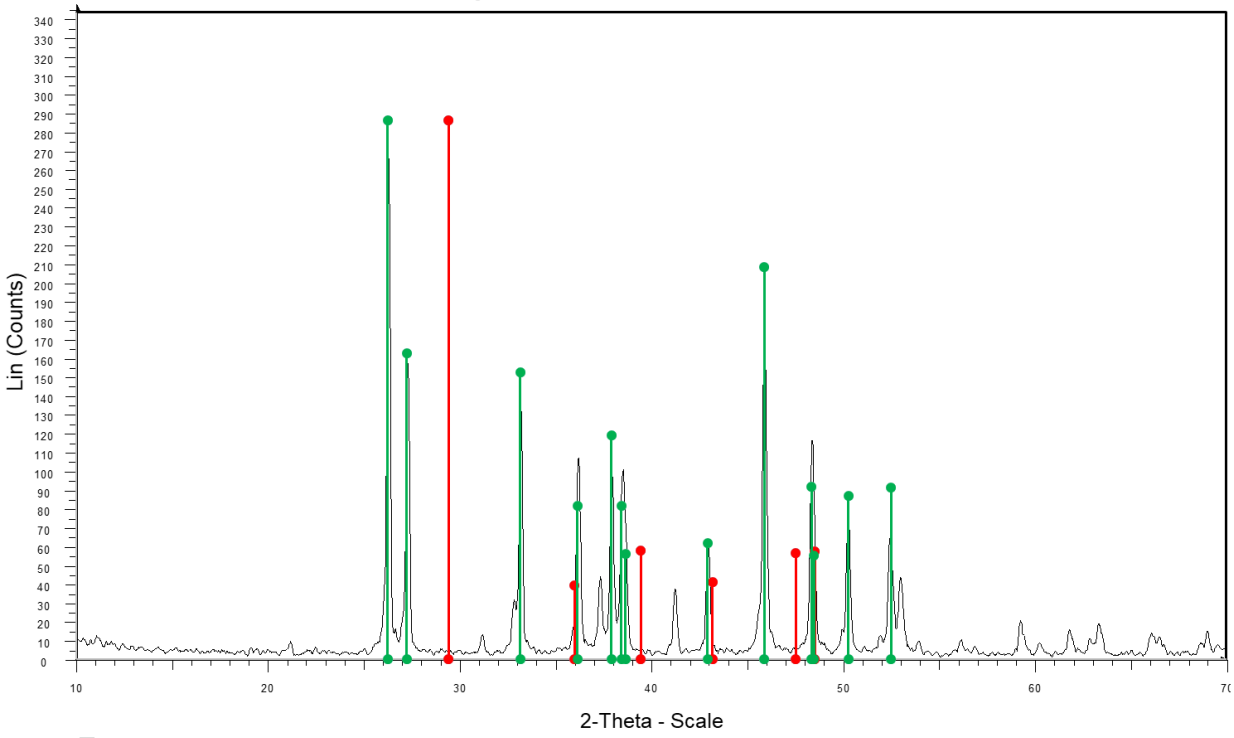

Sample: M2-120-5-0-5C - File: Yesenia Herrera-2017-6-23-M2-120-5-0-5C.RAW - Type: 2Th/Th locked - Start: 10.000 ° - End: 70.000 ° - Step: 0.030 ° - Step time: 1. s - Temp.: 25 °C (Room) - Time Start
Operations: Smooth 0.150 | Import

Sample: M2-134-4-1-2

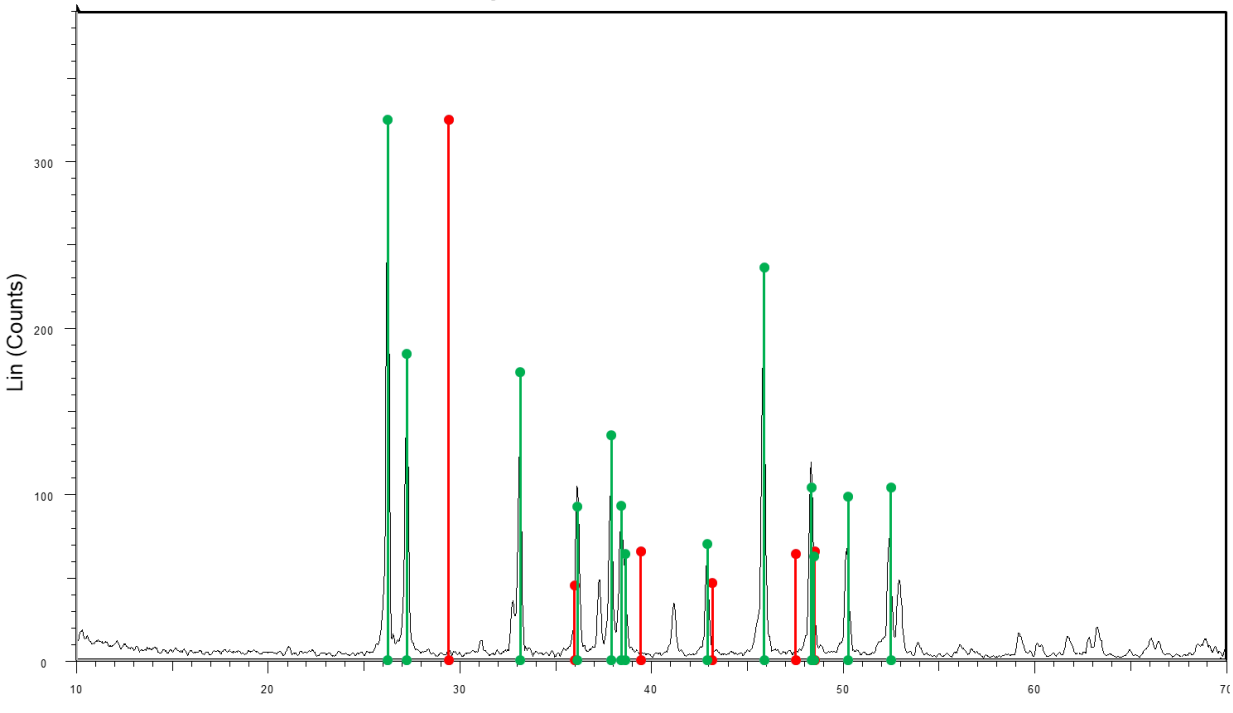

Sample: M2-134-4-1-2 - File: Yesenia Herrera-2017-6-23-M2-134-4-1-2.RAW - Type: 2Th/Th locked - Start: 10.000 ° - End: 70.000 ° - Step: 0.030 ° - Step time: 1. s - Temp.: 25 °C (Room) - Time Started:
Operations: Smooth 0.150 | Import

Sample: M2-140-7-0-7A

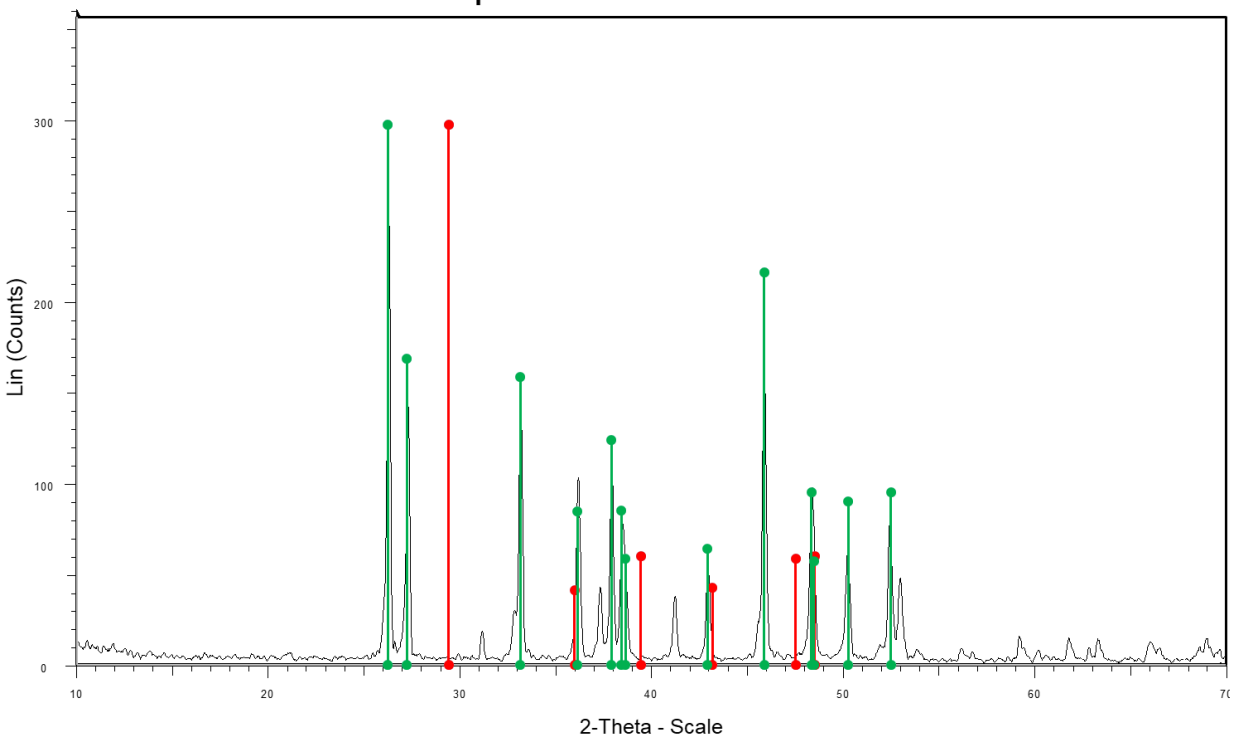

Sample: M2-140-7-0-7A - File: Yesenia Herrera-2017-6-23-M2-140-7-0-7A.RAW - Type: 2Th/Th locked - Start: 10.000 ° - End: 70.000 ° - Step: 0.030 ° - Step time: 1. s - Temp.: 25 °C (Room) - Time Start
Operations: Smooth 0.150 | Import

Sample: M2-136-3-1-1

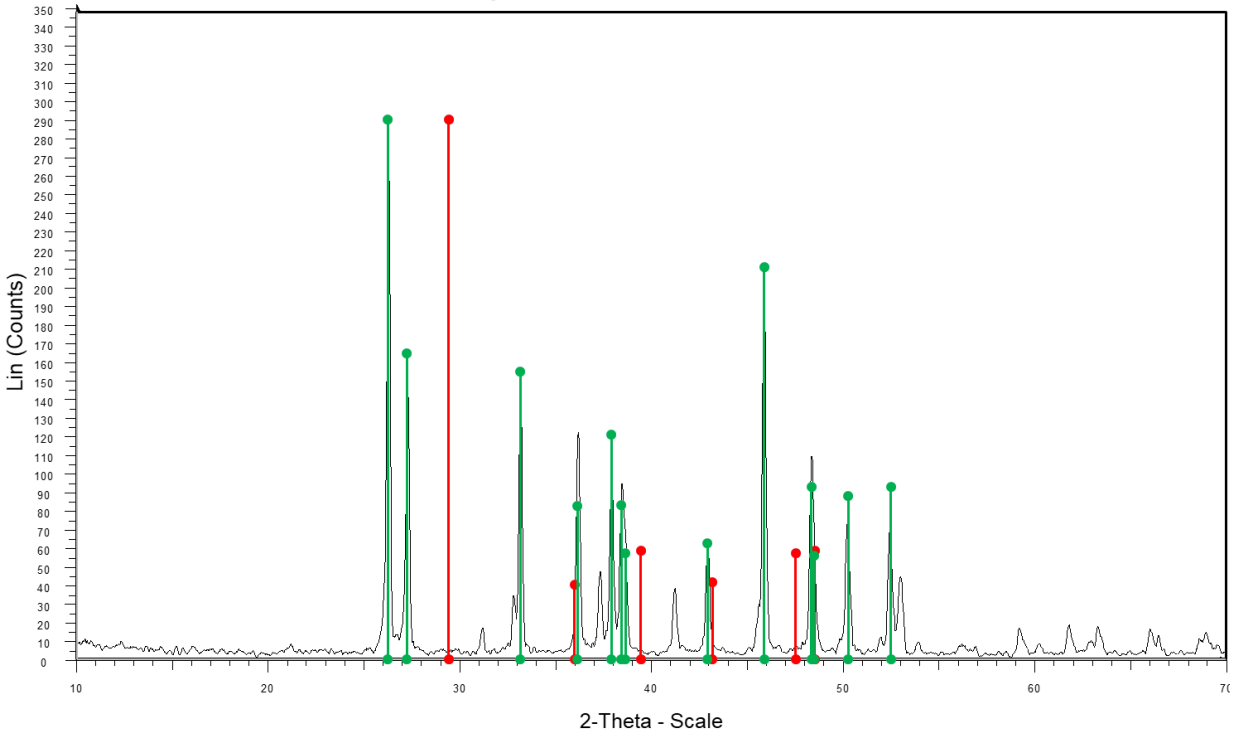

Sample: M2-136-3-1-1 - File: Yesenia Herrera-2017-6-23-M2-136-3-1-1.RAW - Type: 2Th/Th locked - Start: 10.000 ° - End: 70.000 ° - Step: 0.030 ° - Step time: 1. s - Temp.: 25 °C (Room) - Time Started:
Operations: Smooth 0.150 | Import

Sample: M2-140-0-0-8

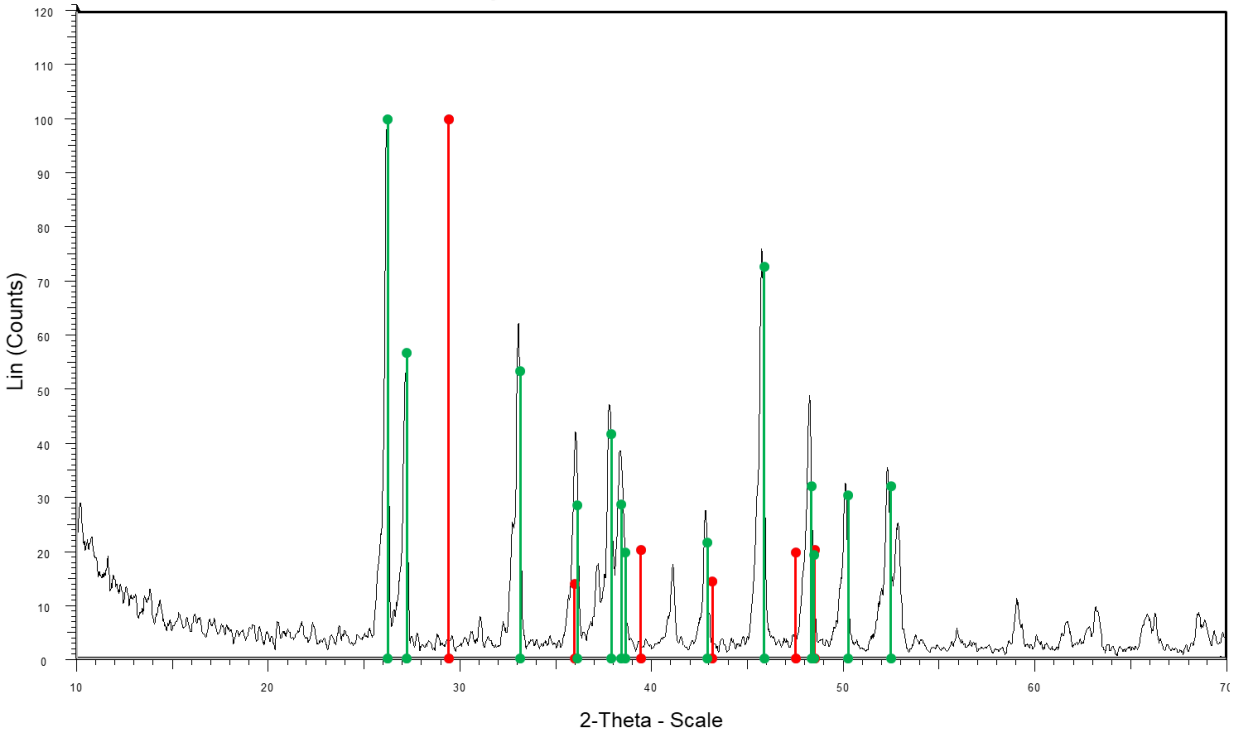

Sample: M2-140-0-0-8 - File: Yesenia Herrera-2017-6-23-M2-140-0-0-8.RAW - Type: 2Th/Th locked - Start: 10.000 ° - End: 70.000 ° - Step: 0.030 ° - Step time: 1. s - Temp.: 25 °C (Room) - Time Started:
Operations: Smooth 0.150 | Import

Sample: M2-120-4-1-5

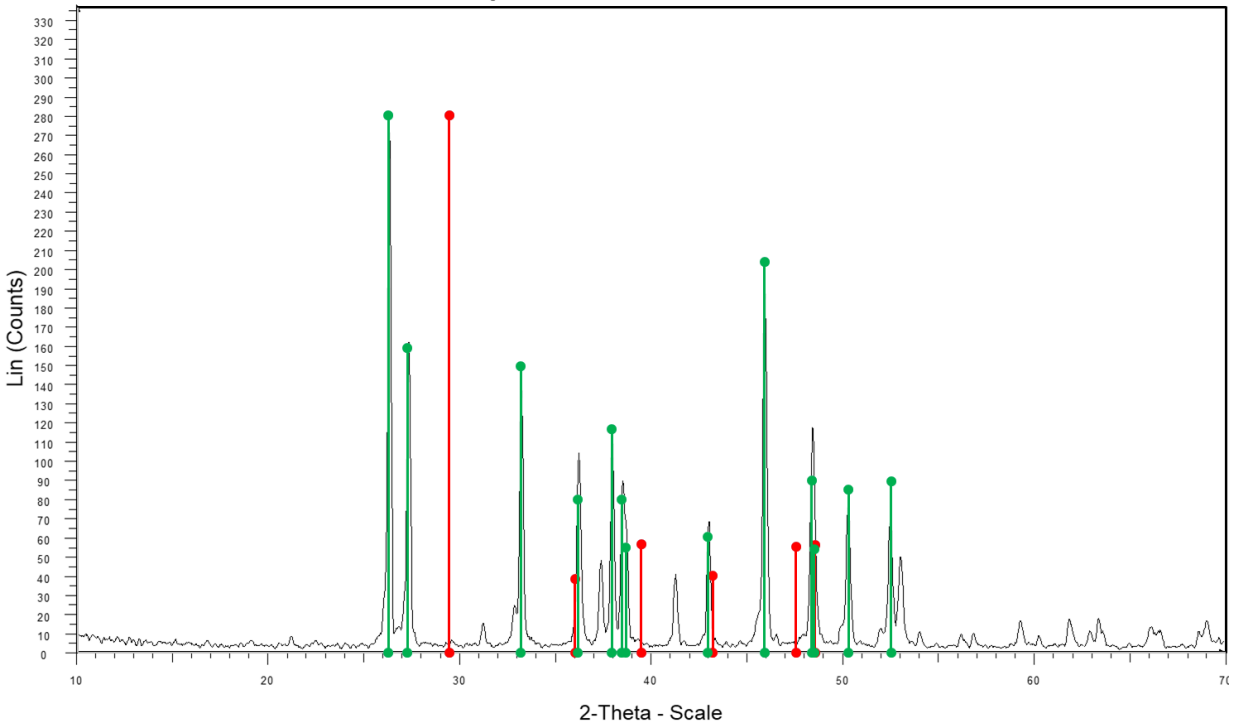

Sample: M2-120-4-1-5 - File: Yesenia Herrera-2017-6-23-M2-120-4-1-5.RAW - Type: 2Th/Th locked - Start: 10.000 ° - End: 70.000 ° - Step: 0.030 ° - Step time: 1. s - Temp.: 25 °C (Room) - Time Started:
Operations: Smooth 0.150 | Import

Appendix 2: M2 Facies Growth Rate Transects

The following figures are transects taken from coral radiographies of samples M2 148-0.6, M2140.7-0.7a, M2 140.7-0.7b, M2 150.7-1.3, M2 120.5-0.5, M2 140.0-0.8, M2134.4-1.2, M2 136.3-1.1, M2144.8-3.1, and M2 145.7-3.1. Transects were analyzed in CoralXDS which uses Luminance as a proxy for relative density. Red dots and yellow bars correspond to high density bands and green dots and grey bands correspond to low density bands. In the radiography transect lighter grey-white sections are higher density and dark grey areas are lower density.

M2 148-0.6

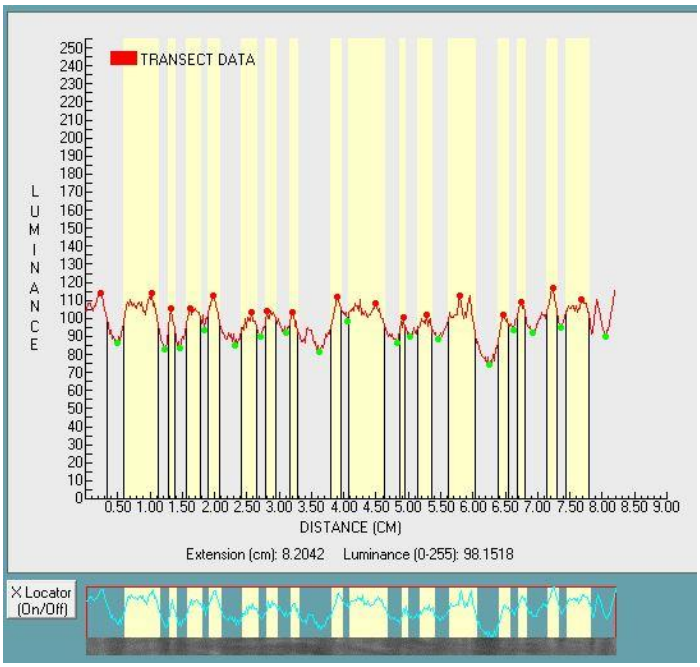

M2140.7-0.7a

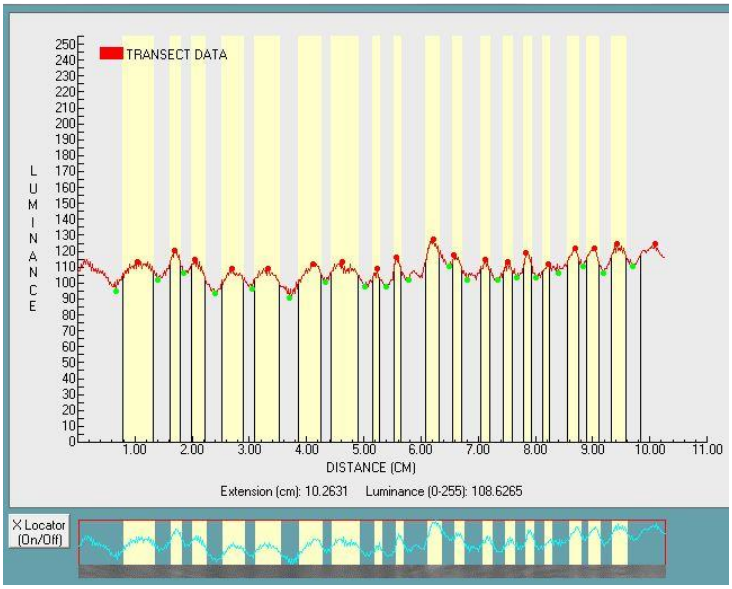

M2 140.7-0.7b

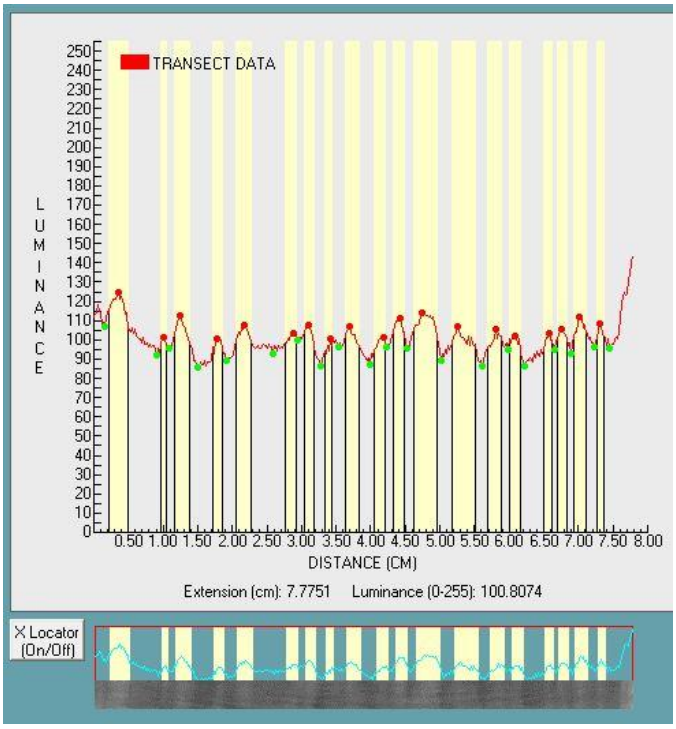

M2 150.7-1.3

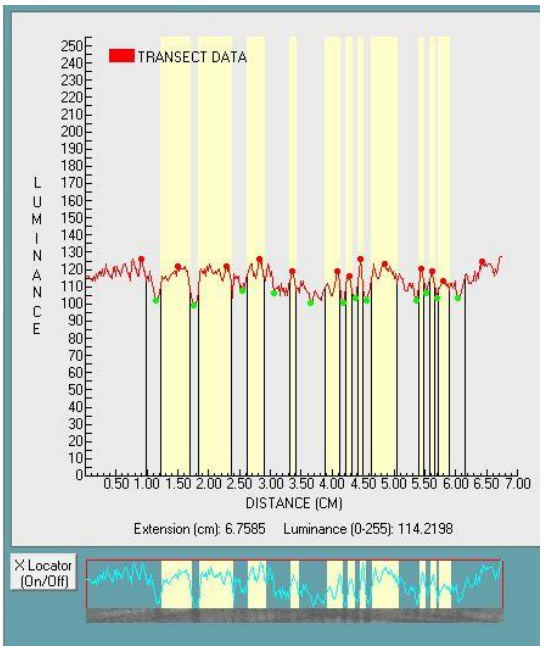

M2 120.5-0.5

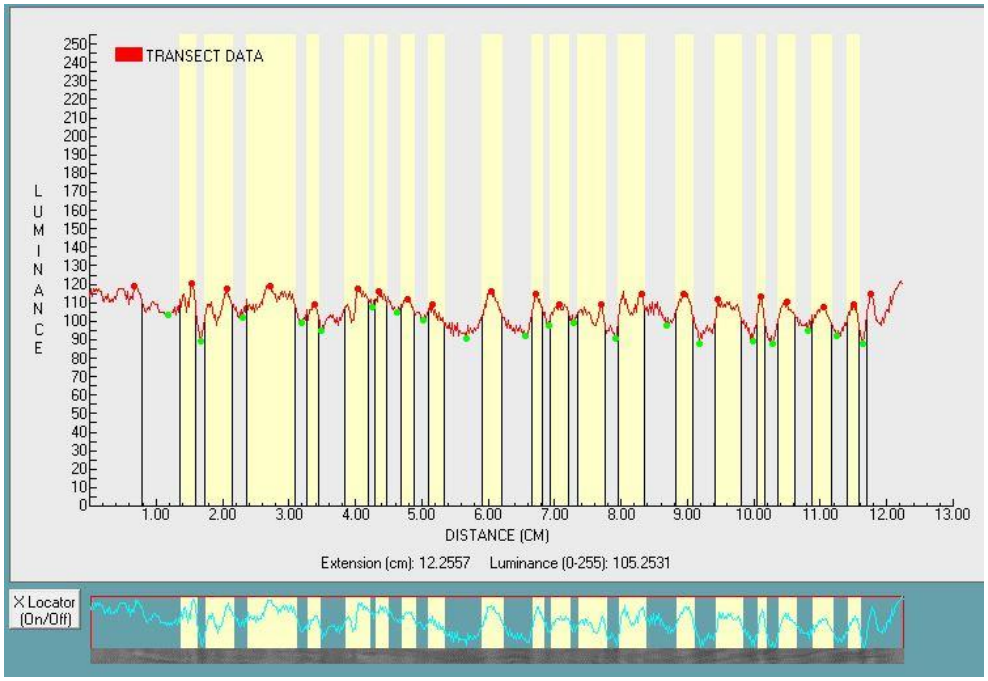

M2 140.0-0.8

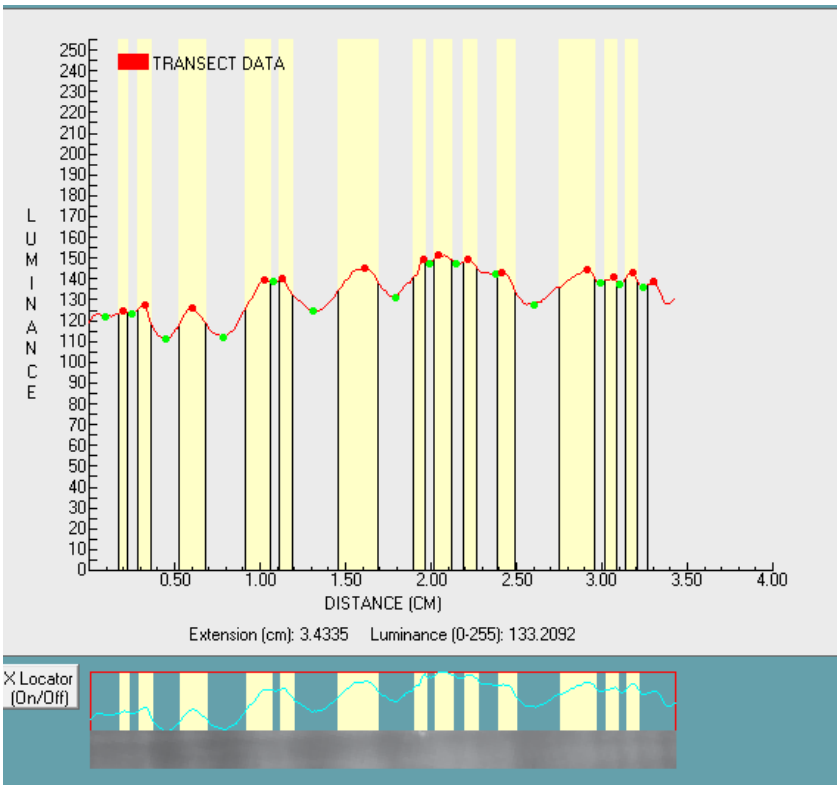

M2134.4-1.2

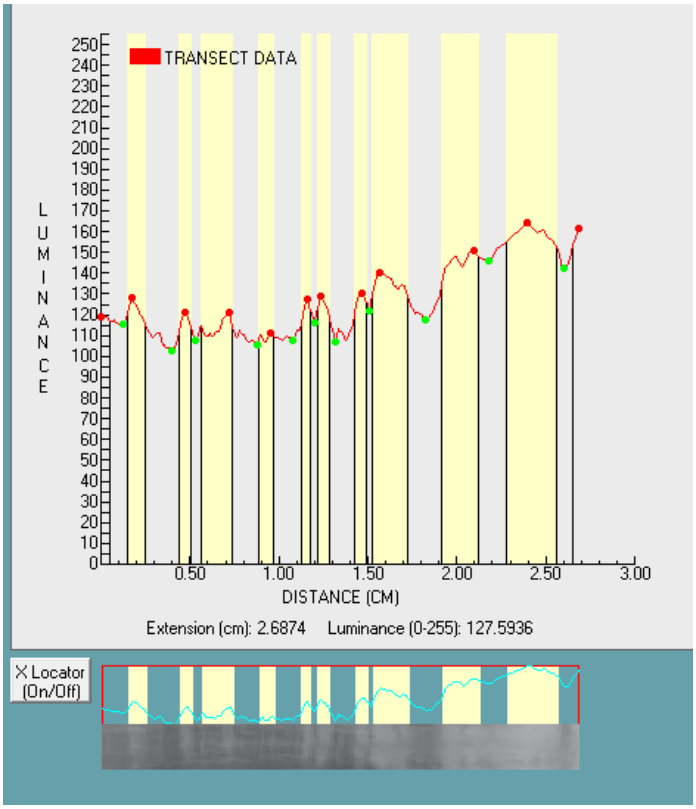

M2 136.3-1.1

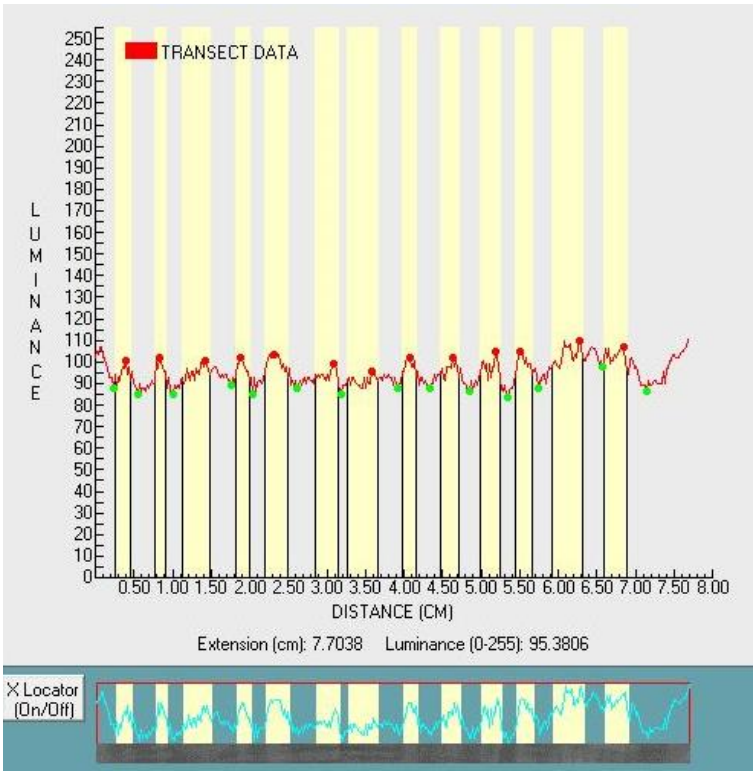

M2144.8-3.1

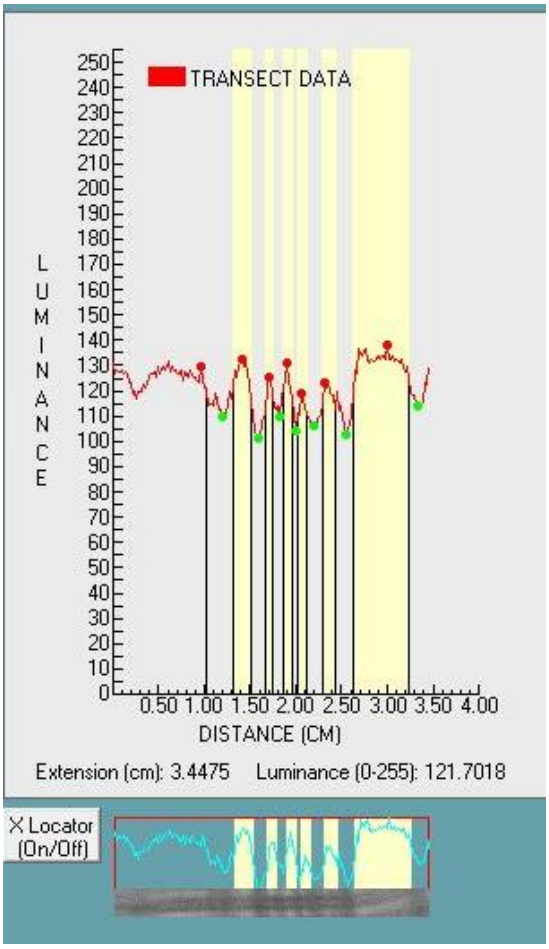

M2 145.7-3.1

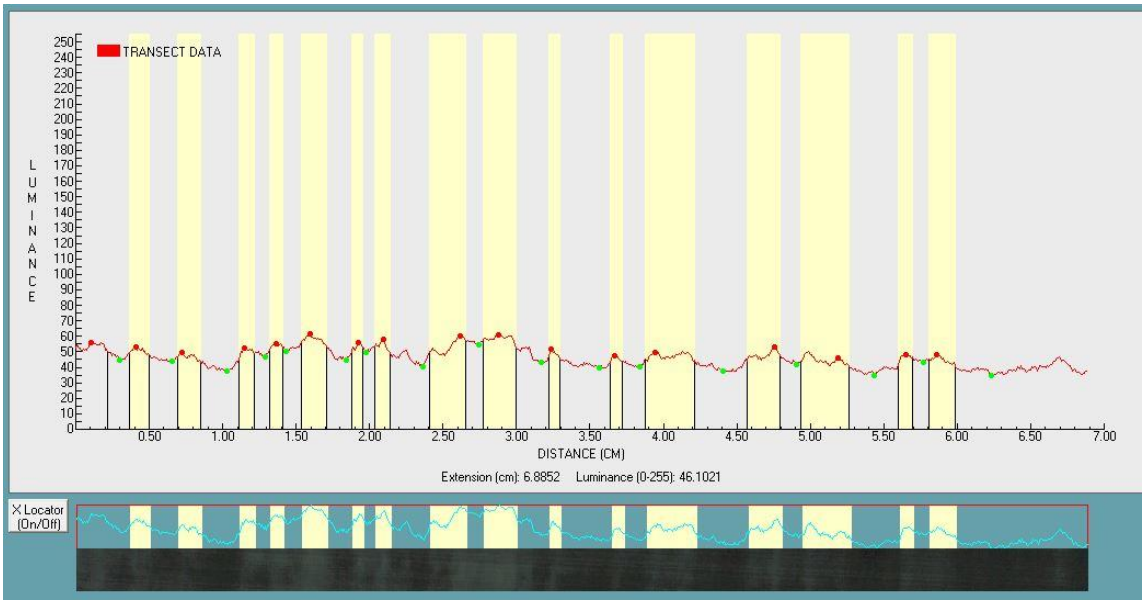

Appendix 3: Cañada Honda Coral Growth Rates by Facies

Facies	Author	Sample ID	Growth Rate (mm)	Growth Rate Error (stdv)
M1 Facies	Diaz, 2005	M1-30	2.78	0.72
	Diaz, 2005	M1-13	2.3	0.2
	Cuevas et al., 2005	M1	2.6	0.18
	Cuevas et al., 2005	M1	2.8	0.7
	Cuevas et al., 2005	M1	2.3	0.02
	Cuevas et al., 2005	M1	3.2	1.3
	Cuevas, 2010	M1-5	0.91	0.13
	Cuevas, 2010	M1-10	2.8	0.37
	Cuevas, 2010	M1-13	2.48	0.19
	Cuevas, 2010	M1-30	2.886	0.04
	Morales, 2015	M1-1Dc	3.55	0.37
	Morales, 2015	M1-1Ee	3.06	0.45
	Morales, 2015	M1-2Ba	2.62	0.48
	Morales, 2015	M1-2E	2.58	0.2
	Morales, 2015	M1-1Gb	2.07	0.14
M2 Facies	Cuevas, 2010	M2-6	3.63	0.24
	Cuevas, 2010	M2-10	1.75	0.17
	Cuevas, 2010	M2-11	1.42	0.14
	Cuevas, 2010	M2-17	3.13	0.45
	Cuevas, 2010	M2-21	2.78	0.62
	Cuevas et al., 2005	M2	1.3	0.7
	Cuevas et al., 2005	M2	1.8	0.45
	Cuevas et al., 2005	M2	3.4	0.5
	Cuevas et al., 2005	M2	4.5	1.6
	Diaz, 2005	M2-10	1.88	0.4
	Diaz, 2005	M2-6	3.44	0.5
	Jimenez, 2018	M2-135	1.95	1
	Jimenez, 2018	M2-146.7	1.98	0.7
	This study	M2120.5-0.5	5.44	0.43
	This study	M2-148-0.6	4.56	0.46
	This study	M2-140.7-0.7b	5.02	0.34
	This study	M2-140.7-0.7a	3.91	0.38
	This study	M2-136.3-1.1	5.28	0.34
	This study	M2-150.7-1.3	4.47	0.72
	This study	M2-144.8-3.1	2.6	0.34
	This study	M2-145.7-3.1	3.63	0.39
	This study	M2-134.4-1.2	2.5	0.35
	This study	M2-140-0.8	2.38	0.3
MZ Facies	Jimenez, 2018	MZ-172.2	1.32	0.9
	Rodriguez 2018	Mz CH-202	4.8	0.026

	Cuevas et al., 2005	MZ	2.4	1.1
	Cuevas et al., 2005	MZ	3.7	0.8
	Cuevas et al., 2005	MZ	3.6	0.9
	Arana, 2018	MZ 165.9-0.3	4.72	0.15
	Arana, 2018	MZ 198.4-0.9	4.91	0.18
	Arana, 2018	MZ 164.1-1.2	5.18	0.17
	Arana, 2018	MZ 118.6-2.1	4.71	0.12
	Arana, 2018	MZ 154.7-2.3	4.63	0.2
	Arana, 2018	MZ 202.4-2.7	4.53	0.12
	Arana, 2018	MZ 148.8-3.3	4.43	0.17
	Cuevas, 2010	Mz-10	3.51	0.79
	Cuevas, 2010	Mz-14	3.05	0.49
	Cuevas, 2010	Mz-16	4.1	0.35
	Cuevas, 2010	Mz-29	4.37	0.42
M3 Facies	Jimenez, 2018	M3-4	1.82	0.83
	Jimenez, 2018	M3-1	1.93	0.82
	Cuevas et al., 2005	M3	1.7	0.8
	Cuevas, 2010	M3-8	1.89	0.32
	Cuevas, 2010	M3-18	2.99	0.55
	Cuevas, 2010	M3-20	2.13	0.53
	Rodriguez 2018	MZ CH-232	5.4	0.026

Appendix 4: Sedimentation Rates

Figure 1 (left) and 2 (right) are transect images and CoralXDS luminance analysis of two foliations used to calculate sedimentation rates for coral M2 136.3-1.1.

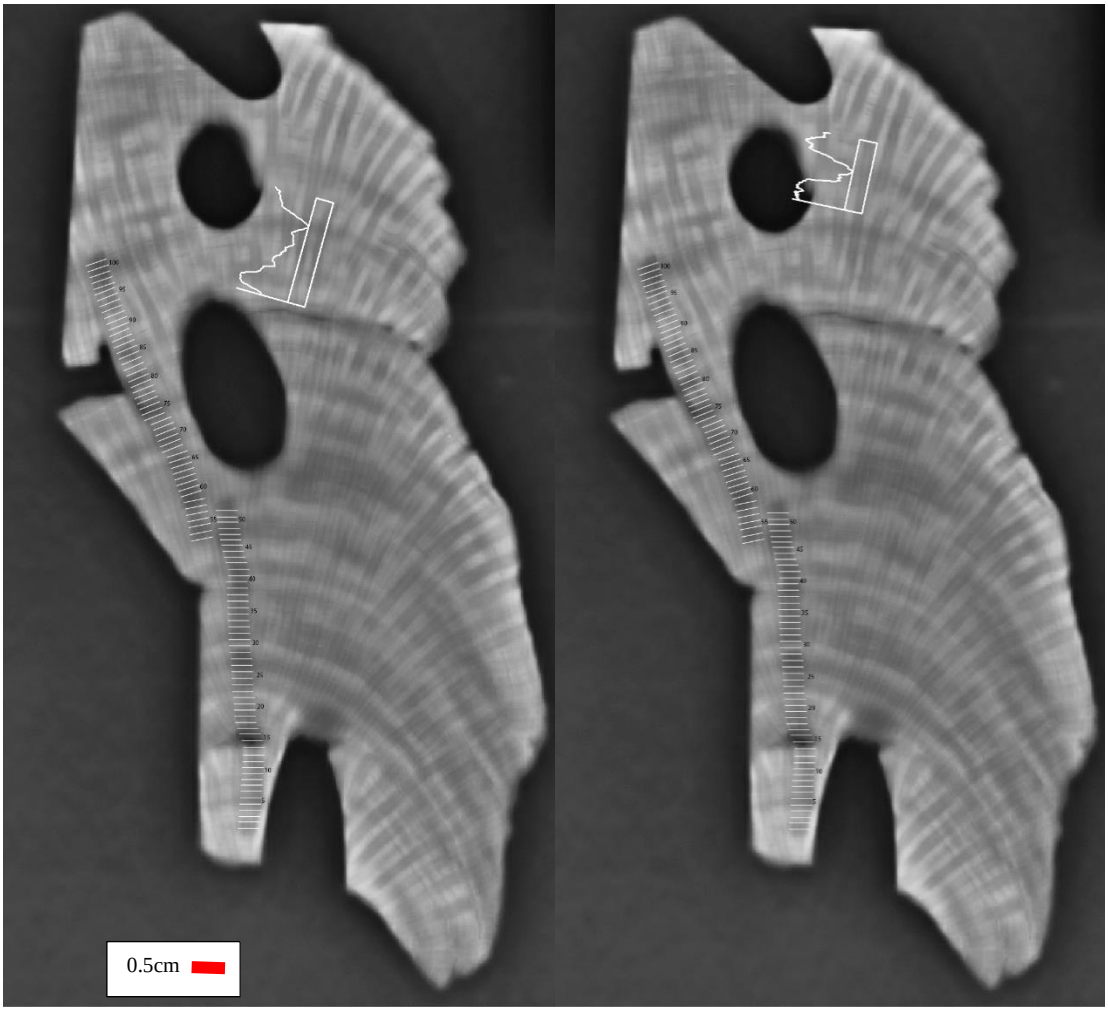

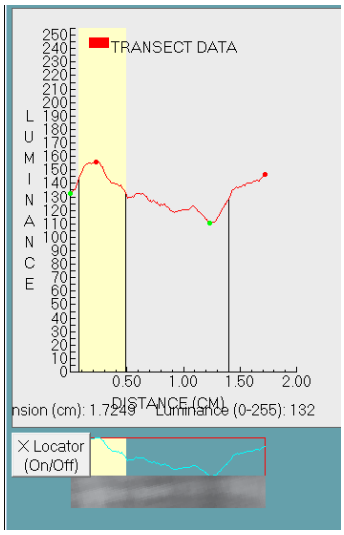

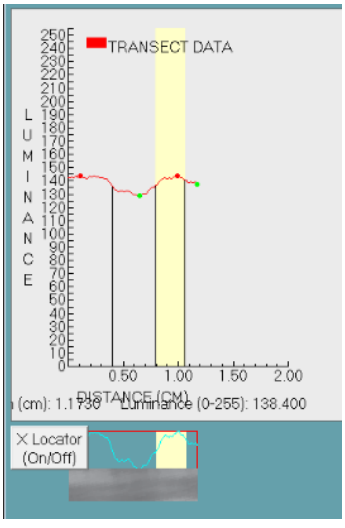

Appendix 5: Stable Isotope Data

Stable isotope ($\delta^{13}C$ and $\delta^{18}O$) data and $\delta^{18}O$-SST for each coral is listed below. Corals are listed in order from oldest to youngest.

M2 140.7-0.7b (7518±46)			
Sample	δ13C (‰)	δ18O (‰)	Average δ18O-SST (°C)
1	-4.05	-2.87	15.31
2	-5.11	-2.45	13.04
3	-3.87	-2.22	11.83
4	-4.31	-2.89	15.41
5	-4.82	-2.25	11.98
6	-3.70	-2.26	12.06
7	-4.68	-2.68	14.30
8			
9	-4.10	-2.49	13.26
10			
11	-4.28	-2.67	14.21
12	-4.32	-2.91	15.50
13	-4.62	-2.62	13.95
14	-4.84	-3.03	16.17
15	-3.84	-2.48	13.21
16	-4.88	-3.18	16.97
17	-4.29	-2.25	11.99
18	-3.51	-2.26	12.06
19	-4.93	-2.88	15.33
20	-3.58	-2.27	12.08
21	-4.36	-2.82	15.02
22	-4.56	-2.09	11.15
23	-3.95	-2.45	13.05
24	-4.58	-2.25	12.00
25	-3.93	-2.36	12.58
26	-5.18	-2.47	13.18
27	-4.14	-1.95	10.40
28	-4.11	-2.25	12.00
29	-4.21	-1.94	10.36
30			
31			
32	-3.74	-1.52	8.09
33	-4.06	-1.76	9.36
34	-4.19	-1.59	8.49
35	-3.44	-1.59	8.48

36	-4.20	-2.03	10.83
37	-4.24	-1.78	9.49
38	-3.67	-1.71	9.11
39	-4.87	-2.39	12.74
40	-4.61	-2.24	11.94
41	-3.78	-2.02	10.75
42	-4.00	-2.40	12.79
43	-4.50	-2.47	13.16
44	-3.82	-1.66	8.85
45	-3.79	-2.15	11.48
46	-4.19	-2.32	12.38
47	-3.74	-1.90	10.13
48	-3.19	-1.82	9.71
49	-3.85	-2.53	13.49
50	-3.97	-2.19	11.67
51	-3.42	-1.68	8.97
52	-4.28	-2.03	10.81
53	-3.56	-1.95	10.37
54	-3.30	-2.01	10.73
55	-3.80	-2.47	13.16
56	-4.60	-2.57	13.69
57	-3.80	-2.28	12.15
58	-3.75	-2.24	11.92
59	-4.05	-2.73	14.55
60	-3.83	-2.25	12.02
61	-3.39	-2.44	12.99
62	-4.10	-2.49	13.27
63	-3.71	-2.33	12.40
64	-3.92	-2.53	13.50
65	-4.03	-2.38	12.69
66	-3.31	-2.23	11.91
67	-3.48	-2.51	13.38
68	-3.68	-2.01	10.72
69	-3.05	-1.90	10.10
70	-3.53	-1.90	10.14
71	-3.22	-1.96	10.45
72	-4.18	-2.40	12.79
73	-3.26	-1.86	9.91
74	-3.33	-2.20	11.73
75	-3.08	-1.75	9.34
76	-3.22	-2.02	10.74
77	-4.33	-2.16	11.50

M2 140.7-0.7a (7508±46)			
Sample	δ13C (‰)	δ18O (‰)	Average δ18O-SST (°C)
1	-4.21	-1.94	10.32
2	-2.95	-1.80	9.62
3	-4.06	-2.53	13.50
4	-4.09	-2.30	12.23
5	-3.60	-1.97	10.51
6	-3.83	-2.44	12.99
7	-3.52	-2.33	12.44
8	-3.52	-2.28	12.15
9	-3.76	-2.14	11.39
10	-3.17	-2.31	12.30
11	-3.42	-2.33	12.43
12	-3.33	-2.03	10.84
13	-3.27	-2.40	12.77
14	-3.74	-2.71	14.43
15	-3.30	-2.00	10.66
16	-3.13	-1.89	10.09
17	-3.75	-1.88	10.04
18	-2.70	-1.70	9.04
19	-3.93	-2.50	13.31
20	-3.33	-1.69	9.03
21	-3.05	-1.96	10.45
22	-3.68	-1.89	10.08
23	-3.25	-1.66	8.86
24	-3.20	-2.05	10.91
25	-4.47	-2.24	11.94
26	-3.48	-1.64	8.75
27	-3.94	-2.04	10.90
28	-4.38	-1.79	9.55
29	-3.16	-1.76	9.38
30	-3.44	-2.08	11.08
31	-4.23	-2.18	11.61
32	-3.74	-1.78	9.48
33	-3.67	-2.25	12.00
34	-3.93	-2.19	11.68
35	-3.44	-2.24	11.93
36	-4.34	-2.57	13.70
37	-3.83	-1.96	10.44
38	-3.15	-1.87	9.99
39	-3.76	-2.51	13.36
40	-3.63	-2.07	11.04

41	-3.36	-1.90	10.11
42	-3.83	-2.46	13.10
43	-4.00	-1.96	10.46
44	-3.24	-1.53	8.14
45	-3.39	-1.92	10.25
46	-4.07	-2.18	11.60
47	-3.40	-1.43	7.60
48	-3.35	-1.67	8.88
49	-3.94	-1.77	9.42
50	-3.39	-1.56	8.34
51			
52	-3.37	-1.40	7.48
53	-4.26	-2.01	10.72
54	-4.11	-1.45	7.73
55	-3.44	-1.37	7.30
56	-4.12	-2.03	10.82
57	-4.11	-1.95	10.39
58	-3.58	-2.13	11.35
59	-4.70	-2.52	13.43
60	-4.21	-2.09	11.14
61	-3.96	-2.17	11.57
62	-4.96	-2.59	13.80
63	-4.29	-2.12	11.30
64			
65	-4.70	-2.85	15.19
66	-5.17	-2.50	13.33

M2 120.5-0.5 (7440±46)			
Sample	δ13C (‰)	δ18O (‰)	Average δ18O-SST (°C)
1	-3.82	-2.08	11.08
2	-4.29	-2.55	13.57
3	-3.15	-2.04	10.85
4	-3.88	-2.22	11.82
5	-3.05	-1.67	8.91
6	-3.47	-2.16	11.49
7	-3.95	-2.20	11.75
8	-3.69	-1.86	9.89
9	-3.47	-1.67	8.92
10	-4.12	-2.25	12.02
11	-4.19	-1.81	9.64
12	-3.49	-1.71	9.12
13	-3.77	-2.07	11.03
14	-3.89	-1.95	10.37
15	-3.26	-1.76	9.38
16	-3.89	-1.99	10.61
17	-4.08	-1.76	9.37
18	-3.52	-1.70	9.08
19	-4.31	-2.18	11.62
20	-3.60	-1.57	8.36
21	-3.40	-1.74	9.26
22	-4.21	-1.99	10.60
23	-4.09	-1.90	10.10
24	-3.85	-1.75	9.30
25	-4.37	-2.00	10.65
26	-4.11	-1.78	9.51
27	-4.20	-1.94	10.35
28	-4.47	-2.18	11.59
29	-3.98	-1.57	8.36
30	-4.18	-1.87	9.95
31	-4.27	-2.20	11.73
32	-4.98	-2.36	12.60
33	-3.80	-1.88	10.03
34	-3.84	-1.88	10.02
35	-4.08	-2.21	11.80
36	-4.61	-2.67	14.21
37	-5.18	-2.41	12.82
38	-4.66	-2.38	12.70
39	-3.76	-1.95	10.40
40	-4.26	-2.11	11.26

41	-4.06	-2.21	11.75
42	-4.39	-2.01	10.71
43	-3.90	-2.18	11.60
44	-4.54	-2.29	12.18
45	-4.03	-1.98	10.54
46	-4.02	-2.17	11.59
47	-4.82	-2.28	12.17
48	-3.53	-1.86	9.90
49	-3.65	-2.06	10.96
50	-4.28	-2.13	11.33
51	-3.40	-1.84	9.78
52	-4.16	-2.26	12.04
53	-3.76	-1.45	7.73
54	-3.85	-2.15	11.47
55	-4.64	-2.35	12.53
56	-3.74	-1.77	9.43
57	-4.03	-2.17	11.57
58	-2.95	-1.92	10.23
59	-3.09	-1.58	8.42
60	-3.53	-1.52	8.10
61	-3.59	-1.76	9.38
62	-3.44	-1.83	9.75
63	-3.45	-1.70	9.06
64	-3.34	-1.39	7.41
65	-4.02	-1.69	9.01
66	-4.13	-2.00	10.66

M2 140.0-0.8			
Sample	δ13C (‰)	δ18O (‰)	Average δ18O-SST (°C)
1	-3.41	-3.90	20.78
2	-1.90	-2.95	15.75
3	-1.78	-3.38	18.00
4	-2.89	-2.97	15.83
5	-1.53	-3.07	16.37
6	-2.78	-3.27	17.45
7	-2.77	-2.66	14.20
8	-1.58	-3.09	16.49
9	-2.58	-3.23	17.22
10	-2.11	-2.52	13.45
11	-1.69	-3.16	16.83
12	-2.88	-3.57	19.02
13	-1.80	-2.23	11.90
14	-1.56	-3.20	17.06
15	-1.52	-2.49	13.27
16	-2.34	-2.92	15.55
17	-1.63	-2.33	12.44
18	-2.39	-2.51	13.38
19	-2.20	-3.41	18.17
20	-1.89	-2.79	14.89
21	-2.16	-2.87	15.32
22	-2.11	-2.76	14.69
23	-1.69	-2.64	14.05
24	-2.52	-2.84	15.15
25	-1.72	-2.59	13.80
26	-2.56	-3.29	17.53
27	-2.22	-2.67	14.25
28	-1.41	-2.38	12.67
29	-2.29	-2.96	15.78
30	-1.41	-2.77	14.78
31	-2.81	-3.37	17.96
32	-1.59	-3.03	16.17
33	-2.41	-2.79	14.88
34	-2.72	-3.47	18.51
35	-2.05	-3.06	16.30
36	-3.31	-3.59	19.14
37	-2.10	-2.97	15.82
38	-1.67	-3.13	16.66
39	-3.10	-3.67	19.59
40	-1.75	-2.94	15.69

41	-2.08	-2.86	15.26
42	-1.83	-2.88	15.38
43	-1.94	-2.79	14.89
44	-1.62	-2.74	14.61
45	-2.93	-3.06	16.30
46	-1.68	-3.01	16.05
47	-2.31	-3.49	18.58
48	-3.16	-3.49	18.62
49	-1.49	-2.72	14.48
50	-2.10	-3.15	16.79
51	-2.94	-3.17	16.90
52	-1.41	-2.72	14.48
53	-2.43	-3.32	17.70
54	-1.76	-2.77	14.75
55	-2.38	-3.13	16.68
56	-1.58	-3.21	17.13
57	-2.61	-3.34	17.79
58	-1.53	-3.21	17.11
59	-1.71	-3.17	16.91
60	-2.00	-2.92	15.54
61	-2.02	-2.99	15.95
62			
63	-2.90	-3.15	16.80
64	-1.98	-2.56	13.65
65	-1.59	-3.31	17.64
66	-2.08	-3.23	17.22

M2 120.4-1.5			
Sample	δ13C (‰)	δ18O (‰)	Average δ18O-SST (°C)
1	-3.85	-2.52	13.43
2	-2.57	-2.38	12.71
3	-3.71	-2.93	15.59
4	-3.25	-2.29	12.19
5	-2.93	-2.58	13.75
6	-3.25	-2.23	11.90
7	-2.47	-2.45	13.07
8	-3.58	-2.65	14.14
9	-2.44	-2.12	11.30
10	-3.18	-2.61	13.90
11	-2.53	-1.92	10.21
12	-2.80	-2.50	13.33
13	-2.73	-2.22	11.83
14	-2.83	-2.37	12.62
15	-2.74	-2.19	11.65
16	-2.85	-2.50	13.31
17	-2.98	-2.09	11.12
18	-2.53	-2.23	11.89
19	-3.51	-2.62	13.97
20	-2.47	-2.14	11.39
21	-3.26	-2.32	12.37
22	-2.94	-2.13	11.35
23	-2.50	-2.40	12.79
24	-3.04	-2.50	13.35
25	-2.95	-2.31	12.32
26	-2.53	-2.06	11.00
27	-2.62	-2.72	14.48
28	-2.97	-2.31	12.29
29	-2.30	-2.37	12.64
30	-3.35	-3.19	17.00
31	-2.50	-2.61	13.90
32	-2.78	-2.76	14.72
33	-3.24	-2.22	11.85
34	-2.25	-2.23	11.88
35	-3.33	-2.46	13.14
36	-2.90	-2.16	11.53
37	-3.04	-2.32	12.35
38	-3.06	-2.10	11.17
39	-2.49	-2.02	10.78
40	-3.45	-2.48	13.23

41	-3.06	-1.96	10.45
42	-3.03	-2.40	12.81
43	-3.95	-2.33	12.43
44	-2.91	-2.25	11.98

M2 134.4-1.2			
Sample	δ13C (‰)	δ18O (‰)	Average δ18O-SST (°C)
1	-2.49	-2.93	15.62
2	-3.09	-3.24	17.27
3	-2.95	-2.88	15.35
4	-2.33	-3.06	16.31
5	-2.87	-3.07	16.36
6	-2.79	-2.65	14.12
7	-2.60	-2.88	15.35
8	-2.92	-2.72	14.50
9	-2.65	-3.16	16.84
10	-2.76	-2.59	13.80
11	-2.29	-2.77	14.76
12	-2.65	-2.60	13.86
13	-2.26	-2.52	13.43
14	-2.68	-3.02	16.10
15	-2.43	-2.53	13.48
16	-2.27	-2.26	12.05
17	-2.46	-2.09	11.14
18	-2.58	-2.37	12.63
19	-2.52	-2.07	11.03
20	-2.08	-1.79	9.54
21	-2.36	-2.00	10.66
22	-2.30	-2.00	10.66
23	-2.29	-1.83	9.75
24	-2.72	-1.89	10.07

M2 136.3-1.1 (7047±57)			
Sample	δ13C (‰)	δ18O (‰)	Average δ18O-SST (°C)
1	-2.56	-2.89	15.40
2	-2.90	-2.82	15.03
3	-2.64	-2.79	14.87
4	-2.84	-2.87	15.30
5	-2.91	-2.87	15.30
6	-3.34	-2.50	13.33
7	-2.50	-2.44	13.01
8	-2.95	-2.52	13.43
9	-2.34	-2.29	12.21
10	-2.73	-2.12	11.30
11	-2.26	-2.30	12.26
12	-2.81	-2.69	14.34
13	-2.49	-1.84	9.81
14	-3.13	-2.80	14.92
15	-3.66	-2.56	13.64
16	-3.55	-2.66	14.18
17	-2.89	-1.70	9.06
18	-2.45	-2.52	13.43
19	-2.93	-3.02	16.10
20	-2.55	-2.58	13.75
21	-2.86	-3.28	17.48
22	-3.49	-3.13	16.68
23	-2.88	-2.64	14.07
24	-3.00	-3.22	17.16
25	-3.48	-2.81	14.98
26	-2.68	-2.67	14.23
27	-2.38	-2.91	15.51
28	-2.64	-2.83	15.08
29	-3.57	-2.71	14.44
30	-2.99	-2.66	14.18
31	-2.86	-3.17	16.90
32	-3.53	-2.67	14.23
33	-3.10	-2.23	11.89
34	-2.66	-2.66	14.18
35	-3.30	-2.98	15.88
36	-3.16	-2.40	12.79
37	-2.55	-2.52	13.43
38	-2.92	-2.66	14.18
39	-3.35	-2.37	12.63
40	-2.72	-1.95	10.39

41	-2.61	-2.39	12.74
42	-3.24	-2.43	12.95
43	-2.78	-1.95	10.39
44	-2.58	-2.23	11.89
45	-3.50	-2.36	12.58
46	-3.68	-2.25	11.99
47	-2.86	-1.88	10.02
48	-2.87	-2.34	12.47
49	-3.52	-2.37	12.63
50	-3.21	-2.30	12.26
51	-2.89	-2.39	12.74
52	-3.28	-2.77	14.76
53	-3.58	-2.19	11.67
54	-2.90	-2.30	12.26
55	-2.89	-2.65	14.12
56	-4.15	-5.19	27.66
57	-3.03	-2.21	11.78
58	-2.65	-2.34	12.47
59	-3.35	-2.69	14.34
60	-3.96	-2.39	12.74
61	-3.04	-2.21	11.78
62	-3.18	-2.50	13.33
63	-3.98	-2.49	13.27
64	-3.42	-2.30	12.26
65	-2.96	-2.57	13.70
66	-3.58	-2.75	14.66
67	-3.32	-2.38	12.69
68	-3.03	-2.82	15.03
69	-3.70	-2.82	15.03
70	-2.77	-2.51	13.38
71	-2.75	-2.96	15.78
72	-3.39	-3.06	16.31
73	-2.79	-2.35	12.53
74	-3.08	-3.13	16.68
75	-3.43	-2.58	13.75
76	-2.46	-2.66	14.18
77	-3.29	-3.14	16.74
78	-2.57	-2.70	14.39
79	-2.47	-2.94	15.67
80	-3.45	-3.23	17.22
81	-2.59	-2.97	15.83
82	-3.70	-3.07	16.36
83	-2.90	-3.11	16.58

84	-2.74	-2.58	13.75
85	-2.97	-2.86	15.24
86	-2.70	-2.79	14.87
87	-3.04	-2.50	13.33
88	-2.70	-2.94	15.67
89	-3.20	-2.61	13.91
90	-3.00	-2.81	14.98
91	-3.48	-2.85	15.19
92	-2.62	-2.78	14.82
93	-3.05	-2.97	15.83
94	-2.85	-2.63	14.02
95	-2.70	-3.02	16.10
96	-3.70	-3.05	16.26

M2 144.8-3.1			
Sample	δ13C (‰)	δ18O (‰)	Average δ18O-SST (°C)
1	-1.74	-2.27	12.08
2	-2.83	-3.00	16.01
3	-2.14	-2.92	15.54
4	-2.59	-2.82	15.06
5	-2.32	-2.85	15.19
6	-2.72	-2.79	14.84
7	-2.65	-2.93	15.61
8	-2.04	-3.06	16.32
9	-2.47	-2.99	15.91
10	-2.36	-2.92	15.58
11	-2.19	-3.09	16.44
12	-2.73	-2.98	15.89
13	-2.69	-3.23	17.22
14			
15	-2.75	-3.21	17.13
16	-1.93	-3.22	17.14
17	-2.06	-2.89	15.38
18	-1.85	-3.16	16.83
19	-2.49	-2.92	15.57
20	-2.76	-3.11	16.57
21	-2.04	-2.78	14.80
22	-2.39	-3.09	16.46
23	-2.87	-2.98	15.88
24	-2.00	-2.99	15.93
25	-2.84	-3.09	16.46
26	-2.30	-3.20	17.06
27	-3.32	-3.23	17.24
28	-2.38	-3.01	16.04
29	-2.85	-2.91	15.51
30	-2.52	-3.25	17.31
31	-2.13	-3.08	16.43
32	-2.52	-2.85	15.20
33	-2.07	-2.94	15.65
34	-2.36	-3.22	17.16
35	-2.55	-3.11	16.57
36	-2.43	-2.61	13.89
37	-2.84	-2.58	13.74
38	-2.76	-3.01	16.03
39	-2.16	-2.71	14.46
40	-3.08	-2.86	15.27

41	-2.69	-2.74	14.58
42	-2.42	-3.04	16.20
43	-2.87	-3.07	16.38

M2 145.7-3.1 (5944±28)			
Sample	δ13C (‰)	δ18O (‰)	Average δ18O-SST (°C)
1	-2.87	-3.02	16.10
2	-1.67	-3.21	17.11
3	-1.75	-2.88	15.35
4	-1.96	-3.40	18.12
5	-2.73	-3.11	16.58
6	-2.18	-2.80	14.92
7	-1.83	-3.56	18.97
8	-2.21	-2.81	14.98
9	-1.85	-3.32	17.70
10	-2.25	-3.25	17.32
11	-1.97	-3.13	16.68
12	-1.62	-3.60	19.19
13	-2.36	-2.89	15.40
14	-1.51	-3.17	16.90
15	-2.13	-2.88	15.35
16	-2.03	-2.85	15.19
17	-2.34	-2.80	14.92
18	-2.38	-2.89	15.40
19	-1.95	-2.49	13.27
20	-2.62	-3.06	16.31
21	-2.56	-2.98	15.88
22	-2.48	-2.46	13.11
23	-2.86	-2.53	13.48
24	-2.78	-2.80	14.92
25	-2.40	-3.09	16.47
26	-2.39	-2.98	15.88
27	-2.46	-3.05	16.26
28	-2.23	-2.57	13.70
29	-2.27	-3.07	16.36
30	-2.14	-2.71	14.44
31	-2.02	-2.73	14.55
32	-2.28	-2.74	14.60
33	-1.78	-2.77	14.76
34	-2.72	-2.91	15.51
35	-1.68	-2.47	13.17
36	-2.49	-3.14	16.74
37	-1.94	-2.52	13.43
38	-2.24	-3.08	16.42
39	-2.49	-3.06	16.31
40	-2.71	-2.94	15.67

41	-2.40	-2.91	15.51
42	-2.60	-3.61	19.24
43	-2.74	-3.00	15.99
44	-1.99	-3.25	17.32
45	-2.80	-2.98	15.88
46	-2.38	-3.48	18.55
47	-2.44	-3.56	18.97
48	-2.88	-3.29	17.54
49	-2.68	-3.61	19.24
50	-2.55	-3.23	17.22
51	-2.45	-3.71	19.77
52	-2.41	-3.26	17.38
53	-1.99	-3.33	17.75
54	-2.25	-3.70	19.72
55	-2.24	-2.91	15.51
56	-1.81	-3.49	18.60
57	-2.13	-3.63	19.35
58	-2.31	-3.74	19.93
59	-1.64	-3.23	17.22
60	-1.73	-3.61	19.24
61	-2.07	-3.14	16.74
62	-1.60	-3.10	16.52
63	-2.21	-2.90	15.46
64	-1.63	-2.91	15.51
65	-2.19	-3.10	16.52
66	-1.75	-3.27	17.43
67	-2.19	-3.52	18.76
68	-2.50	-3.90	20.79
69	-2.17	-3.37	17.96

Appendix 6: Sr/Ca Data

Sr/Ca values for corals M2 145.7-3.1 and 140.7-0.7b and Sr/Ca-SST calculated with six calibration equations (Table 2). Table 1 list the equations which corresponds to each Sr/Ca-SST calculated. Figures 1 and 2 shows the (in blue) samples selected for Sr/Ca analysis based on the $\delta^{18}O$ record (in red) for each coral.

Table 1. Sr/Ca-Calibration equation key.

Sr/Ca-SST Calibration Equation Key			
Key	SST Equation Source	Location	Sr/Ca-SST Calibration Equation
SST1	Jimenez, 2018	Baharaona Bay, Domincan Republic	SST=((-Sr/Ca)+10.7867)/0.0676
SST2	Saenger et al. 2008 (1)	South shore reef, Bermuda	SST=((-Sr/Ca)+11.74)/0.095
SST3	Flannery and Poore, 2013	Dry Tortugas, Florida	SST=((-Sr/Ca)+10.205)/0.0392
SST4	Saenger et al. 2008 (2)	St. Croix, U.S. Virgin Islands	SST=((-Sr/Ca)+10.98)/0.077
SST5	Smith, 2006	Looe Key, Florida	SST=((-Sr/Ca)+9.962)/0.0282
SST6	Swart et al., 2002	Biscayne National Park, Florida	SST=((-Sr/Ca)+10.165)/0.0471

Table 2. Sr/Ca values for coral M2 145.7-3.1 and 140.7-0.7b and Sr/Ca-SST. SST1 to 6 correspond to the calibration equations listed in Table 1.

M2 145.7-3.1 (5944±28)							
Sample	Sr/Ca (mmol/mol)	SST1 (°C)	SST2 (°C)	SST3 (°C)	SST4 (°C)	SST5 (°C)	SST6 (°C)
4	9.23	23.05	26.43	24.91	22.74	26.00	19.88
8	9.43	20.05	24.30	19.74	20.11	18.82	15.58
12	9.37	21.00	24.98	21.38	20.95	21.10	16.94
19	9.43	20.11	24.34	19.84	20.17	18.96	15.66
25	9.25	22.66	26.16	24.24	22.40	25.08	19.32
28	9.34	21.46	25.30	22.16	21.35	22.19	17.60
29	9.47	19.42	23.85	18.64	19.56	17.30	14.67
35	9.49	19.22	23.71	18.31	19.39	16.83	14.39
42	9.37	21.00	24.98	21.38	20.95	21.10	16.94
45	9.39	20.73	24.79	20.91	20.71	20.45	16.56
51	9.52	18.71	23.35	17.43	18.94	15.62	13.66
55	9.49	19.11	23.63	18.11	19.29	16.56	14.23
58	9.43	20.09	24.33	19.81	20.15	18.92	15.64
63	9.44	19.87	24.17	19.43	19.96	18.39	15.32
68	9.59	17.76	22.67	15.78	18.10	13.32	12.28
M2 140.7-0.7a (7508±46)							
Sample	Sr/Ca (mmol/mol)	SST1	SST2	SST3	SST4	SST5	SST6
2	9.30	22.03	25.71	23.15	21.85	23.57	18.42
6	9.19	23.61	26.84	25.88	23.24	27.36	20.69
12	9.42	20.23	24.43	20.05	20.27	19.25	15.83
14	9.30	21.92	25.63	22.96	21.75	23.30	18.26
18	9.28	22.36	25.95	23.72	22.14	24.36	18.89
25	9.33	21.56	25.38	22.34	21.44	22.44	17.74
32	9.21	23.26	26.58	25.26	22.93	26.50	20.18
36	9.22	23.21	26.55	25.18	22.88	26.39	20.11
38	9.13	24.49	27.46	27.39	24.01	29.45	21.94
42	9.25	22.66	26.16	24.25	22.41	25.09	19.33
44	9.38	20.80	24.84	21.03	20.77	20.62	16.65
46	9.37	21.01	24.98	21.39	20.95	21.12	16.95
53	9.37	20.96	24.95	21.30	20.91	20.99	16.88
55	9.40	20.58	24.68	20.65	20.58	20.08	16.33
59	9.39	20.59	24.68	20.66	20.58	20.11	16.35

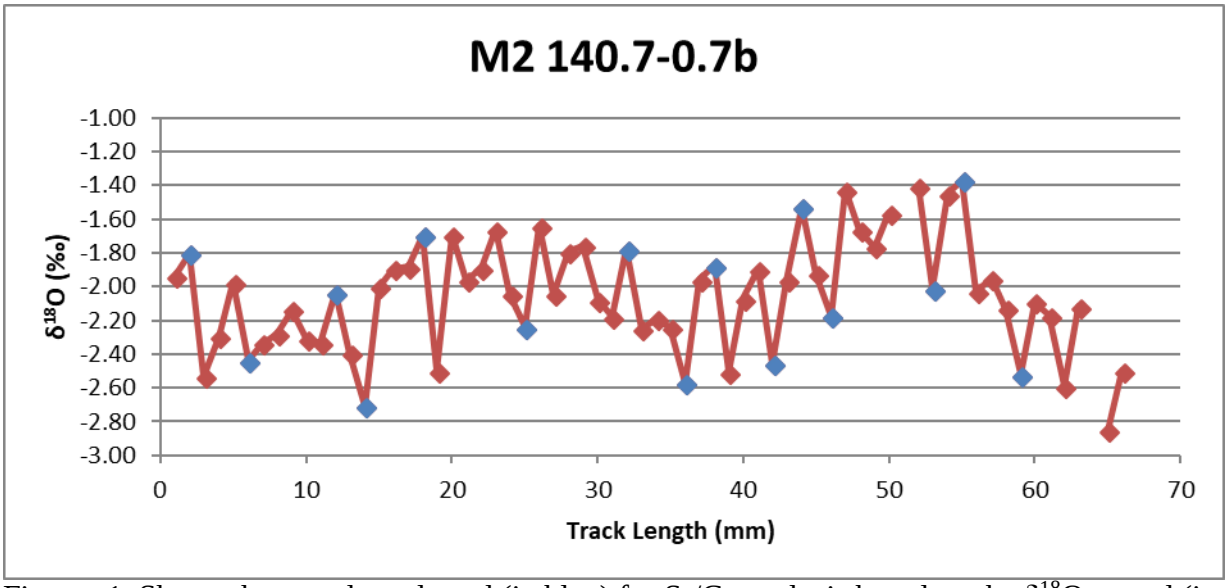

Figures 1. Shows the samples selected (in blue) for Sr/Ca analysis based on the $\delta^{18}O$ record (in red) for coral M2 140.7-0.7b.

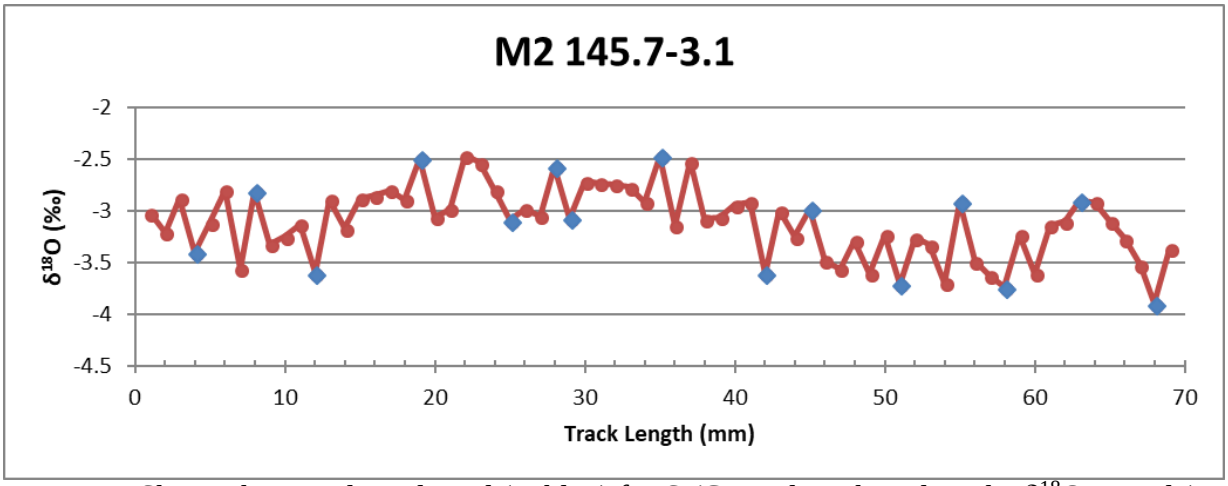

Figures 2. Shows the samples selected (in blue) for Sr/Ca analysis based on the $\delta^{18}O$ record (in red) for coral M2 145.7-3.1.

Appendix 7: Residual Oxygen Isotope Data

Residual $\delta^{18}O$ ($\Delta\delta^{18}O$) for corals M2 145.7-3.1 and 140.7-0.7b. $\Delta\delta^{18}O$ were calculated using $\delta^{18}O$-SST and Sr/Ca-SST calculated with the calibration equation by Jimenez (2018). $\Delta\delta^{18}O$, $\delta^{18}O$-SST, and Sr/Ca-SST listed below.

M2 145.7-3.1 (5944±28)				M2 140.7-0.7a (7508±46)			
Sample	Sr/Ca-SST (°C)	Average δ18O-SST (°C)	Δδ18O (‰)	Sample	Sr/Ca-SST (°C)	Average δ18O-SST (°C)	Δδ18O (‰)
4	23.05	18.12	0.92	2	22.03	9.62	2.33
8	20.05	14.98	0.95	6	23.61	12.99	1.99
12	21.00	19.19	0.34	12	20.23	10.84	1.76
19	20.11	13.27	1.28	14	21.92	14.43	1.41
25	22.66	16.47	1.16	18	22.36	9.04	2.50
28	21.46	13.70	1.46	25	21.56	11.94	1.81
29	19.42	16.36	0.57	32	23.26	9.48	2.58
35	19.22	13.17	1.14	36	23.21	13.70	1.78
42	21.00	19.24	0.33	38	24.49	9.99	2.72
45	20.73	15.88	0.91	42	22.66	13.10	1.80
51	18.71	19.77	-0.20	44	20.80	8.14	2.37
55	19.11	15.51	0.68	46	21.01	11.60	1.77
58	20.09	19.93	0.03	53	20.96	10.72	1.92
63	19.87	15.46	0.83	55	20.58	7.30	2.49
68	17.76	20.79	-0.57	59	20.59	13.43	1.34

Appendix 8: Growth Rate Data

Annual growth rate data for each coral listed in mm/yr below.

M2 148-0.6	M2 140.7-0.7a	M2 140.7-0.7b	M2 150.7-1.3	M2 120.5-0.5	M2 140-0.8	M2 134.4-1.2
6.94	7.52	8.27	6.13	3.75	1.12	2.91
2.77	1.98	3.74	7.90	6.32	2.42	1.25
3.37	5.54	5.32	6.92	9.08	3.89	3.24
5.15	3.36	5.71	5.73	5.72	1.99	2.33
3.77	7.12	7.68	3.36	4.54	3.37	0.92
3.77	2.77	5.71	1.98	3.95	4.41	2.08
6.34	2.97	7.29	1.98	3.95	1.21	1.00
2.77	2.97	3.74	7.71	8.09	1.73	3.91
7.93	4.15	5.52	1.78	7.50	1.99	3.66
2.77	2.77	4.73	1.38	2.76	3.63	3.74
4.56	2.97	4.92	4.35	4.14	2.68	
7.73	5.54	3.94		6.12	1.21	
2.97	5.14	3.55		8.68	1.30	
4.56	3.17	3.35		5.92		
2.97	4.75	4.33		6.32		
	1.98	3.35		3.16		
	2.37	4.14		5.13		
	3.36	5.12		5.33		
				2.96		

M2 136.3-1.1	M2 144.8-3.1	M2 145.7-3.1
5.16	3.55	3.28
3.57	1.97	4.18
6.95	1.58	2.09
3.77	2.56	2.16
6.55	3.35	3.43
4.17		1.57
6.95		3.73
4.96		3.66
5.16		4.48
4.57		4.18
4.77		2.39
6.75		6.94
		3.66
		6.64
		2.01

Appendix 9: Coral Radiographies and Coral Slabs

Radiographies and coral slab for each coral used in this study. Sample names listed below each radiography. The white square in each image is 4.8 by 4.8 centimeters.

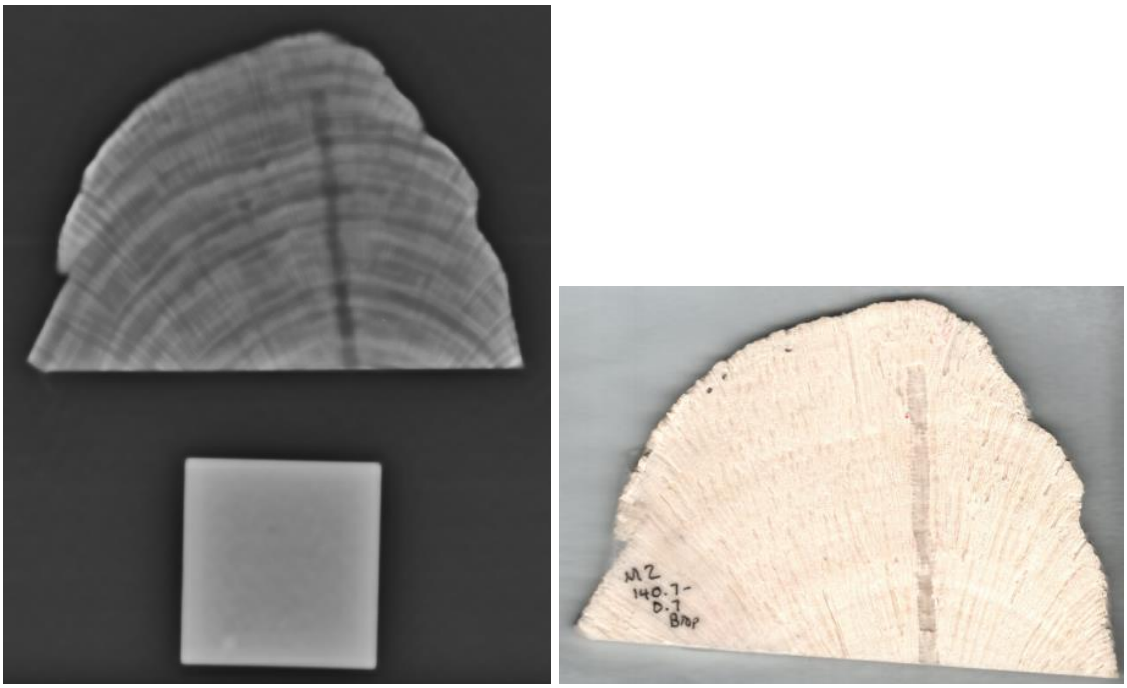

M2 140.7-0.7b

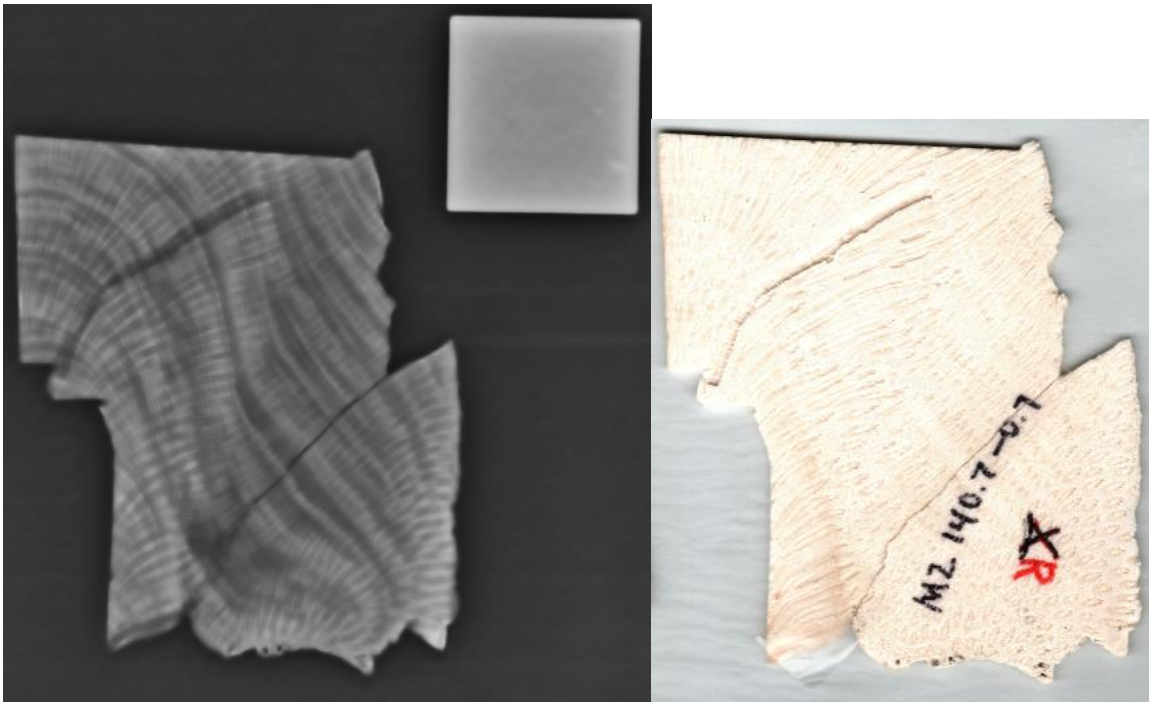

M2 140.7-0.7a

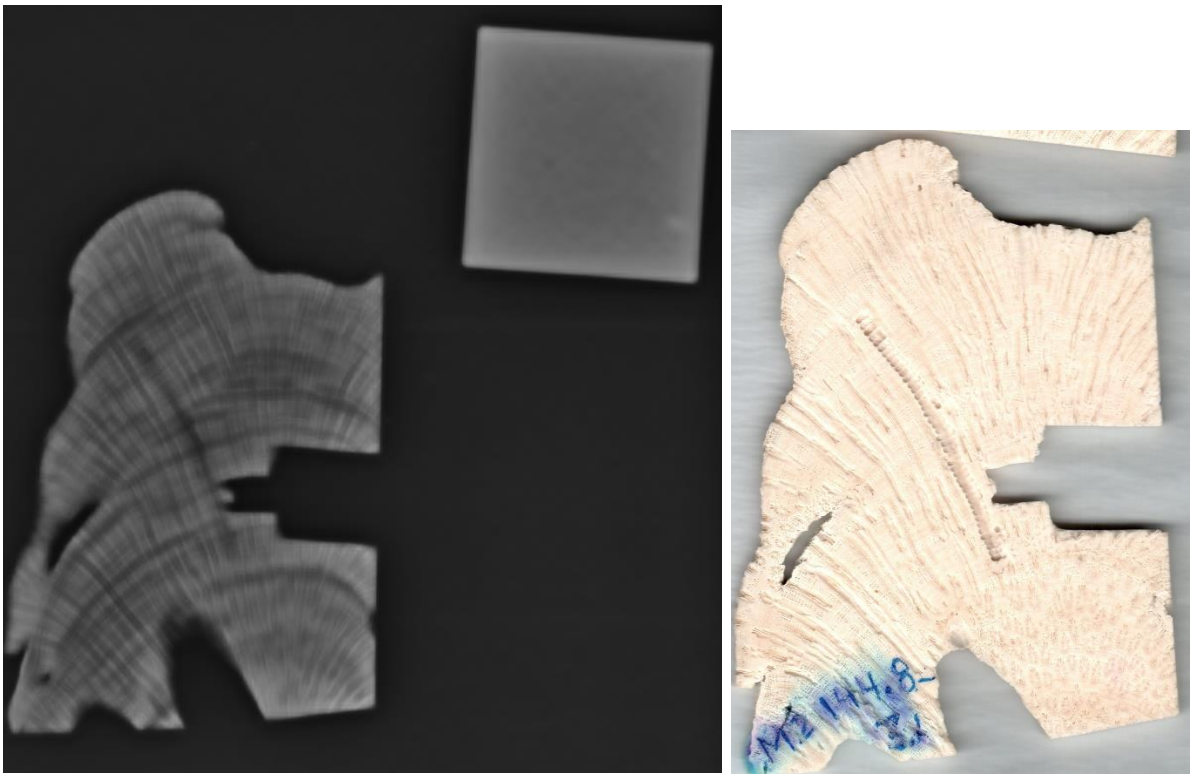

M2 144.8-3.1

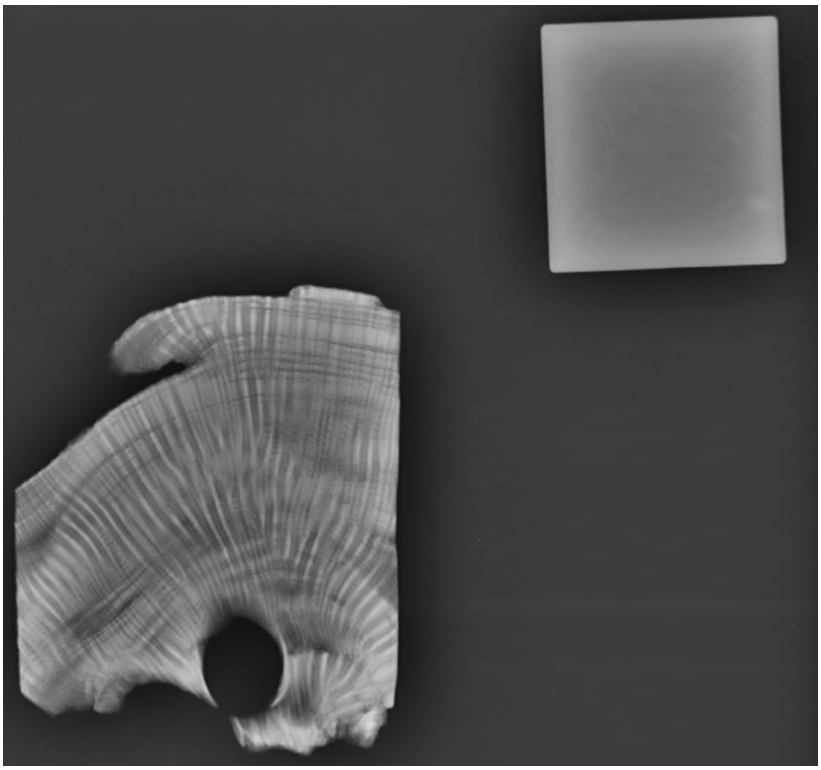

M2 120.4-1.5 (This section was used to calculate growth rates because the slab sampled for geochemical analysis was not flat.)

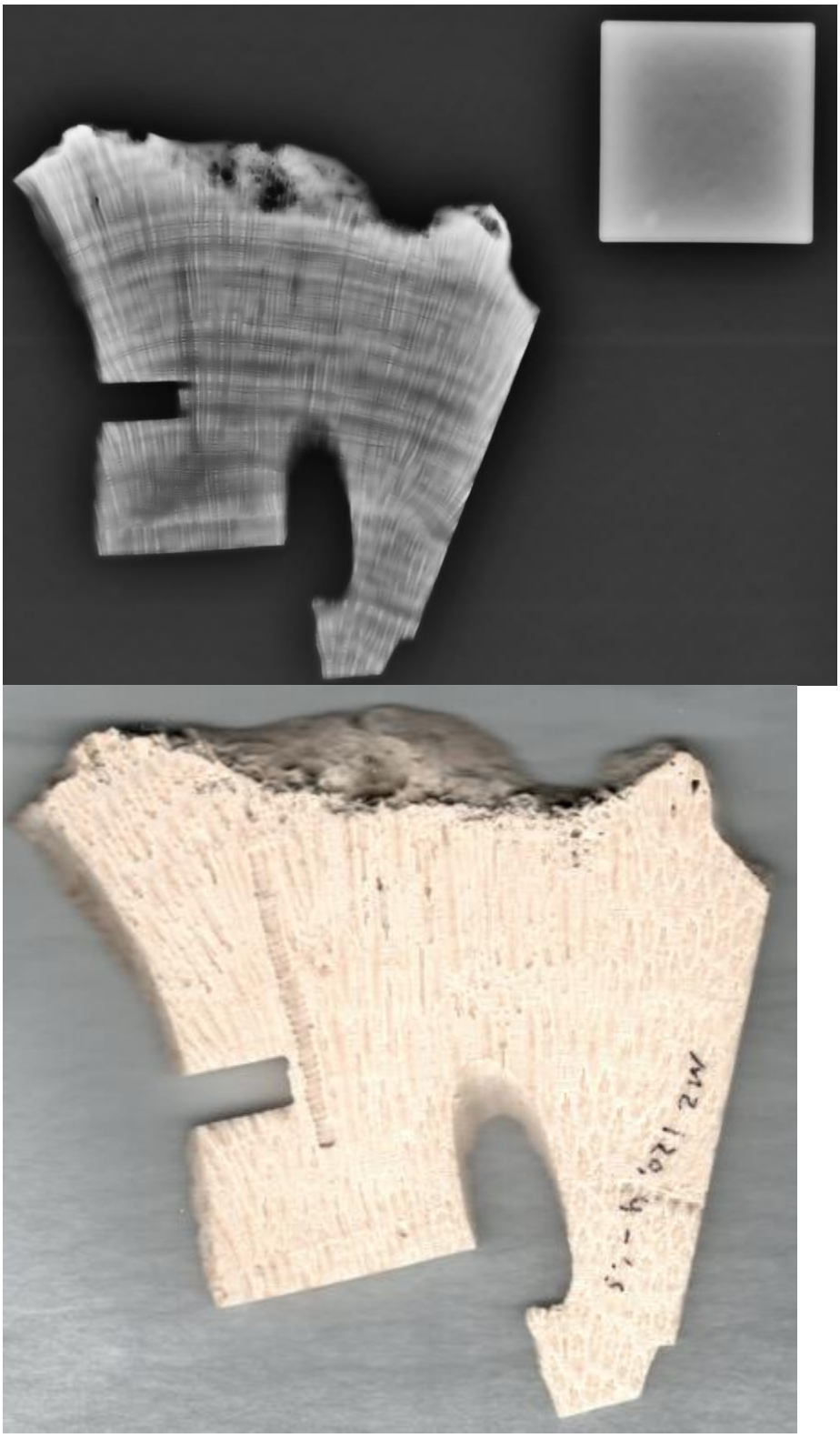

M2 120.4-1.5 (This section is not flat and therefore cannot be used for growth rates.)

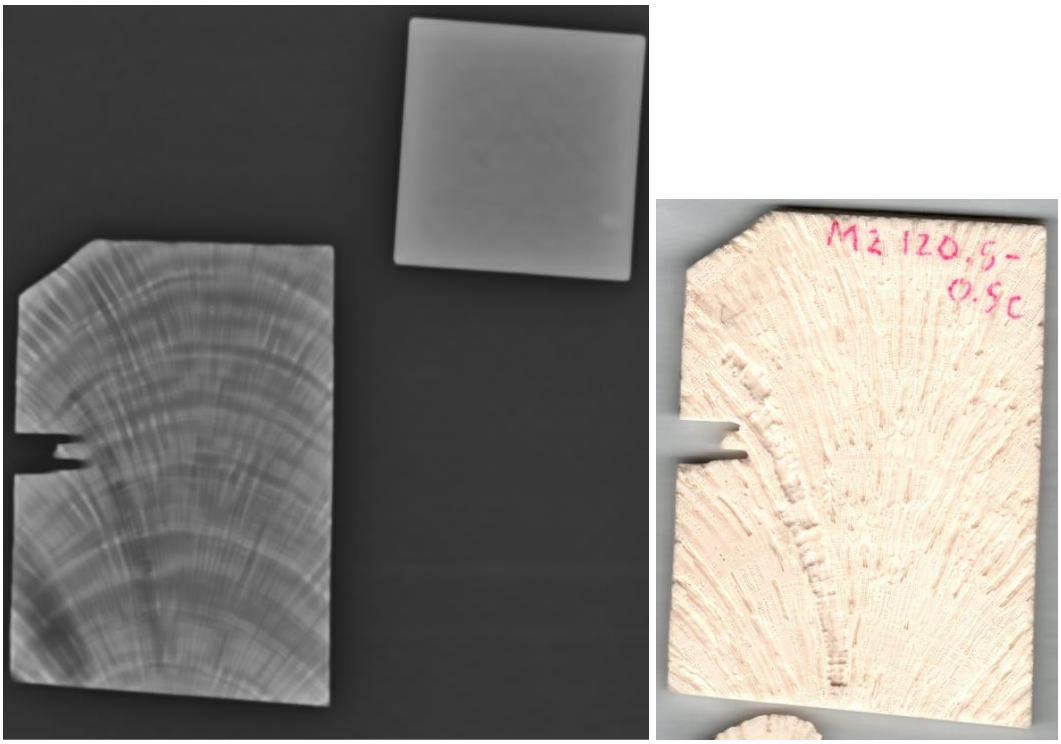

M2 120.5-0.5

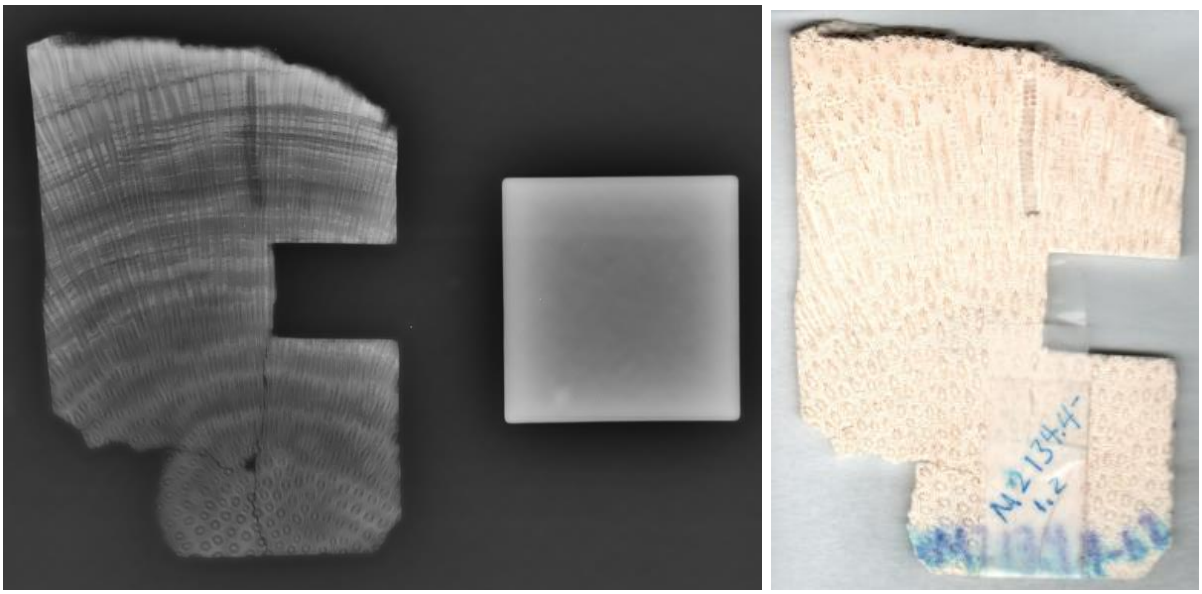

M2 134.4-1.2

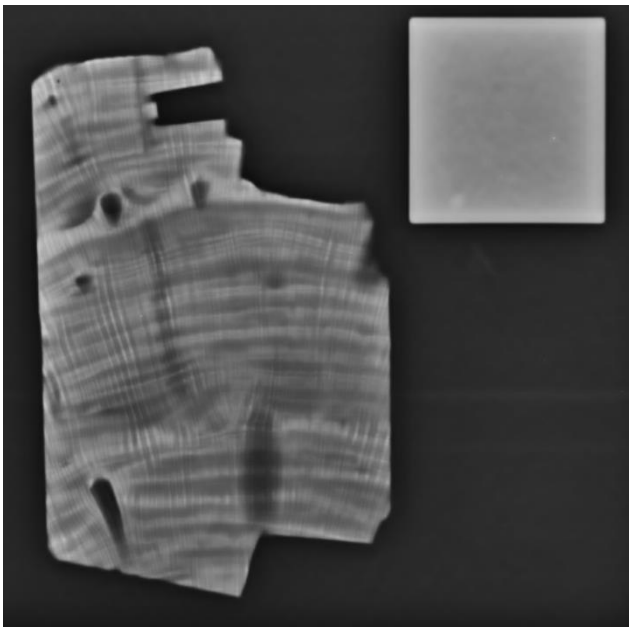
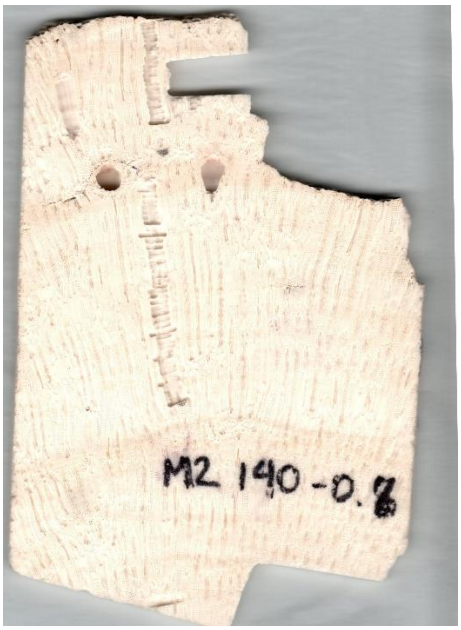

M2 140-0.8

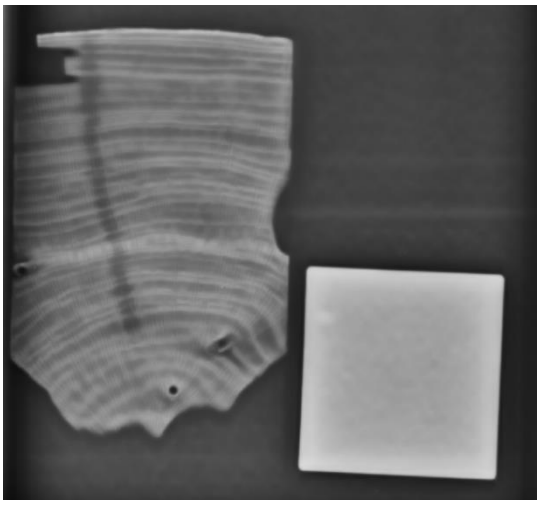
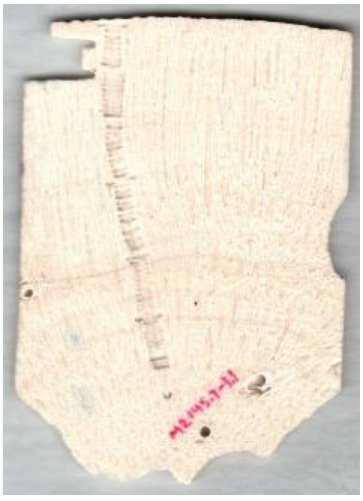

M2 145.7-3.1

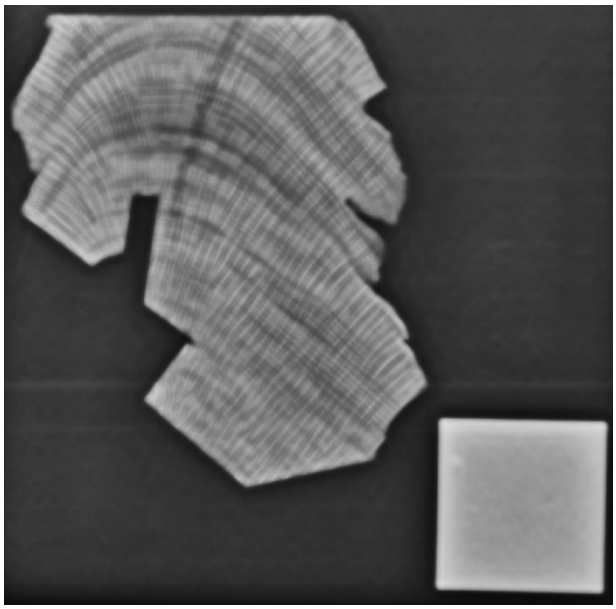

M2 150.7-1.3

The following figures show the coral slabs and their radiographies were before samples were taken from the slab for SEM and XRD analysis.

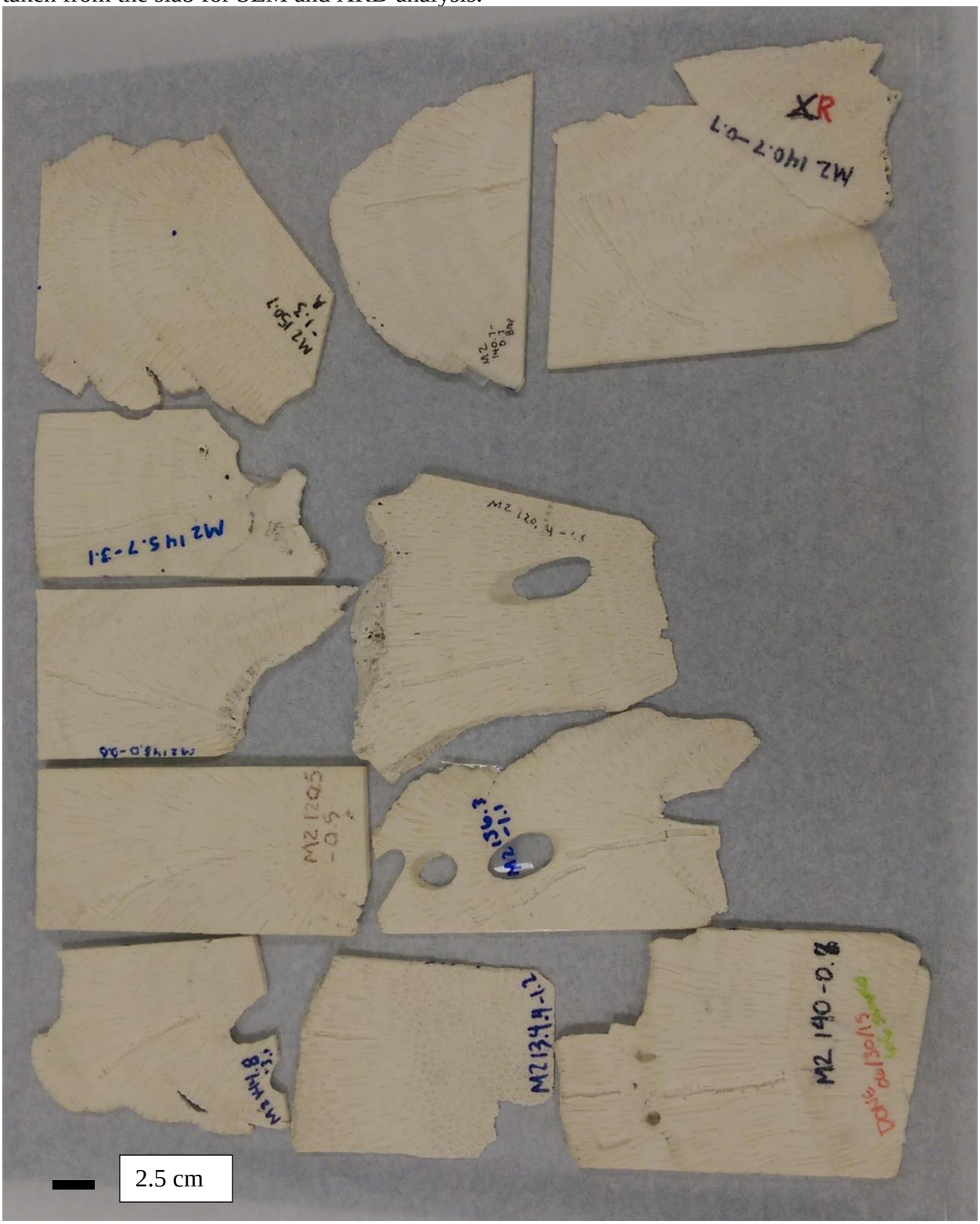


2.5 cm